X-525-70-200

PREPRINT

NASA TM X- 65313

K_U-BAND TRACKING AND DATA RELAY SATELLITE GROUND ANTENNA STUDY

JUNE 1970

GSFC

GODDARD SPACE FLIGHT CENTER

GREENBELT, MARYLAND

X-525-70-200

K_u-BAND TRACKING AND DATA RELAY SATELLITE GROUND ANTENNA STUDY

Leonard F. Deerkoski
Howard Estep
Paul A. Lantz
Nicholas A. Raumann

June, 1970

GODDARD SPACE FLIGHT CENTER
Greenbelt, Maryland

K_u-BAND TRACKING AND DATA RELAY SATELLITE GROUND ANTENNA STUDY

Leonard F. Deerkoski

Howard Estep

Paul A. Lantz

Nicholas A. Raumann

ABSTRACT

An array of four 42-foot diameter reflector antennas on a single pedestal is the most attractive ground antenna configuration to provide the 70 db gain required for the 16 GHz Tracking and Data Relay Satellite (TDRS) to ground communication link. A continuous uninterrupted communication channel precludes the use of a radome because of water film losses under precipitation. A 17-foot diameter acquisition antenna at the center of the array enables the system to acquire and track the TDRS within a 1/4 degree cone about the boresite axis of the full array. The acquisition antenna can also be used for command uplink to the TDRS while simultaneously tracking and receiving with the full array.

CONTENTS

CONTENTS (Continued)

ILLUSTRATIONS

ILLUSTRATIONS (Continued)

ILLUSTRATIONS (Continued)

TABLES

SYMBOLS

Symbol	Meaning
a_1, a_2, a_3, a_4	constants
B, BW	antenna beamwidth, degrees
c	velocity of light, 9.835×10^8 ft/sec
C_F	cost of receiver front end, dollars
d	subreflector diameter
D	main reflector diameter
f	focal length of subreflector
F	frequency, hertz
$\mathcal{F}$	focal length of the main reflector
G	gain
G_E	gain of one array element
G_T	total array gain
$G_w(s)$	torque system transfer function
J_a	antenna inertia, slug-ft^2
k_1, k_2, k_s	constants
k_w	wind coefficient, ft-lbs/(mph)^2
ℓ, ℓ_a, ℓ_o, ℓ_r	transmission loss
L	frame side length
M	parameter relating σ to D
P	drive motor rating, hp
Q	rain rate, mm/hr
r	radius of hub, feet

SYMBOLS

Symbol	Meaning
R	radome radius, feet
s	Laplace operator
t	water film thickness, mils
T	noise temperature, °K
T_a	antenna noise temperature, °K
T_{ac}	acceleration torque, ft-lbs
T_f	friction torque, ft-lbs
T_w	wind torque, ft-lbs
T_{wf}	wind torque fluctuation, ft-lbs
T_m	mean absorption temperature of atmosphere, °K
T_r	noise temperature of radome, °K
T_s	system noise temperature, °K
T_{sk}	sky noise temperature, °K
T_1	position loop time constant, seconds
V_0	maximum wind velocity, mph
$V_1(t)$	standard deviation of wind velocity, mph
w	frame width, feet
W	diameter of feed
α	transmission coefficient
α_r	transmission coefficient of radome and water film
α_s	transmission coefficient due to ohmic losses
α_f	transmission coefficient of feed and cables
α_t	$\alpha_r \cdot \alpha_f$
β_n	servo noise bandwidth, Hertz

Symbol	Meaning
δ	skin depth
ϵ	dielectric constant
ϵ_d	error due to dynamic lag of servo, radians
ϵ_f	error due to friction, radians
ϵ_s	error due to atmospheric scintillations
ϵ_{th}	error due to receiver noise, radians
ϵ_w	error due to wind torque, radians
λ	wavelength
η_h	hub blockage
η_m	membrane blockage
η_a	aperture efficiency
η_B	aperture blockage
η_D	efficiency due to subreflector diffraction
η_F	feed efficiency
η_0	antenna efficiency
Γ	reflection coefficient
σ	rms surface accuracy
$\sigma_{S.R.}$	rms surface accuracy of subreflector
$\sigma_{M.R.}$	rms surface accuracy of main reflector
ρ	density, gm/m^3
μ_g	gearing efficiency
μ_t	torque bias ratio
ω_c	position loop bandwidth, radians/second

SYMBOLS

Symbol	Meaning
ω_n	lowest structural resonance, radians/second
ω_r	rate loop bandwidth, radians/second
θ_{sat}	angular position of satellite, radians
θ_{ANT}	orientation of antenna axis, radians
θ_{ww}	power density spectrum, $(\text{ft-lbs})^2$/radians/second
ϕ	zenith angle
ATS	applications technology satellite
CNR	carrier to noise ratio
TDRS	tracking and data relay satellite
TDRSS	tracking and data relay satellite system
EIRP	effective isotropic radiated power
GSFC	Goddard Space Flight Center
NF	noise figure
\$, $\$_A$, $\$_E$, $\$_s$	cost, dollars

ACKNOWLEDGMENT

The authors wish to acknowledge the contributions of numerous individuals within the Tracking and Data System Directorate and especially the Advanced Development Division. Also acknowledged are the contributions of Mr. Andrew J. Rolinski of the Antenna Systems Branch to the Economic Section of this report.

K_u-BAND TRACKING DATA RELAY SATELLITE GROUND ANTENNA STUDY

1 INTRODUCTION

Several reports have been published on the Tracking and Data Relay Satellite System (TDRSS). This report is the first study devoted exclusively to the ground antenna requirements in support of the TDRSS. The ground antenna requirements are derived from the overall system goals postulated below.

a. A K_u-band downlink carrier

b. A continuous uninterrupted communication channel

c. Minimize impact on the Tracking and Data Relay Satellite (TDRS)

In order to minimize the power and antenna gain requirements of the TDRS spacecraft, the ground antenna gain should be maximized. There are several reasons for this approach.

a. A Thor-Delta launch vehicle is currently being considered for the TDRS and severe weight and power constraints can be expected.

b. A 1-watt transmitter at K_u-band provides an 8 to 1 advantage in efficiency over a 20-watt transmitter.

c. Reducing spacecraft gain would increase its field of view at the ground and thereby increase the possibility of simultaneous communication with two ground stations. For example, a one foot diameter antenna at K_u-band could simultaneously communicate with the Goddard Space Flight Center (GSFC) and the Manned Spacecraft Center in Houston.

The communication link between TDRS and ground requires consideration of propagation also. Propagation characteristics are a function of the environmental

conditions at the ground antenna and are therefore unique for a given location. In order to realistically consider all the parameters that will affect the communication link and therefore the ground antenna, a specific example was constructed and fully evaluated. The location of the ground station was chosen to be near GSFC to provide convenient access to its data processing facilities. The assumed spacecraft parameters are outlined in Section 2 of this report. Although specific values of spacecraft gain, bandwidth and power are selected, it is only the spacecraft EIRP (+84.5 dbm) that affects the communication link. Therefore a new set of spacecraft parameters will require only an adjustment of the results presented in this report.

This report establishes the TDRS ground antenna requirements for this example and presents the most attractive alternative for meeting those requirements. The feasibility of a radome, the comparison of single aperture versus multi-aperture arrays both technically and economically, tracking and reliability are all considered in detail.

The logical organization of the report is given in Figure 1-1. Section 3 briefly summarizes the results of the study while Sections 9 and 10 present the detailed system considerations and costs, respectively, which led to our conclusions. It is suggested that sections 4 through 8 be omitted in a first reading of this report because these sections contain details that are intended to answer specific questions and necessarily require a more intense review

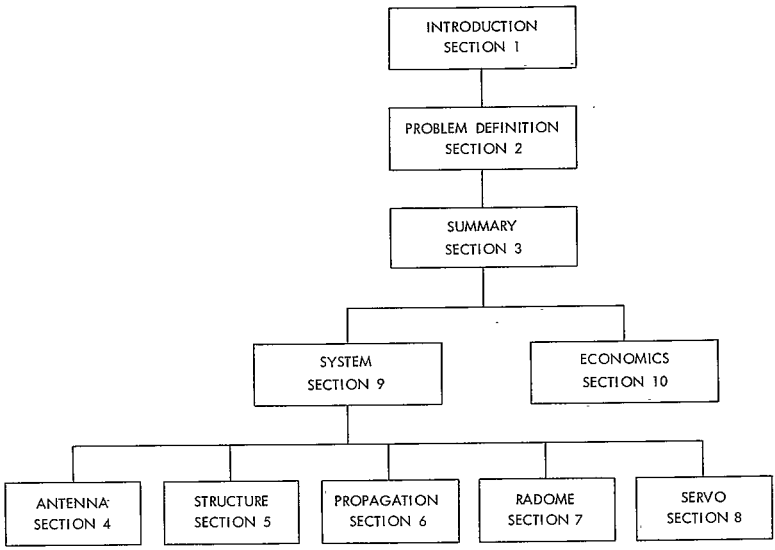

Figure 1-1. Organization of Report

2 PROBLEM DEFINITION

The objective of this report is to make a preliminary study of the feasibility of locating a ground antenna system near GSFC in support of the TDRS downlink channel. The requirements of the ground antenna are determined from the spacecraft parameters listed in Table 2-1. The spacecraft antenna is assumed stable

Table 2-1

TDRS Spacecraft Parameters

Spacecraft Antenna	4 ft. dia. paraboloid
Downlink Frequency	15.7-17.7 GHz
Spacecraft Gain	43.5 db
Bandwidth	2.0 GHz
Transmitter Power	20 watts
Spacecraft Losses	2.0 db

and continuously pointing toward GSFC with an angular accuracy of ±0.1°, corresponding to less than 0.1 db loss in spacecraft gain due to pointing error.

The number and location of the TDRS spacecraft have not yet been determined. Propagation effects are, however, a function of elevation angle and a range of spacecraft positions must be defined. Each TDRS spacecraft is at synchronous altitude and the elevation of any visible TDRS spacecraft will be defined by its longitude position relative to GSFC as in Figure 2-1. We have assumed that the TDRS spacecraft is within 60° longitude of GSFC and the minimum elevation angle to the spacecraft is therefore 15°. The maximum elevation angle to a TDRS spacecraft will be 45° and will occur when the spacecraft is at

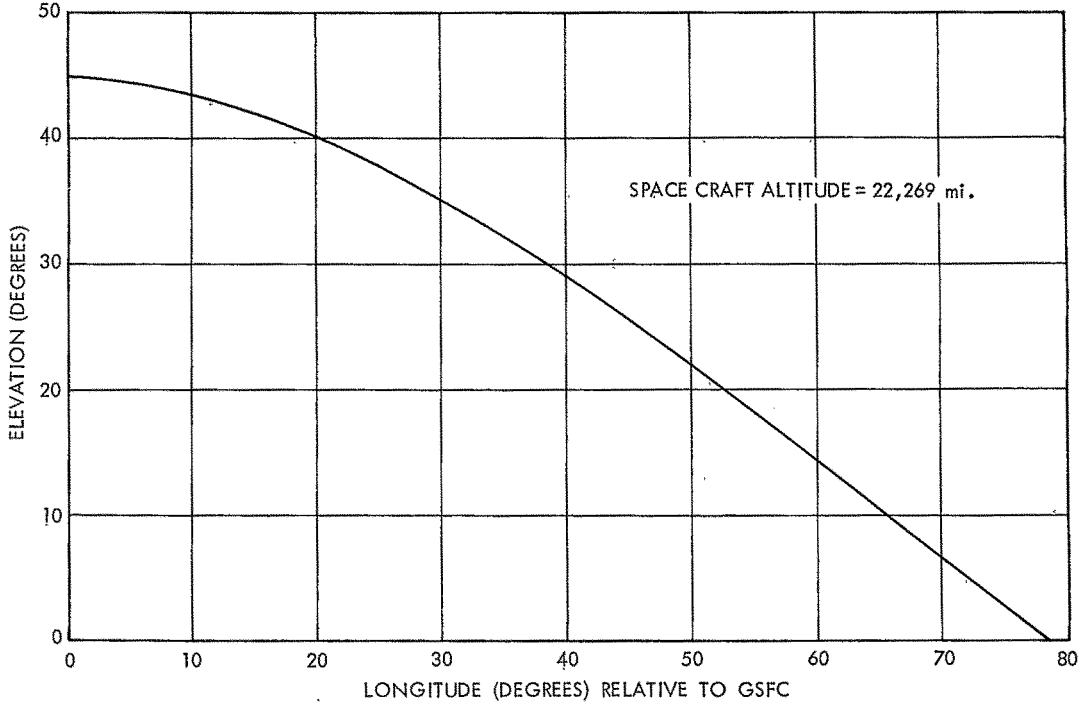

Figure 2-1. Elevation of TDRS Spacecraft as Seen From GSFC

the same longitude as GSFC. The range of elevation angles that will be considered in this report is therefore 15° to 45°.

The TDRS spacecraft are at synchronous altitude but they are not stationary. A synchronous orbit traces out a distorted figure eight in space within a period of 24 hours. The figure eight itself moves, but the major contribution to spacecraft velocity is its motion along the figure eight path. ATS-1, for example, has a ±2° peak to peak latitude excursion from the equatorial plane. The maximum angular velocity of this spacecraft is roughly 0.0167°/min. For the pointing accuracy required of the TDRS ground antenna, the ground antenna pointing would need to be updated at least three times per minute to follow an orbit similar to that of ATS-1. For this reason, tracking is considered a requirement of the TDRS ground antenna system and will be included in this report.

3 SUMMARY

3.1 Conclusions

The environmental conditions in the vicinity of GSFC requires a 10 db CNR margin for the TDRS to ground communication link to guarantee acceptable data quality. A 70 db gain ground antenna with tracking capability is required to provide the 30 db minimum CNR at the receiver under favorable weather conditions. At 16 GHz the 70 db gain can presently be achieved with a 95-foot diameter single aperture parabolic reflector antenna with σ = 0.030 inch rms and 55% efficiency. However, in comparison with a 4 element adaptively phased multi-aperture array on a single pedestal the single aperture antenna is less desirable. Four 42-foot diameter parabolic reflectors mounted on a common pedestal with a 17-foot diameter acquisition antenna located at the array center is the most attractive ground antenna configuration. A multi-aperture antenna on separate pedestals can provide the required 70 db gain, but the bandwidth limitation of the array precludes this configuration.

The four element array provides two orthogonal phase monopulse tracking channels, requiring only listening feeds in each array element. The acquisition antenna has a 3 db beamwidth (BW) of 0.25°. A tracking feed in the acquisition antenna provides sufficient pointing accuracy to place the spacecraft within the 2 db BW of the full array which can then accept the tracking function. After the full array has accepted the tracking function, the acquisition antenna would be available for command uplink to the TDRS.

Enclosing the antenna within a radome relieves the servo tracking system of wind errors; however, the 1 db transmission loss of the radome requires a 115-foot diameter antenna (Figure 10-2) to provide the equivalent gain of an exposed 95-foot diameter reflector. Moderate rainfall and heavy rainfall cause

a 4 db and 12 db CNR reduction, respectively, due to water accumulation on the radome surface (Section 9 of this report). This CNR reduction is in addition to that resulting from propagation through the atmosphere. The communication performance reliability for an exposed antenna is 2 to 6 times better than that for a gain equivalent radome enclosed system. The advantages of a radome for improving tracking reliability are not sufficient to justify the corresponding reduction in communication performance reliability. An exposed ground antenna is recommended.

An AZ/EL tracking pedestal is structurally the most attractive mount. The required tracking accuracy for both the single aperture and multi-aperture systems makes a hydrostatic bearing on the azimuth axis essential. This requirement exists irrespective of the presence of a radome.

The conclusion of this report is that the TDRS ground antenna should have the following features:

a. Four 42-foot diameter reflectors mounted on a common pedestal

b. Surface accuracy, each reflector: σ = 0.013"

c. Listening feeds only in each reflector

d. Adaptively phased tracking receiver

e. AZ/EL tracking pedestal

f. Center mounted 17' diameter acquisition/command antenna

g. No radome.

The antenna system described above has a 1/4° acquisition cone. The 3 db BW of this adaptively phased array is 0.1°.

A four element array on a single pedestal is as cost effective as a gain equivalent single aperture antenna. A four element array of 42-foot diameter

reflectors with no radome will provide a minimum CNR of 20 db with 98.7% reliability and a minimum CNR of 10 db with 99.8% reliability when the TDRS is located 60° longitude from GSFC. At 53° longitude from GSFC the reliabilities are 99.5% for 20 db CNR and 99.9% for 10 db CNR.

3.2 Recommendations For Further Study

The most attractive ground antenna configuration, the 4 element array on a single pedestal, is unconventional and a further study of its more detailed technical characteristics is required. As a minimum, the following items require further analysis.

a. Optimum feed/reflector combination. Including as alternatives the conventional Cassegrain, the near field Cassegrain and the dual shaped reflector feed systems.

b. Tracking capability including error channel slope and sensitivity.

c. Collimation of the array elements.

d. Receiver requirements for phasing and combining.

e. Mutual coupling between array elements.

f. Structural considerations of this unconventional configuration.

g. Command uplink to the TDRS from the acquisition antenna.

h. Detailed cost analysis of the entire antenna system.

Although the radome was ruled out for this application based upon current technology, improvements in water repellent surfaces in conjunction with improved surface design could significantly reduce its disadvantages. However, until experimental evidence of the improved performance is available, the use of the radome adds an unnecessary risk factor to the system.

The servo system presented in this report is sufficient to provide an acceptable total system reliability. However, digital control systems could improve serve performance and reduce wind error which is the greatest tracking problem for the system. Computer modeling and simulation of these more advanced servo techniques is desirable.

4 ANTENNA CONSIDERATIONS

The gain requirement for the TDRS ground antenna is established as 70 db in Section 9.3 of this report. However, further analysis may change that requirement and this Section will consider gains ranging from 69 to 73 db, which approaches the gain limitation imposed by reflector surface tolerances. The maximum achievable gain occurs at that wavelength such that the surface tolerance [1] is

$$\sigma = \frac{\lambda}{12.6} \tag{4-1}$$

as determined from the gain diminution expression

$$-\text{db} = 684(\sigma/\lambda)^2 \tag{4-2}$$

That is, for a given surface tolerance the gain of a reflector will increase as D/λ increases until that point is reached where the incremental increase in gain is just offset by the incremental gain diminution (Eq. 4-2). This may be shown analytically by normalizing the surface tolerance with respect to the antenna diameter

$$\sigma/D = 10^{-M}$$

The gain of the reflector becomes

$$G(\text{db}) = 10 \log \eta_0 + 20 \log \pi D/\lambda - 684(10^{-M} D/\lambda)^2 \tag{4-3}$$

Setting $dG/d(D/\lambda) = 0$ yields the diameter for maximum gain

$$D/\lambda = \frac{10^M}{4\pi} \tag{4-4}$$

$$= 10^{(M-1.1)}$$

Assuming the antenna efficiency (η_0) with no surface errors is 55% the maximum gain as determined from Eqs. 4-3 and 4-4 is

$$G_{max}(db) = 20M - 19 \tag{4-5}$$

and for gains ranging from 69 to 73 db the parameter M must vary from 4.4 to 4.6 (Figures 4-1, 4-2). The parameter M is ultimately determined by thermal stresses [2] in the reflector.

4.1 Gain-Limited Antennas

The earliest quantitative analysis [3] yields a value of M = 4 (Figure 4-3 taken from Ref. [3]) which is comprised of the effects of gravity, solar heating, wind and atmospheric turbulence. [The effects of atmospheric turbulence make it almost impossible to evaluate the performance of a gain-limited antenna on a conventional test range.] However, the increasing demand for greater gain appears to have developed the technology to provide it. A literature survey of precision reflectors is given in Appendix A. The normalized surface tolerances of these examples are superimposed in Figure 4-3.

Surface tolerances may be routinely measured to 1/20,000 diameters (M = 4.3) and with additional refinement measurements of 1/40,000 diameter (M = 4.6) may be achieved. Inserting these parameters into Eq. 5 yields maximum gains of 67 and 73 db respectively. Eq. 4-3 is plotted (Figure 4-4) vs D/λ for values of $\sigma = \lambda/12.6$, $\lambda/20$, $10^{-4}D$, $10^{-4.6}D$ together with the measured gains taken

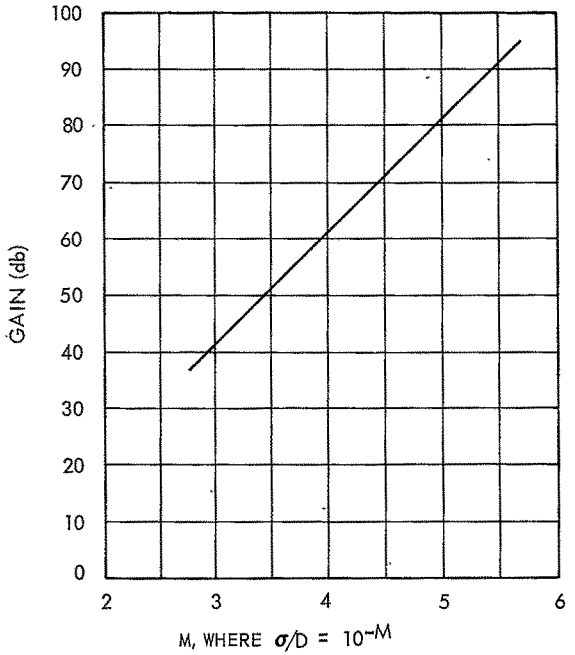

Figure 4-1. Maximum Antenna Gain vs M

from the above mentioned examples. The closeness-of-fit of the measured data with the curve M = 4.6 suggests the measurements were taken immediately after the surface adjustment was completed, however, two data points (I and J in Appendix A) are the results after several days of thermal cycling, therefore we conclude that the required gain (69-73 db) can be achieved.

4.2 Feed Configurations

Cassegrain antennas have demonstrated a superior figure-of-merit (G/T) and are widely used in communication links with synchronous satellites. The

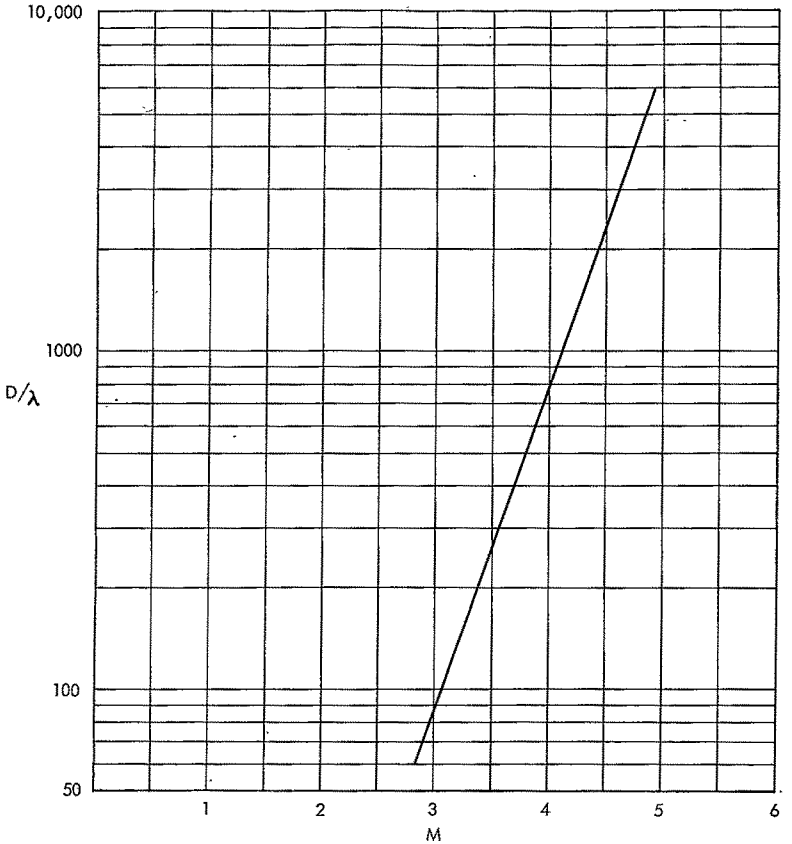

Figure 4-2. Antenna Diameter vs Normalized Surface Tolerance

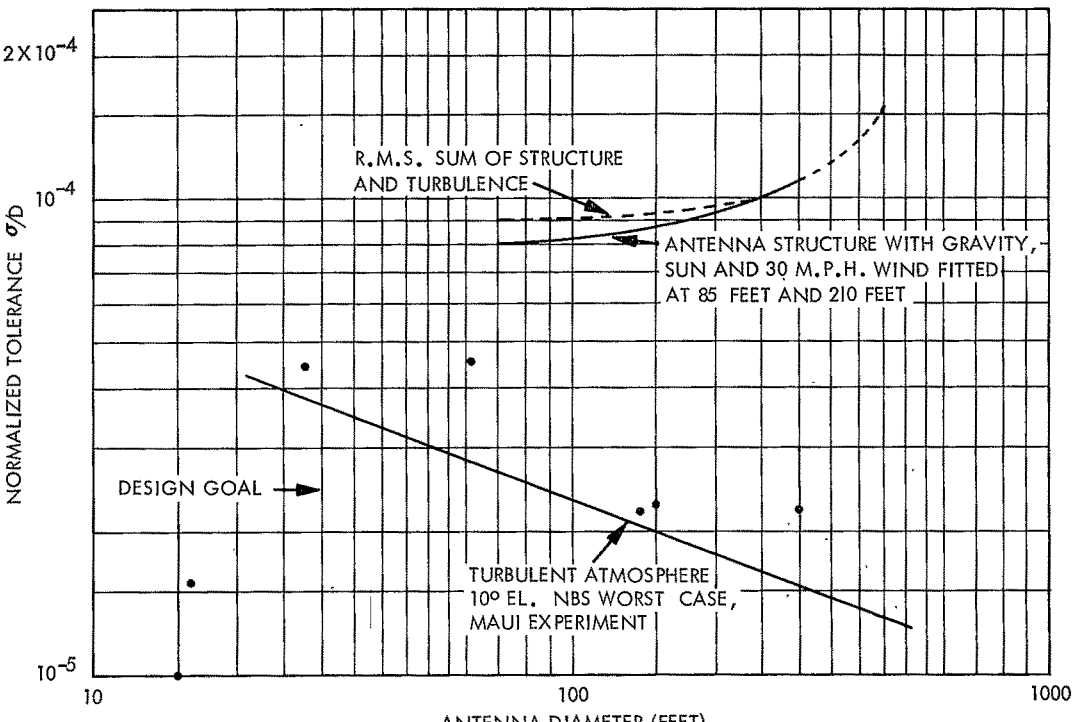

Figure 4-3. Normalized Surface Tolerance vs Antenna Diameter

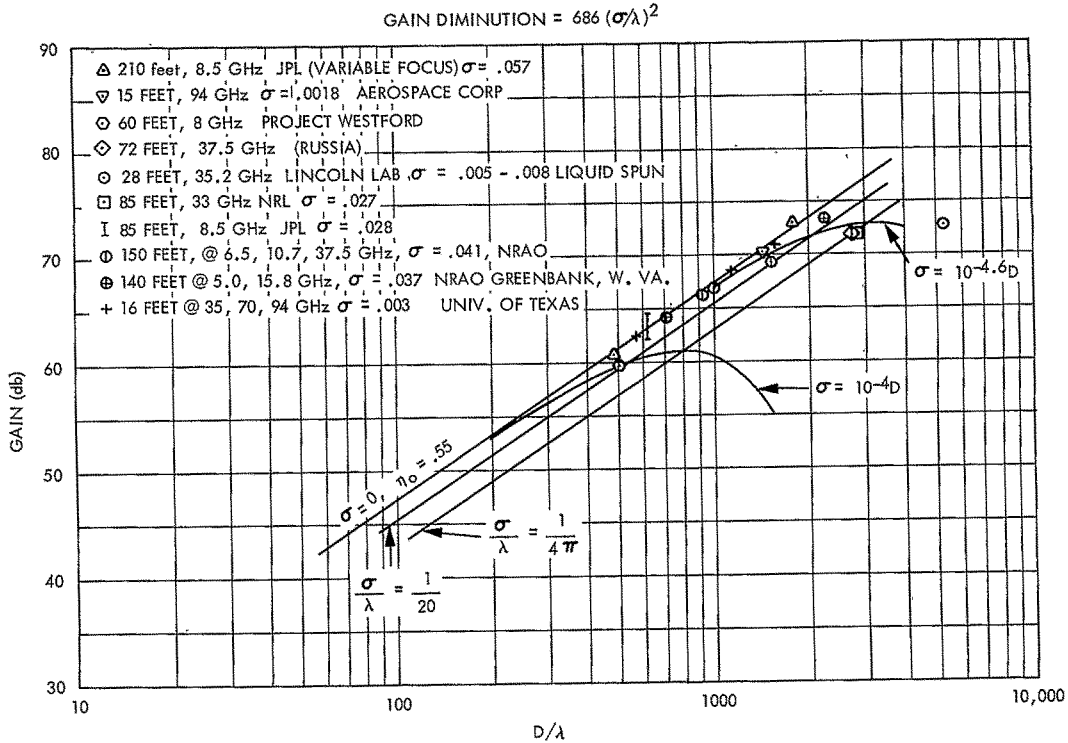

Figure 4-4. Antenna Gain vs Surface Tolerance

first configuration to be considered is the conventional Cassegrain (Figure 4-5) with a $D/\lambda = 3000$ (roughly corresponding to a gain of 73 db).

It has been shown [4] that the effects of surface tolerances is lessened in deep dishes. A suitable compromise between the diffraction effects of high incidence angles (on the subreflector) and a low value for F/D leads to the choice F/D = 0.3. Other objectives in Cassegrain design are to maintain low values of d/D and m while placing the feed as near the vertex of the main reflector as is prudent. Also, the feed horn design is made easier when the angle ϕ_0 is made large.

The Cassegrain configuration can be completely characterized by the triangle formed by the edge rays and the foci (Figure 4-6), from which we get the relationship

$$d/2 = \frac{f}{\text{Cot } \phi_0 + \text{Cot } \theta_0} \tag{4-6}$$

Introducing the additional relationships

$$\frac{\text{Tan } (\theta_0/2)}{\text{Tan } (\phi_0/2)} = m \text{ (magnification)} \tag{4-7}$$

$$\text{Tan } (\theta_0/2) = \frac{D}{4m\mathcal{F}} \tag{4-8}$$

we get, after some algebra,

$$\frac{f}{\mathcal{F}} = \frac{d}{D}(m + 1)\left[1 - \frac{1}{m}\left(\frac{D}{4\mathcal{F}}\right)^2\right] \tag{4-9}$$

Setting $f/\mathcal{F} = 1$ and $\mathcal{F}/D = .3$ yields

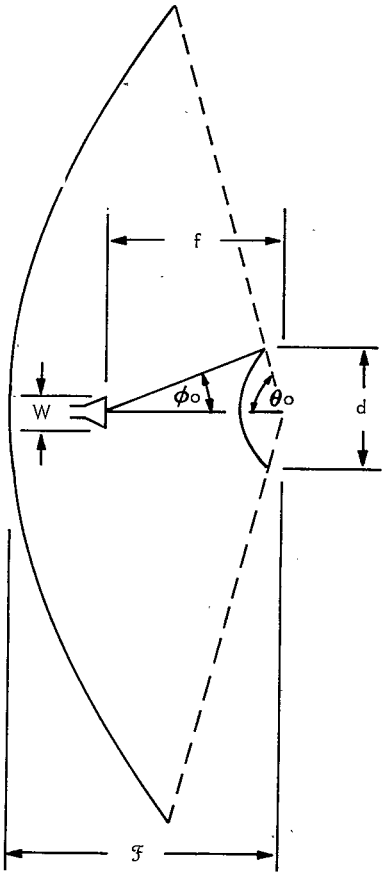

Figure 4-5. Cassegrain Antenna Geometry

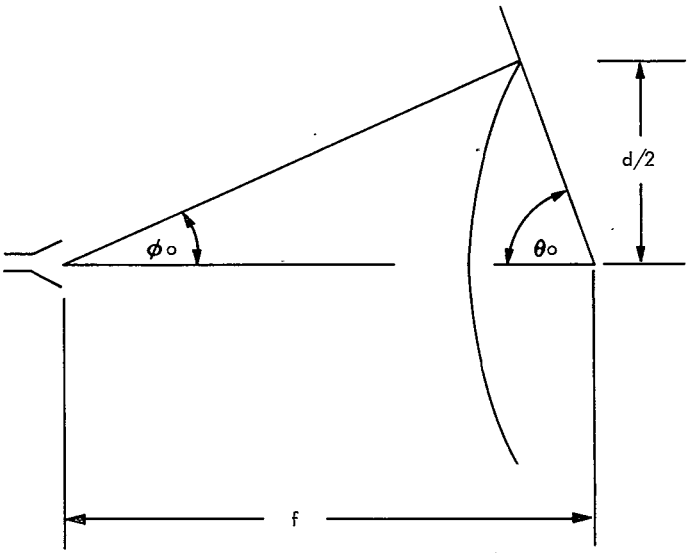

Figure 4-6. Cassegrain Feed Geometry

$$\frac{D}{d} m = m^2 + .307 m - .693$$

or approximately

$$m = \frac{D}{d} \tag{4-10}$$

A study of noise temperatures of Cassegrain antennas [5] indicates the figure-of-merit is optimum when the subreflector edge illumination is -14 db. This requires the feed horn to satisfy the relationship

$$W/\lambda \, \mathrm{Sin} \, \phi_0 = 1.2$$

or

$$\phi_0 \sim \frac{1.2\lambda}{W} \tag{4-11}$$

Combining Eqs. 4-7, 4-8 and 4-11 yields

$$\frac{1.2\lambda}{W} = \frac{D}{2m\mathcal{F}} \tag{4-12}$$

Introducing Eq. 4-10 into Eq. 4-12 yields

$$\frac{1.2\lambda}{W} = \frac{d}{2\mathcal{F}} \tag{4-13}$$

Next we impose the far-field spacing criterion of the feed horn, i.e.,

$$2W^2/\lambda = f \tag{4-14}$$

or

$$2W\left(\frac{2.4\mathcal{F}}{d}\right) = f$$

whence

$$W = \frac{d}{4.8} \tag{4-15}$$

Inserting Eq. (4-15) into Eq. 4-13 yields

$$d = 3.4\sqrt{\lambda\mathcal{F}} \tag{4-16}$$

With $\mathcal{F}/D = 0.3$ and $D = 3000\lambda$ we get $d = 102\lambda$, $d/D = 0.034$, $m = 29.2$ and $W/\lambda = 21.2$. The high values of m and W/λ make feed designs very difficult. When $D = 1500\lambda$ the parameters are: $d = 72\lambda$, $d/D = .048$, $m = 20.2$ and $W/\lambda = 15$.

In conventional feed horn design the phase error across the aperture is not permitted to exceed $\lambda/16$ which determines the relationship between the length of the horn and the aperture width viz

$$L/\lambda = 2(W/\lambda)^2 \tag{4-17}$$

i.e., the length of the horn throat is equal to the far-field spacing of the feed. With W/λ = 15-20 this distance becomes appreciable and it becomes desirable to permit the feed horn to be placed nearer the subreflector.

With an $\mathcal{F}/D = 0.3$ the dish is very deep and the feed horn still lies inside the dish (i.e., is shielded from the hot earth) when $f/\mathcal{F} = 0.5$ (Figure 4-7). The feed horn lies in the main reflector aperture plane when $f/F = 0.307$. Selecting the value $f/\mathcal{F} = 0.5$ and repeating the above exercise for a D/λ = 3000-1500 yields the following parameters:

D/λ	$\mathcal{F}/D$	d/D	m	W/λ	$f/\mathcal{F}$
3000	0.3	0.017	29	21.2	0.5
1500	0.3	0.034		14.7	0.5

The values of m and W/λ are not appreciably altered. In the foregoing the parameter d/D has been a dependent variable. If this parameter is to be selected independent of the other parameters we must analyze the effects of subreflector surface tolerances. These irregularities make an rms contribution to the overall phase error, therefore, in effect to render this contribution negligible we require

$$\begin{aligned} \sigma_{s.r.} &= \frac{d}{D}\sigma_{m.r.} \\ &= \frac{d}{D}\,\frac{\lambda}{12.6} \end{aligned} \tag{4-18}$$

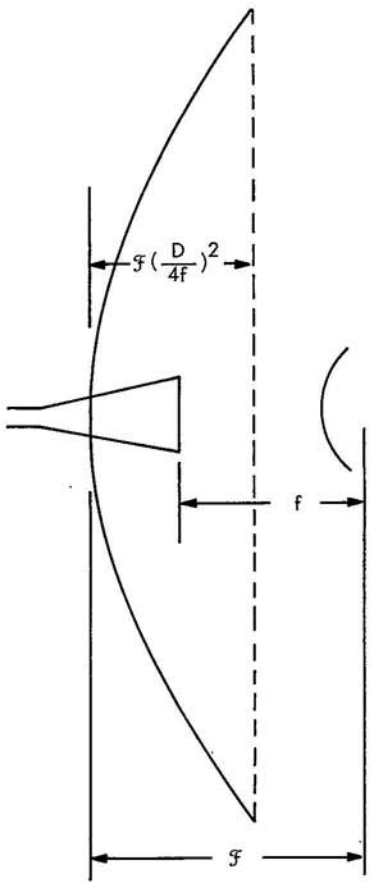

Figure 4-7. Cassegrain Geometry

since $D/\lambda = 3000$ we have $\sigma_{s.r.}/d = 10^{-4.6}$. Setting an arbitrary lower limit for $\sigma_{s.r.} \geq 0.005$ in. yields an upper bound for $d \leq 200''$ or 200λ at K_u-band. This is an equivalent upper bound of $d/D = 0.066$. Eq. 4-9 yields Table 4-1.

Table 4-1

Cassegrain Antenna Design Parameters
$\mathcal{F}/D = 0.3$

	$f/\mathcal{F} = 1$		$f/\mathcal{F} = 0.5$	
d/D	m	W/λ	m	W/λ
0.04	12.3	8.85	5.62	4.05
0.05	9.85	7.1	5.36	3.86
0.06	7.7	5.65	4.04	2.94

Since aperture blockage must also be minimized the value $d/D = 0.04$ is selected for both $D/\lambda = 3000$ and $D/\lambda = 1500$ (corresponding to 73 db and 69 db gain respectively) reflector sizes. The final choice of the value for $f/\mathcal{F}$ ($0.5 \leq f/\mathcal{F} \leq 1.0$) will be decided from feed development considerations.

The configurations arrived at above require packaging of receiver components in the feed support cone and an equipment room must be attached to the reflector support structure. A configuration that would permit packaging all the equipment on the aximuth turntable would be much more convenient to service and considerable weight would be removed from the reflector support structure. Such a configuration is the near-field Cassegrain (Figure 4-8).

The subreflector is a paraboloid, with $\mathcal{F}/D$ identical to that of the main reflector, illuminated by a plane phase front emerging from the near-field feed.

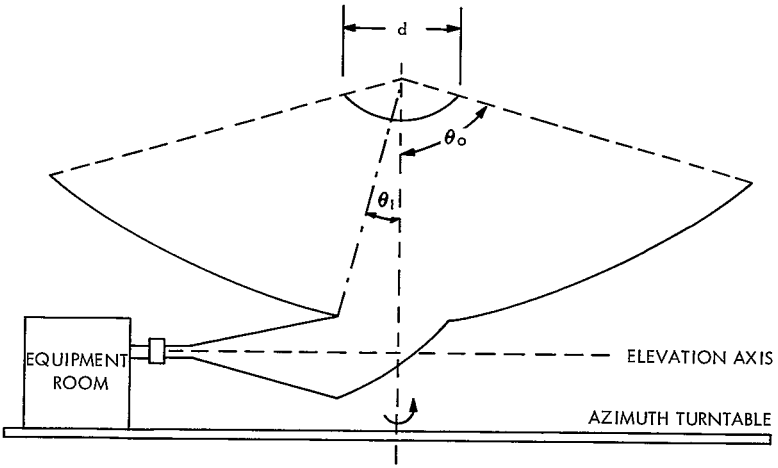

Figure 4-8. Near Field Cassegrain Antenna

The near-field feed dimension d is chosen such that $2d^2/\lambda << F$. The reflection coefficient of the feed is approximately

$$\Gamma \simeq d/D$$

Setting the near-field spacing such that

$$\mathcal{F} = 0.1\frac{d^2}{\lambda}$$

$$\frac{\mathcal{F}}{D} = 0.1\frac{d}{\lambda}\frac{d}{D}$$

then with $\mathcal{F}/D = 0.3$, $D/\lambda = 3000$ we get $d/\lambda = 95$ and $d/D = 0.0316$. With $D/\lambda = 1500$, $\mathcal{F}/D = 0.3$ we find $d/\lambda = 67$, $d/D = 0.0447$. The feed horn is a version of

the Telestar ground based antenna (Andover, Me.) which has undergone considerable development.

When operating an antenna in the gain-limited region any increase in efficiency results in a marked reduction in cost. The data of Figure 4-4 is based on an antenna efficiency of 55% resulting from conventional feed techniques. Improved feed designs and shaped reflectors [6] have resulted in an antenna efficiency of approximately 80%. This improvement is comprised of 14% improvement in feed design, i.e., a conventional feed pattern radiates 17% of the energy in sidelobes — multimode feed design [7] has suppressed these sidelobes, making available for collimation an additional 14%. The aperture illumination resulting from a conventional feed will have an edge taper of -10 db or an aperture efficiency of 88%. By shaping the contours of the subreflector and main reflector a uniform aperture distribution is obtained which is equivalent to an increase in efficiency of 12%. These techniques are amenable to listening feeds only — the tracking capability is impaired and the standard practice is to provide separate listening and tracking feeds.

Studies have been made [8] to optimize both tracking and communication functions (i.e., sum and difference patterns) with circular polarization and theoretical calculations indicate the feed horn must support 12 different modes (6 modes are required for linear polarization). Several attempts to obtain high efficiency — low noise circularly polarized feeds have been reported [9-12] which yield computed efficiencies of 70% for the sum channel and 25-35% for the difference channels. The Haystack feed [13, 14] yields an overall measured efficiency of 62% (this antenna does not use special reflector contours) which is comprised of the factors

feed efficiency	η_F	=	0.90	
aperture efficiency	η_a	=	0.80	(-15 db taper)
Subreflector				
diffraction	η_d	=	0.96	
aperture blockage	η_B	=	0.90	
Overall Efficiency	=	$\eta_F \eta_a \eta_d \eta_B$		
	=	0.62		

Use of shaped reflectors would yield an additional 12% or an overall efficiency of 74% from a multimode listening-tracking feed appears feasible.

The design of multimode feeds is a very difficult task wherein the propagation velocity and amplitude of the various modes, in a common waveguide, must be carefully controlled. In order to provide mode purity the feed horn flare can assume very large dimensions [15] hence this design should be undertaken only in the event a large single antenna element is chosen and packaging problems prevent the use of separate listening and tracking feeds.

To summarize, an antenna efficiency of 65% is attainable from separate listening and tracking feeds, 60% is available from a multimode feed that provides both listening and tracking functions, and an additional 12% may be obtained by resorting to shaped contours in the subreflector and main reflector. The costs of feed development appear to be warranted in the case of an overall gain requirement of 73 db. A gain requirement of 70 db may make multimode feed development uneconomical.

4.3 Arrays

The gain requirement can also be achieved through the use of an array of smaller aperture antennas. The array elements can be mounted on a common pedestal or can each be mounted on separate pedestals. A conceptual drawing

of the three configurations is given in Figure 4-9. The gain requirement for the identical array elements is determined from the total array gain by Eq. 4-19.

$$G_E = G_T - 10 \log N \qquad (4\text{-}19)$$

G_E = array element gain, db

G_T = total array gain, db

N = number of array elements

The size of the array elements is determined by the $\sigma/D = 10^{-4.6}$ relation. For a 73 db gain requirement ($D/\lambda = 3{,}000$) the relative size of a two and four element array versus that for a single aperture antenna is shown in Figure 4-10. The reduction in aperture area in using an array is clearly indicated in this figure.

The gain requirement for the ground antenna is established in Section 9 of this report to be 70 db. This would require a single aperture antenna of approximately 95-foot diameter with σ = 0.030 inch rms and 55% efficiency (Figure 4-4). An array of two 62-foot diameter antennas or four 42-foot diameter antennas could provide equivalent array gain. These arrangements allow for a conservative 0.7 db loss in the combining process. The combining losses are compensated by the increased efficiency available from each array element, since only listening feeds will be required. An element efficiency of 65% is considered reasonable.

The tracking requirement for the antenna has been established in Section 2 of this report. The efficiency advantages of using listening-only feeds in a high gain antenna are discussed in Section 4-4. The array of aperture antennas on a single pedestal provides a convenient tracking capability that requires only listening feeds in the array elements. The array provides phase monopulse tracking

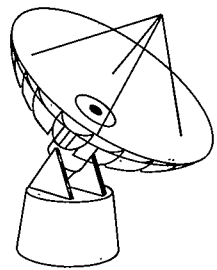

SINGLE APERTURE

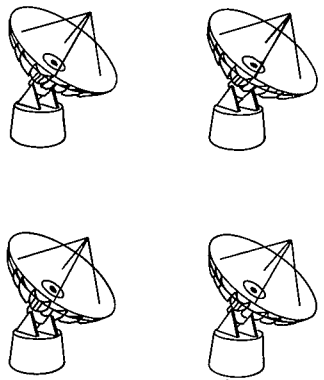

MULTI-APERTURE ARRAY
SEPARATE PEDESTALS

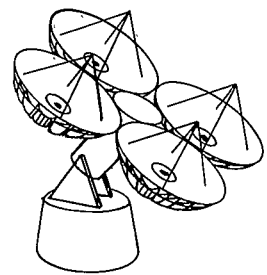

MULTI-APERTURE ARRAY
COMMON PEDESTAL

Figure 4-9. Conceptual Drawing, Antenna Configurations

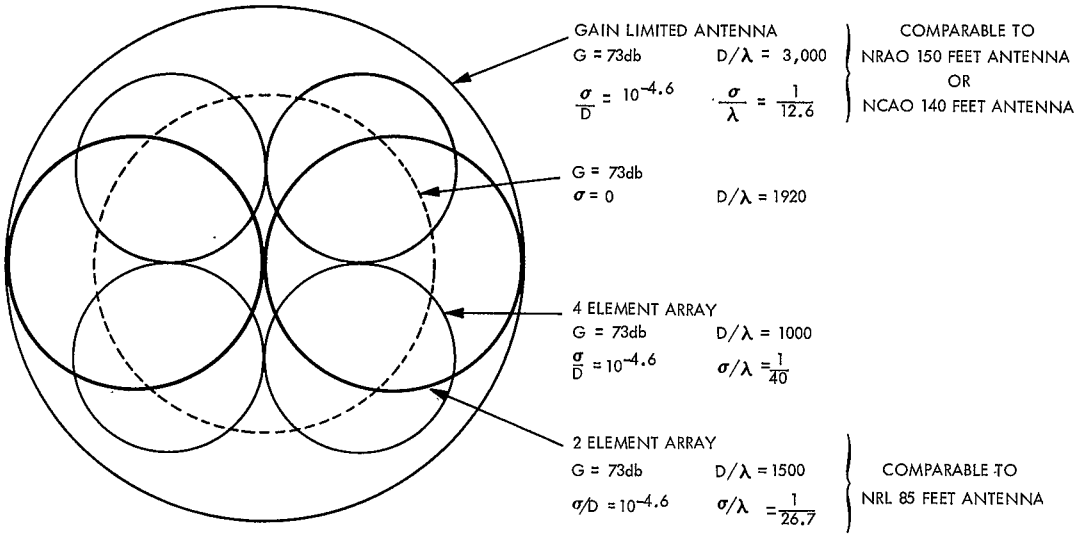

Figure 4-10. Relative Antenna Dimensions

by comparing the relative phase received at the array elements. A two element array on a single pedestal would provide only one error channel and would still require a tracking feed to provide the orthogonal error channel. The four element array can achieve the entire tracking function with any three or all four of the array elements. The four element array is therefore required to take full advantage of the multi-aperture configuration.

The phase monopulse function would be performed on a coherent pilot transmitted from the spacecraft within its 2 GHz downlink bandwidth. To obtain a 30 db CNR in this error channel, a one milliwatt spacecraft pilot and a 20 KHz tracking bandwidth in the receiver would be sufficient.

There is a second advantage in tracking with the four element array on a single pedestal. By using adaptive combining in the receiver, the array elements are phased and weighted prior to combining to provide maximum array gain. The phasing function of the receiver has the effect of electronically scanning the radiation pattern of the array so as to maintain the peak of the array pattern on the spacecraft at all times. The effect of the feature is to reduce the required servo tracking accuracy. Instead of basing the tracking accuracy on the total array beamwidth (0.04°) the tracking accuracy is now based only on the beamwidth of the array elements (0.1°). The advantages of this will be discussed in detail in Section 9-4 of this report.

The separation between array elements determines the bandwidth capability of the array as in Equation 4-20.

$$3 \text{ db Bandwidth} = \frac{c}{2S\sin(x)} \qquad (4\text{-}20)$$

c velocity of light (9.835×10^8 ft/sec)

S maximum element separation

x angle of spacecraft relative to array boresite

For 70 db total array gain using four 42 foot diameter elements on a common pedestal, the separation between diagonal elements will be 60 feet. In the case of a gain equivalent array on separate pedestals, the minimum separation between elements would be 175 feet to prevent shadowing [16] down to 15° elevation. The separation between diagonal elements would therefore be 250 feet. Using these separations, the maximum array bandwidth for a given loss is given in Table 4-2. The value of x used in Table 4-2 was 0.05°, one half the 3 db beamwidth of an array element. Based upon the bandwidth limitations of the array on separate pedestals, the array must be placed on a common pedestal to provide the required 2 GHz bandwidth. Note that the 0.05° value of x was the worst case condition. However, as discussed in Section 9.4 of this report, the local wind conditions in the vicinity of GSFC require the array to perform adequately at 0.05° from boresite.

The feasible alternatives are therefore the single aperture antenna and the 4-element array on a common pedestal. A detailed comparison of their respective

Table 4-2

Array Bandwidth Capabilities

Array Configuration	Maximum Bandwidth			
	3 db loss	2 db loss	1 db loss	0.5 db loss
4-Element Array Common Pedestal	8.8 GHz	7.33 GHz	4.88 GHz	3.66 GHz
4-Element Array Separate Pedestals	0.64	0.54	0.36	0.12

tracking reliability is discussed in Section 9.4. A cost effectiveness study of the alternatives is given in Section 10. The four element array on a single pedestal offers superior tracking capability and is as cost effective as the single aperture antenna.

REFERENCES FOR SECTION 4

1. J. Ruze. "The Effect of Aperture Errors on the Antenna Radiation Patterns", Nuove Cimento (Suppl.), Vol. 9, pp. 364-380, 1952

2. J. Robieux. "Influence of the Precision of Manufacture on the Performance of Antennas", Ann. Radio Elect., Vol. 11, pp. 29-56, Jan. 1956

3. P. D. Potter, et al. Large Antenna Apertures and Arrays for Deep Space Communications, JPL Tech Report 32-848, Nov. 1965

4. J. Ruze. "Antenna Tolerance Theory — A Review", Proc. IEEE Apr. 1966, pp. 633-640

5. Study of Gain-to-Noise-Temperature Improvement for Cassegrain Antennas, Contract No. NAS5-9845. General Electric Co., Research and Development Center, Schenectady, New York, Mar. 1967, p. 141

6. V. Galindo. "Design of Dual Reflector Antennas with Arbitrary Phase and Amplitude Distributions", P-GAP July 1964, p. 403

7. P. D. Potter. "A New Horn Antenna with Suppressed Sidelobes and Equal Beamwidths", The Microwave Journal p. 71-78, June 1963

8. P. W. Hannan. "Optimum Feeds for all Three Modes of a Monopulse Antenna, Theory and Practice", P-GAP Sept. 1961, pp. 444-461

9. P. D. Potter, A. C. Ludwig. Beamshaping by Use of Higher Order Modes in Conical Horns, Northeast Electronics Research Engineering Meeting (NEREM) Boston, Mass., Nov. 1963, p. 92

10. P. A. Jensen. A Low-Noise Multimode Cassegrain Monopulse Feed with Polarization Diversity, NEREM, Boston, Mass., Nov. 1963, p. 94

11. V. Galindo, C. Y. Pon. Control and Optimization of a Multimode Square Feed for Sum and Difference Patterns, NEREM, Boston, Mass., Nov. 1963, p. 96

12. P. Foldes, S. Komlos. A New Multimode Monopulse Feed, NEREM, Boston, Mass., Nov. 1963, p. 100

13. K. J. Keeping. Design and Construction of a Multimode Circularly-Polarized Monopulse Tracking Feed for High Power Applications in a Cassegrain Reflector System, 1965 IEEE International Convention Record, Part 5, 101.

14. K. J. Keeping, Early Test Results with the Circularly-Polarized Tracking Feed in the Haystack Antenna, NEREM Record, Nov. 1965, p. 18

15. K. Tomiyasu. A 17.5 Foot Long Multi-Conical Taper for $TE_{0,1}$ Mode at X-band, NEREM Record, Nov. 1968, p. 24

16. Investigation and Study of a Multi-Aperture Antenna System, Electronic Communications, Inc., Final Report Contract NAS5-3472, April, 1964. Prepared for the Goddard Space Flight Center, Greenbelt, Maryland.

APPENDIX A

LITERATURE SURVEY OF PRECISION REFLECTORS

A. P. D. Kalachev, A. E. Salomonovish, Radiotekhn i. Elektron, 4 (3) 1961

Dia = 22 meters

σ = 0.6 mm (M = 4.56)

Gain 72 db at 8.mm

Thermal gradients controlled with diffuse white paint. Separation introduced between reflector panels to permit expansion.

B. 28-foot Liquid Spun Reflectors for Millimeter Waves, Proc. I.R.E. June 1962, p. 1541

σ = 0.008" (M = 4.62)

G = 67.4 db @ 35.2 GHz, D/λ = 1000

$\mathcal{F}/D$ = 0.43

The authors state that sunlight on the reflector affects gain and the above data was gathered at night.

C. Radio Astronomy With the Australian 210-foot Telescope, Proc. I.R.E. Nov. 1963

σ = 5 mm (M = 4.1)

D. Project WESTFORD, Proc. I.R.E. May 1964

Dia = 60'

σ = 0.016" (M = 4.65) Measurements made at night

$\mathcal{F}/D$ = 0.3

Gain = 59.8 db (8.35 GHz)

E. The Haystack Microwave Research Facility IEEE Spectrum Feb. 1965

G. G. Weiss

Dia = 120'

σ = 0.020 (M = 4.857)

A subsequent paper "Performance Measurements of the Haystack Antenna", Inst. Elec. Engrs., Proc. June 1966, gives a surface tolerance of 0.053 (M = 4.43) and states that temperature problems proved to be significant. The antenna acts like a Hugh partition, cold below, hot above. This antenna is enclosed inside a 150-foot diameter radome. Further analysis (Feasibility Study for Re-rigging the Haystack Antenna, M. S. Zarghamee AD 651796, Feb. 1967) indicates thermal problems exist inside the radome. The most recent reference to the Haystack problem (MIT Needles Haystack for Better Performance — Microwaves, June 1968, p. 16) states that after a seven week program of computer-aided adjustment of the reflector surface the gain at 2 cm wavelength has increased 1.5 db which indicates the new rms surface tolerance is 0.042" (η = 4.53). Adjustments of 0.01" were required.

F. L. M. Keane, The AFCRL 29-Foot Millimeter Wave Antenna, AFCRL-65-726, Oct. 1965

F = 35 GHz

G = 66.4 ± 0.5 db

σ = 0.012" peak

$\mathcal{F}/D$ = 0.3

D/λ = 1050

d/D = 0.069

The reflector was painted with diffuse white paint.

G. A 16-foot Diameter Millimeter Wavelength Antenna System, Its Characteristics and Its Application, C. W. Tolbert, A. W. Straiton, L. C. Krause. P-GAP Mar. 1965, p. 225

$F = 94$ GHz

$\sigma = 0.003 \quad (M = 4.68)$

$D/\lambda = 1530$

$G = 70.9 \pm .3$ db

The antenna employs a prime focus feed with -10 db edge illumination. The antenna is enclosed in a steel astrodome which has an 18-foot shutter. Considerable difficulty was experienced in measuring patterns on the test range due to atmospheric turbulence. Reflector and support structure are made of Invar.

H. A 2.8 Arc-min. Beamwidth Antenna: Lunar Eclipse Observations at 3.2 mm. H. E. King, E. Jacobs, J. M. Stacey, PGAP Jan. 1966, p. 82

Dia = 15 ft.

$\sigma = 0.0018$ at zenith, 0.0031 at $60°$

$\mathcal{F}/D = 0.3$

$d/D = 0.066$

$G = 70.33 \pm 0.44$ db at 94 GHz

$\eta_0 = 53.6\%$

The reflecting surface was painted with diffuse white paint (thickness = 0.001 ± 0.00025"). The temperature difference between the surface and ambient was less than 8°F. The temperature rise when looking at the sun was less than 20°F. The reflector is fed with a diagonal horn feed that provides -13.2 db edge illumination.

I. M. M. Small. The New 140-foot Radio Telescope. Sky and Telescope, Nov. 1965

σ = 0.037" (M = 4.65)

Gain = 75 db at 15.8 GHz

D/λ = 2710

Design studies began in the fall of 1955. Construction began August 1957 completed Feb. 1965.

J. Construction and Performance of the 150-foot NRC Antenna at Algonquin Radio Observatory, Ontario, Canada. M. H. Jeffery. Structures Technolc for Large Radio and Radar Telescope Systems. MIT Press 1967

σ = 0.040 in (M = 4.65)

G = 70.5 db at 10.7 GHz

D/λ = 1635

After initial adjustment (at night) of the reflector surface to 0.025" errors of 0.35" were found the following day. The surface was adjusted 4 times t reach a value of 0.028" for the surface. Additional errors of 0.023" fabri tion, backup structure of 0.028", and gravity deflection 0.020" yields the overall rms value cited above.

5 STRUCTURAL CONSIDERATIONS

5.1 Mechanical Characteristics of Structure

It is difficult to discuss structural considerations without having a specific design approach in mind. However, certain general design characteristics can be established which are necessary in meeting the requirements for this application. Since various approaches are possible, emphasis will be placed in the discussion on a single 95-foot reflector and a gain equivalent quadruple arrangement of four 42-foot reflectors. The latter approach is unconventional and very little data exists of an empirical nature to characterize this antenna; hence, characteristics of a 95-foot antenna will be used where applicable. (The USSR has built a multiple-dish antenna for tracking its Venus 4 Lander. This antenna consists of eight 52-foot reflectors.)

Structural characteristics vary considerably between an antenna that is enclosed in a radome and an antenna that is exposed to the environment. Some of the structural advantages of a radome protected antenna are listed below:

(1) The antenna need not be designed to survive high winds. As a consequence, a lighter structure results.

(2) The antenna need not be designed to carry snow loads.

(3) Temperature control inside the radome reduces thermal distortions of the antenna.

(4) The antenna is subjected to gravity force only. This force is predictable and methods of compensation can be implemented.

(5) The absence of wind loads permits the use of substantially lower horsepower drive systems.

(6) Since no correction is necessary for wind gusts, the servo bandwidth can be low, and hence the natural frequency of the structure can be low (0.5 Hz).

(7) A lighter structure combined with a smaller drive system will yield a better pointing accuracy and a smoother low speed characteristic of the antenna.

In spite of these mechanical advantages, RF considerations (Section 7) preclude the use of a radome for the TDRS requirements. For this reason, the antenna structure considerations that follow will assume an exposed antenna and the resulting system characteristics will be compared (Section 9) to those resulting from the use of a radome.

Table 5.1 identifies some of the more important characteristics of the structure that have to be met.

5.2 Pedestal Requirements

There are three common types of pedestals in use, each of these having a unique axis arrangement:

(1) Azimuth-Elevation mount

(2) X-Y mount

(3) Polar mount

All two axis pedestals have a gimbal lock zone which is in line with the major (or lower) axis of the mount. Gimbal lock occurs at zenith for the azimuth-elevation mount, at the horizon for the X-Y mount and at the celestial north pole for the polar mount. However, gimbal lock is not a consideration in this application since operation is anticipated between 15° and 45° elevation. Since the satellite to be tracked has a synchronous orbit, dynamic considerations of the

Table 5.1

Mechanical Characteristics of Structure

Approach	Single Reflector	Quadruple Reflector
Diameter of Reflector	95 ft.	45 ft.
Surface Accuracy	0.030" rms	0.013" rms
Desired Pointing Accuracy	0.005°	0.009°
Natural Frequency	3.55 Hz	
Hemispherical Coverage, azimuth	0 - 360°	
elevation	0 - 90°	
Axis Rates, velocity	0 - 0.1°/sec	
acceleration	0 - 0.1°/sec^2	
Windloading, operation	0 - 30 mph	
operation, reduced acc'y	30 - 45 mph	
drive to stow	45 - 60 mph	
survival, stowed	60 - 120 mph	
Snow load depth	24 inches	
Ice load depth	1 inch	

pedestal are practically nonexistent and hence, the choice of a mount can be based almost exclusively on mechanical considerations. The azimuth-elevation mount offers several advantages over the other two mounts. Some of these advantages are compactness, low inertia and lighter structure.

Servo considerations establish the lowest natural frequency the pedestal must have in order to meet tracking accuracy during wind gusts. Without having

a specific design in mind, it is very difficult to estimate this frequency. Use can be made of data available from existing pedestals; by plotting natural frequency vs dish diameter, an empirical curve can be drawn. This curve is shown in Figure 5-1 and has been based on data from several antennas. Using this curve, it seems that a natural frequency of 3.55 cps is realizable for a 95-foot dish.

As will be shown in the servo section of this study (Section 8), pedestal friction is a prime consideration for pointing accuracy and low speed performance of the antenna. Hence low friction is an essential requirement for this application. Similar to the natural frequency case, an empirical curve can be drawn for friction in mounts with conventional (roller) bearings. This curve is given in Figure 5-2. The friction for a 95-foot antenna is 8.4×10^4 foot-pounds. As is shown in the servo section, this amount of friction is in excess of the amount permissible and, consequently, the use of hydrostatic bearings becomes mandatory. Hydrostatic bearings increase cost and decrease reliability of the system.

5.3 Drive System and Gearing Considerations

Satellite dynamics as seen from the antenna indicate maximum axis rates of 0.0002°/sec (Section 8.1), which is an order of magnitude smaller than sidereal rate (0.00417°/sec.). To make optimum use of the dynamic range of the drive system requires that the maximum rate of the antenna be 0.0002°/sec. Using a 300 rpm motor, a gear ratio (motor to antenna axis) of 10^7:1 is required. This ratio is impractical and, in addition, antenna slewing would be extremely slow. A more practical approach would be to set the maximum antenna velocity at 0.1°/sec. Since the dynamic range (ratio of maximum velocity to minimum smooth velocity) of a good drive system is about 1000:1, smooth tracking at least at the maximum target rates will be assured. The gear ratio for this condition is about 20,000:1

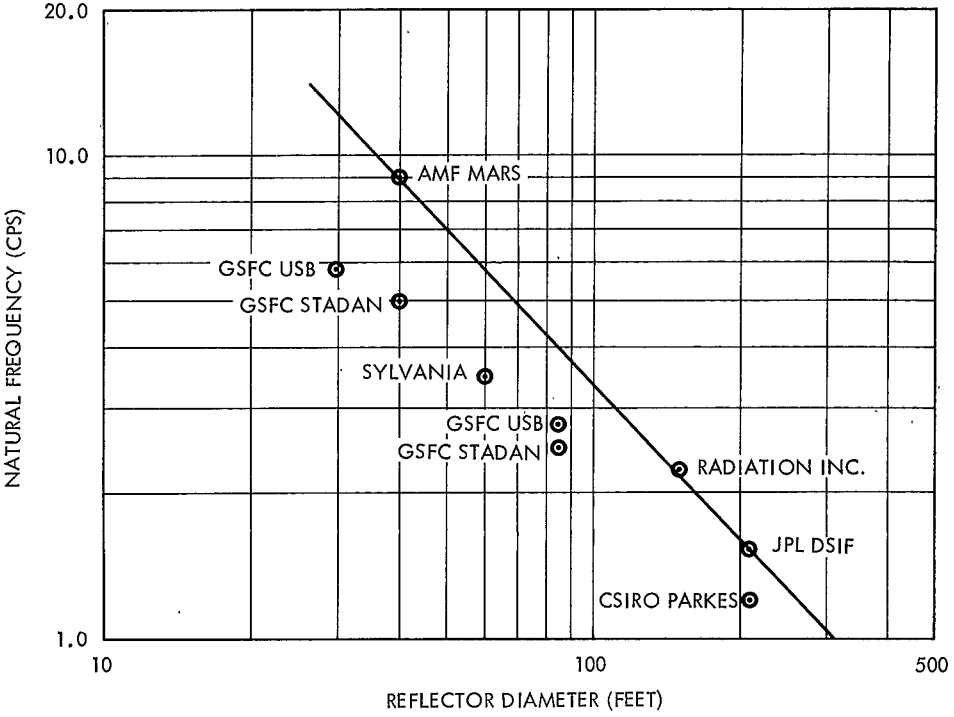

Figure 5-1. Natural Frequency of Antenna Structure vs Reflector Size

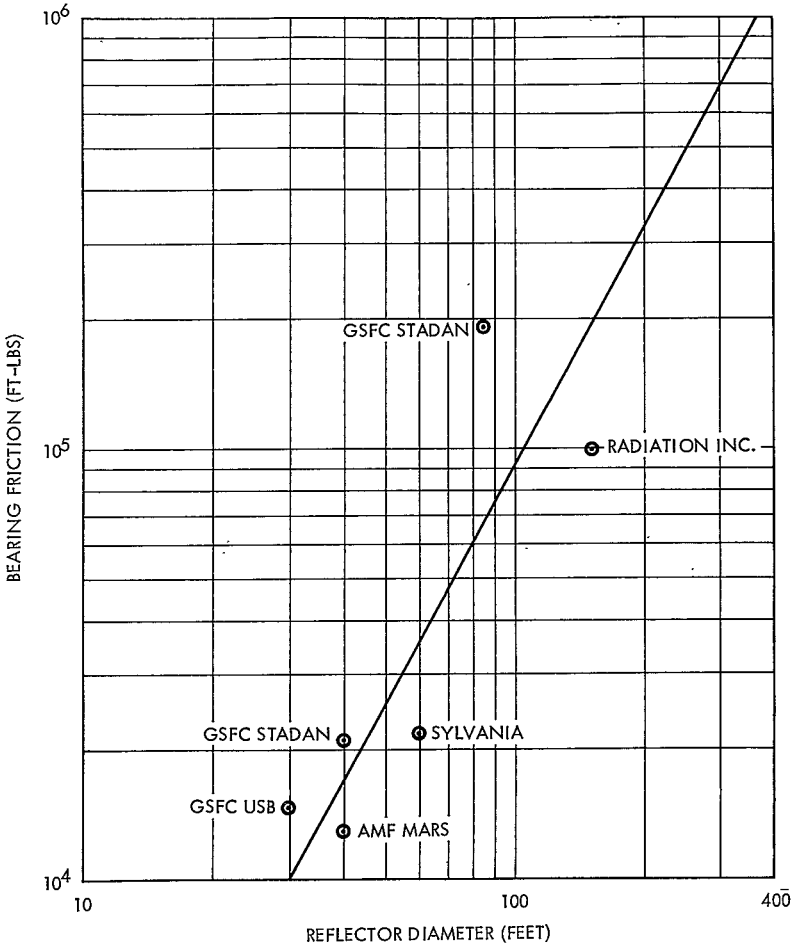

Figure 5-2. Roller Bearing Friction vs Reflector Size

which is feasible. Slewing is still slow. It will take, for example, 30 minutes to move the antenna 180° in azimuth. However, slewing rates can be increased by adding a clutching arrangement that would bypass portions of the gear train.

In order to establish the horsepower rating of the drive system, wind torque and inertia torque have to be estimated. Here again, empirical data is used to establish wind coefficients and antenna inertia for a 95-foot dish antenna. Figures 5-3 and 5-4 show these quantities vs reflector size. The wind torque is computed as

$$T_w = k_w V_0^2 = 670(30)^2 = 6.03 \times 10^5 \text{ foot-pounds}$$

where

T_w = wind torque, ft.-lbs.

k_w = wind coefficient, ft. - lbs./(mph)^2

V_0 = average wind velocity, mph

The acceleration torque is computed as

$$T_a = \ddot{\theta}_a J_a = 0.00175 \times 2 \times 10^6 = 3.50 \times 10^3 \text{ ft.-lbs.}$$

where

T_a = acceleration torque, ft. lbs.

$\ddot{\theta}_a$ = maximum antenna acceleration, rad/sec^2

J_a = antenna inertia, slug-ft.^{2}

Having computed the above quantities, the horsepower rating of the drive system can be established using 75% gearing efficiency and 25% torque bias:

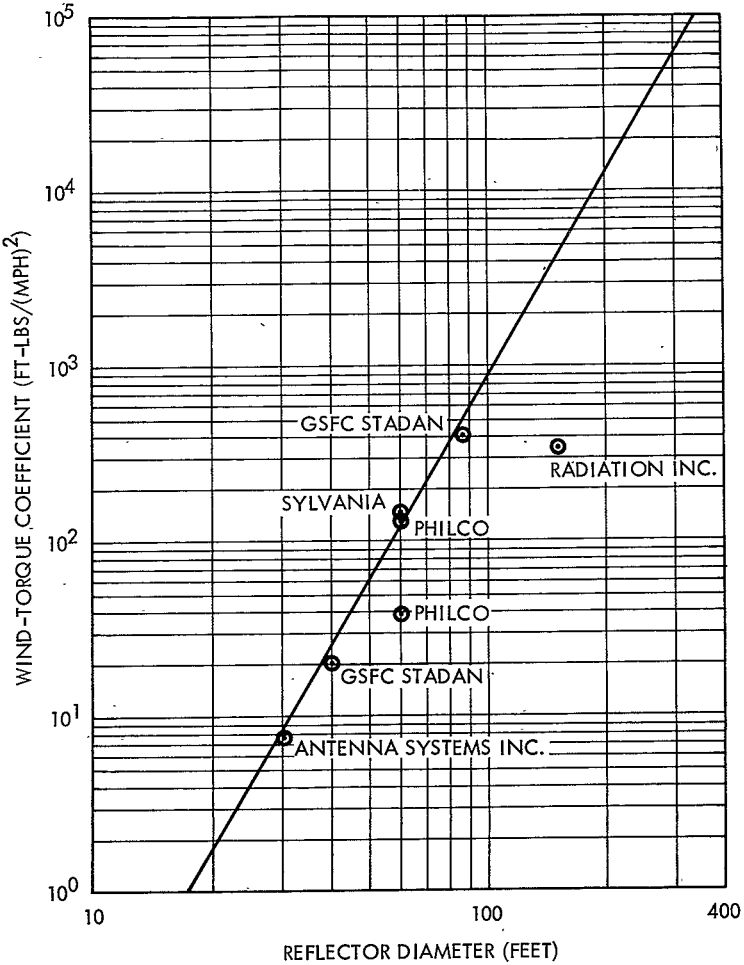

Figure 5-3. Wind-Torque Coefficient vs Reflector Size

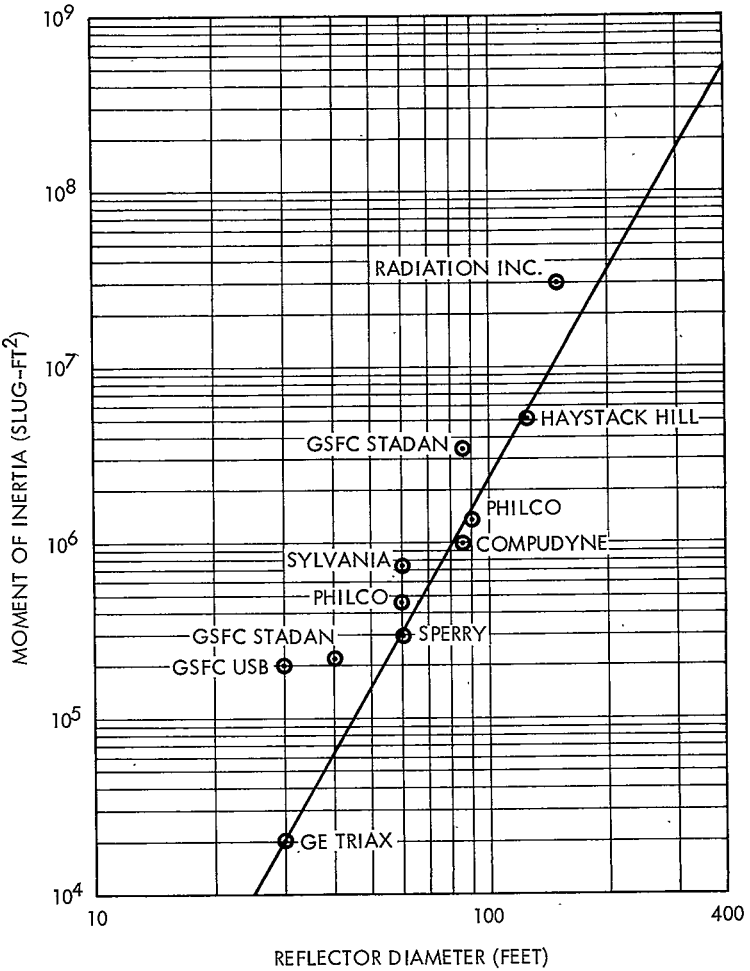

Figure 5-4. Moment of Inertia vs Reflector Size

$$P = \frac{1}{\mu_g}(1 + \mu_t)\frac{(T_a + T_w + T_f)}{5250}\dot{\theta}_a$$

$$= \frac{1}{0.75}\frac{(1 + 0.25)(3.50 \times 10^3 + 6.03 \times 10^5 + 8.4 \times 10^4)}{5250}(0.0166)$$

$$= 3.65 \text{ hp}$$

where

P = drive motor rating, hp

μ_g = efficiency of gearing

μ_t = torque bias ratio (an opposed drive system is required for elimination of backlash in gear train)

T_f = friction torque, ft.-lbs.

$\dot{\theta}_a$ = maximum antenna velocity, rpm

The drive system has to be capable of delivering 3.65 hp which is a low requirement considering the antenna size, and hence, does not pose a serious problem.

5.4 Antenna Surface Considerations

Radio frequency considerations dictate a required surface accuracy of 0.030" rms for the 95-foot reflector and 0.013" rms for the 42-foot reflector. One fundamental limitation of surface accuracy is that of measuring this accuracy. Hence, the antenna size-to-tolerance ratio becomes important. Best estimates are that standard surveying techniques using theodolites and tapes permit measurement accuracies of about one part in 20,000. Photogrammetic measuring techniques can measure to one part in 40,000 with 68% confidence and one part in 20,000 with 95% confidence. Present surveying methods using laser beams can probably improve the accuracy to one part in 100,000. Using

lasers then, the surface accuracy could be measured to 0.011" rms for the 95-foot reflector (0.0054" rms for 42-foot reflector.) Using the empirical approach, tolerances of existing antennas can be plotted vs. reflector diameter and the curves in Figure 5-5 are obtained. It is evident, that using a good structural approach a tolerance of about 0.017" rms is realizable for the 95-foot antenna (0.01" rms for the 42-foot antenna) under ideal conditions.

However, this antenna will be exposed to the environment and the surface accuracy will degrade from this ideal condition. There is little data available

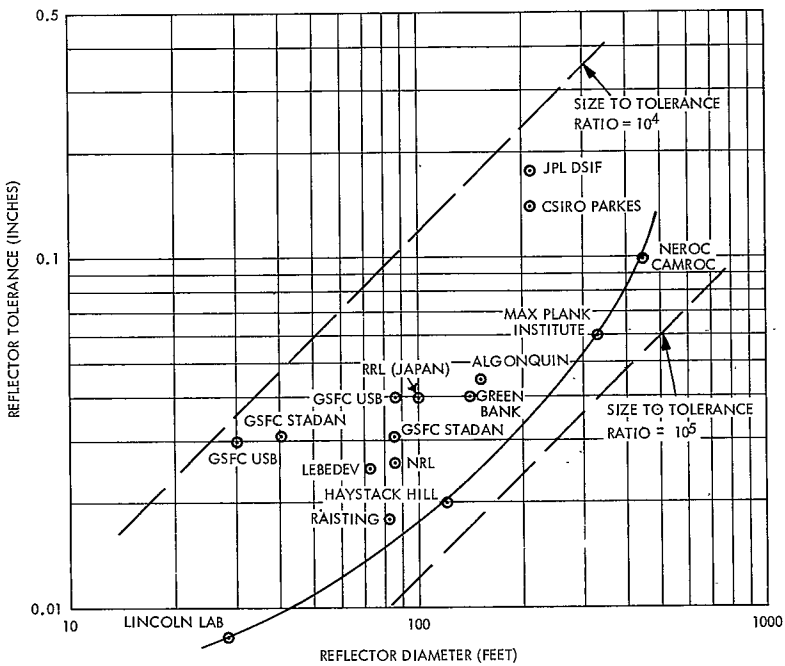

Figure 5-5. Reflector Tolerance vs Reflector Size

dealing with environmental effects on surface tolerance. The Rohr Corporation in its proposal for the Rosman II antenna (Reference 1) estimates surface accuracy to degrade with increase in wind velocity as shown in Figure 5-6. If this curve is used in a proportional manner then the 0.017" rms tolerance at zero wind velocity will increase to 0.025" rms (0.015" rms for the 42-foot array) at 30 mph. No applicable data could be found for the effects of precipitation and temperature on the surface.

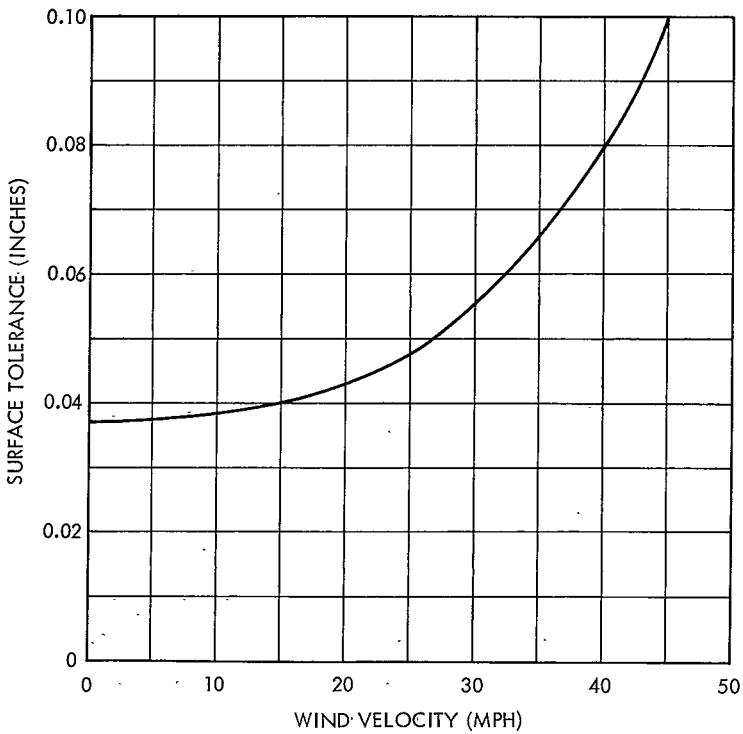

Figure 5-6. Surface Tolerance vs Wind Velocity for Rosman II Antenna

5.5 Mechanical Errors

This antenna will be used as a data acquisition terminal only and not as an angle tracking system. Hence, mechanical errors are defined as those that contribute to the difference between the radio-frequency axis of the antenna and the position of the satellite. These errors are necessarily of short duration as compared to the time constant of the servo system, since long term errors can be compensated out through systematic calibration. Mechanical errors can be classified as errors due to gravity, alignment and manufacturing tolerance, wind and thermal deflections. All of these errors except those due to wind can be either calibrated out or are of long enough duration to make their effect negligible. For wind errors, only the random component or gustiness of the wind is of concern. If the assumption is made that the variation of the wind about the mean is 25% (see Section 8.3) the effects of windgusts of 7.5 mph must be evaluated. Reference 1 gives wind errors for an 85-foot antenna at 20 mph:

Pedestal bending:	2 arc seconds
Pedestal windup:	22 arc seconds
Translation of feed Rotation of primary reflector	24 arc seconds

If these values are scaled linearly to a 95-foot antenna, corrected by the wind ratio squared and summed in a root-mean-squared fashion, a total mechanical error of 0.00047° results. The effect of feed translation on the system's RF performance must also be considered, but this analysis depends on the detailed mechanical design and is considered beyond the scope of this report.

REFERENCE FOR SECTION 5

1. Rohr Corporation: Technical Proposal for 85-Foot Diameter X-Y Mount Satellite Tracking Antenna, 1963

6 PROPAGATION

6.1 Attenuation

Gaseous water vapor and oxygen are the primary causes of attenuation in the atmosphere when no precipitation is present. The amount of attenuation is a function of the atmospheric temperature, pressure and humidity. For any given set of meteorological conditions the total atmospheric attenuation will be related to zenith attenuation (ℓ_0) and zenith angle (ϕ) by the expression

$$\ell_a = \ell_0 \cdot \sec \phi \qquad (6\text{-}1)$$

where ℓ_0 and ℓ_a are expressed in db. This expression is useful to zenith angles of 85°. The value of ℓ_0 used in the above expression is highly dependent on the atmospheric model used in its calculation. Recent millimeter communication studies [1-3] have indicated that no single model is universally recognized. A report by Altshuler [4] on earth-space communications contains two models that conservatively estimate atmospheric attenuation for the standard atmosphere and for the atmosphere with precipitation. These models are given in Figures 6-1 and 6-2.

The total atmospheric attenuation based upon these models is indicated in Figure 6-3 for several meteorological conditions. The attenuation is significantly affected by the rain cloud water density assumed, and these numbers are indicated along with rain rate in Figure 6-3.

For the TDRS ground antenna problem, the spacecraft location will be the fixed parameter and meteorological conditions the variable. Figure 6-4 expresses this relationship in a form useful for our application. The probability of occurrence for each rain rate condition is indicated on the upper part of this graph. Rain rate probabilities were calculated for the Washington, D.C. area

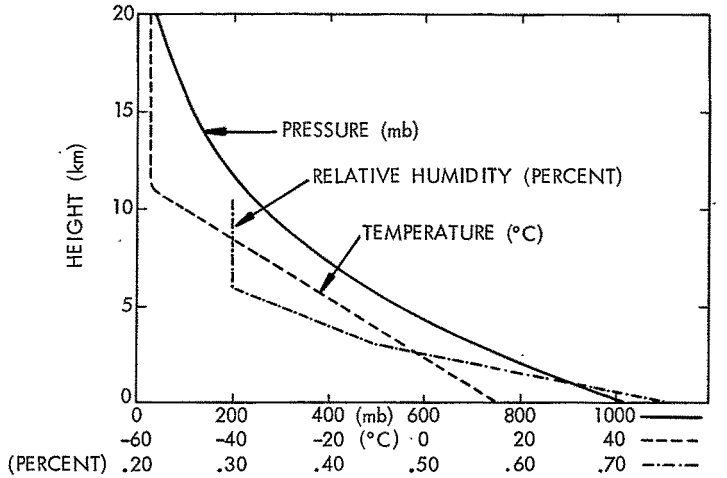

Figure 6-1. Model of Standard Atmosphere (Reference 4)

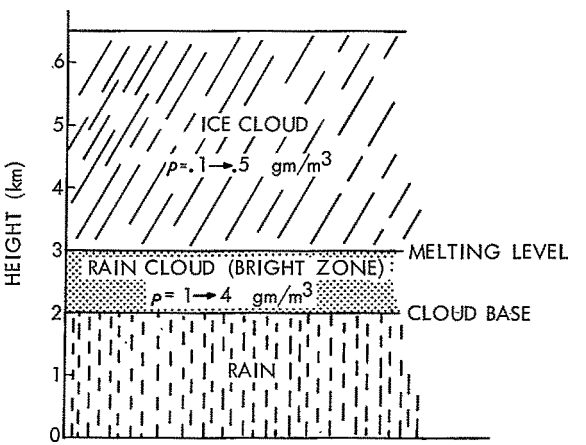

Figure 6-2. Model of Atmosphere with Precipitation (Reference 4)

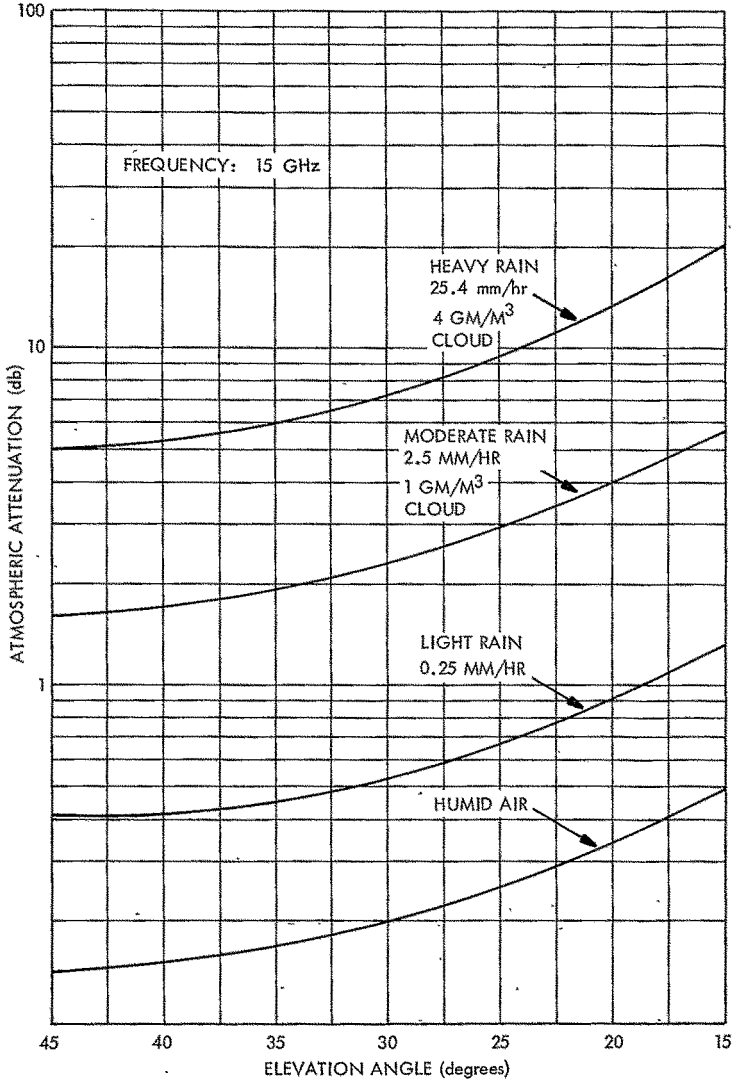

Figure 6-3. Atmospheric Attenuation for Several Meteorological Conditions (Reference 4)

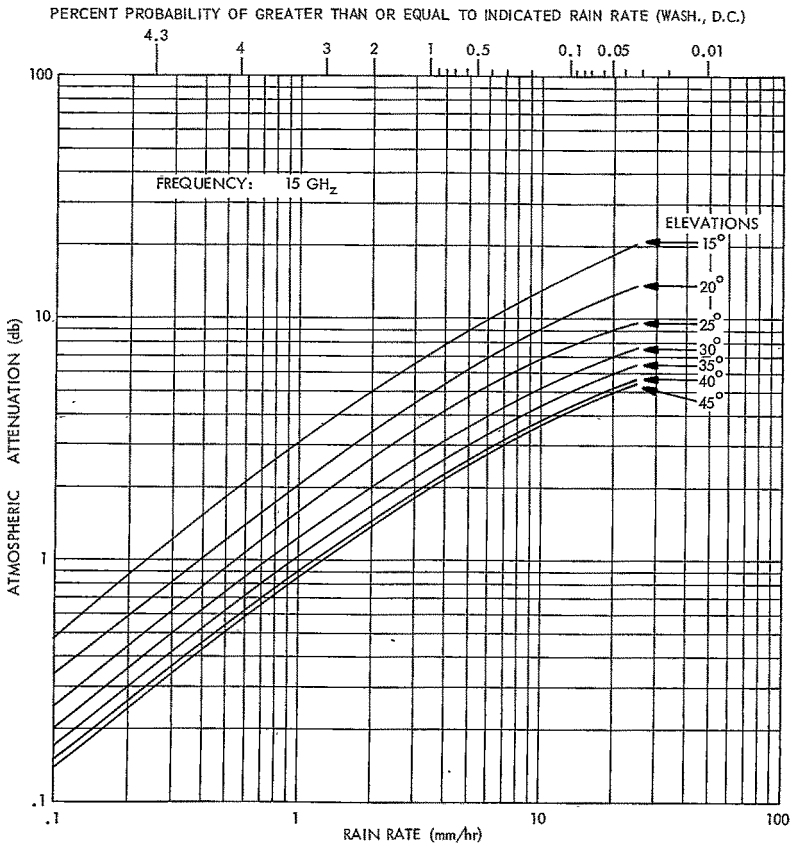

Figure 6-4. Atmospheric Attenuation vs Rain Rate

from 60-year averages published by the Weather Bureau [5]. The probability distribution of rain rates is given in Figure 6-5. Rain accumulations measured at less than one hour intervals may be of concern for some applications and curves for measurements at 1 minute, 1/2 hour and one hour intervals are indicated in Figure 6-6.

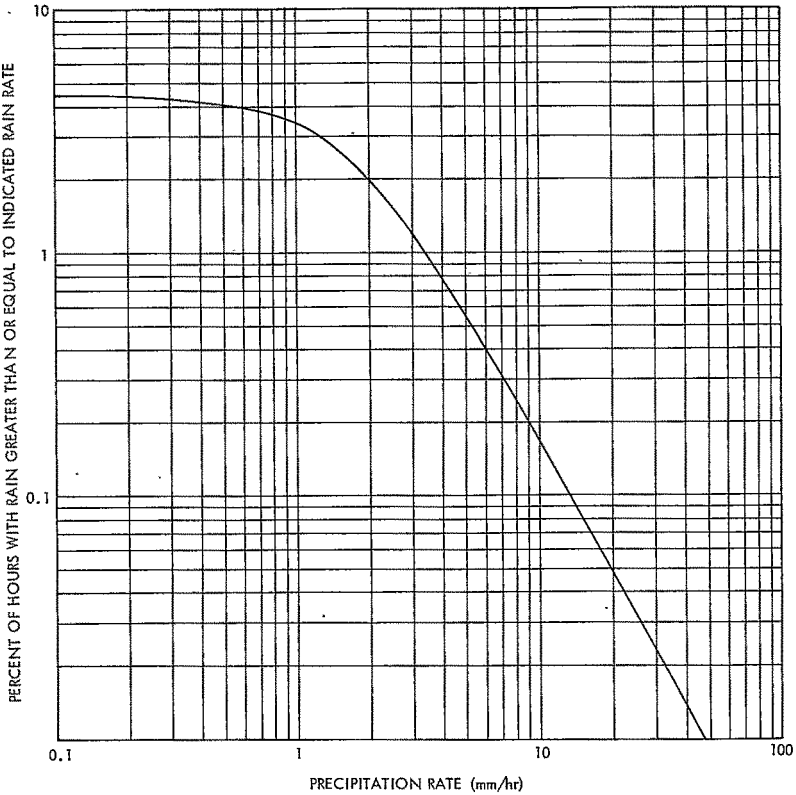

Figure 6-5. Probability Distribution of Rainfall Rates, Washington, D.C.

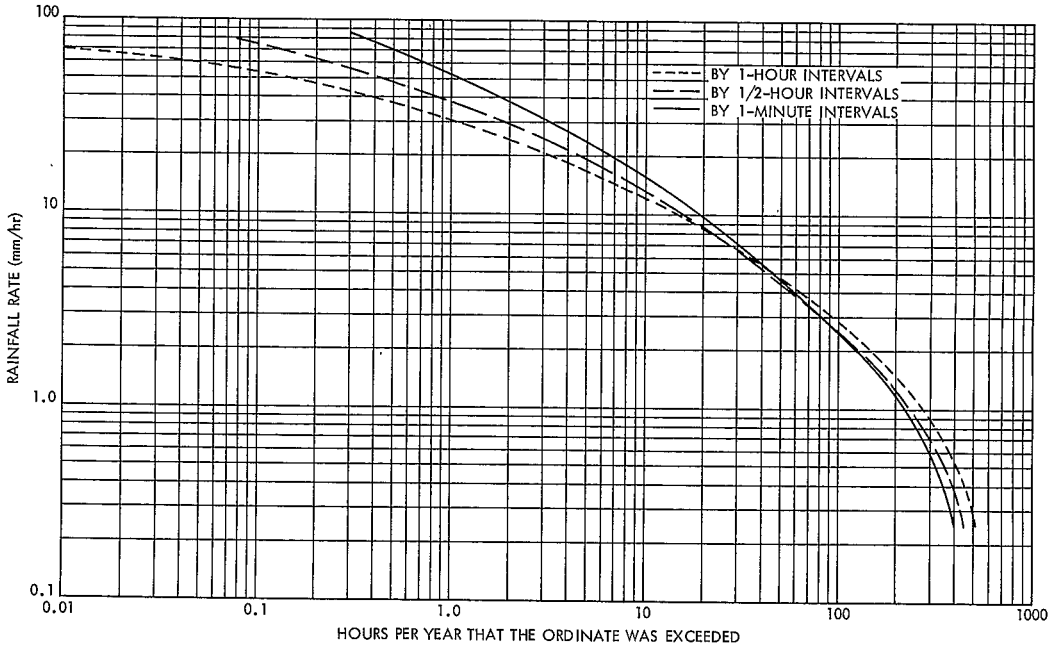

Figure 6-6. Rainfall Distribution for Washington, D.C.

The attenuation due to dry snow or hail [4] is lower than that of rain for a given liquid water content while wet snow has been found to attenuate more. The probability of significant snow attenuation compared to that of rain for the Washington, D.C. area is negligibly small and will not be considered further.

6.2 Sky Noise

With no precipitation in the propagation path, the sky temperature can be calculated from the expression

$$T_{sk} = (1 - \alpha)\, T_m \tag{6-2}$$

where α is the transmission coefficient of the atmosphere and T_m is the mean absorption temperature of the atmosphere. Assuming a horizontally stratified atmosphere, the total sky temperature will actually consist of a summation of noise temperature contributions from the several atmospheric layers proportionately reduced by the attenuation between that layer and the antenna. Thus, the sky temperature can be more accurately stated as:

$$T_{sk} = \sum_{k=1}^{n} \left[(1 - \alpha_k)\, T_m \cdot \alpha_1 \cdot \alpha_2 \cdot \ldots \cdot \alpha_{k-2} \cdot \alpha_{k-1} \right]$$

where n is the number of stratified layers and α_k is the transmission coefficient of the kth layer with $k = 1$ being the layer closest to the earth surface.

When precipitation is present in the transmission path, the need for the more rigorous sky noise temperature equation increases since rain drop density and rain cloud density are highly dependent on altitude. However, measurements have indicated that the simplified expression (Eq. 6-2) gives acceptable results.

Wulfsburg measured sky noise at 15 and 35 GHz [6] and compared them to calculated values. The calculated values used for comparison were derived from the equation

$$T_{sk}(\phi) = \left(\alpha_0^{\sec \phi}\right) T_m \qquad (6\text{-}3)$$

where

$$\alpha_0 = 1 - (T_{sk})_{zenith}$$

is a combination of Eqs. 6-1 and 6-2. α_0, the zenith transmission coefficient for meteorological conditions existing at the time of measurement, was used to determine the sky temperature $T_{sk}(\phi)$ at any zenith angle ϕ for an estimated mean absorption temperature of 260° for the atmosphere. Using Eq. 6-3 for comparison, Wulfsburg found that his measured and calculated sky noise distributions corresponded well as shown in Figure 6-7 at 35 GHz. These measurements were made in the Boston area.

Using the same expression (Eq. 6-3), the sky noise temperature was calculated based upon the attenuation curves given in Figure 6-4. The results are shown in Figure 6-8. The mean atmospheric absorption temperature was assumed 280°K in these calculations. This mean absorption temperature was chosen since we are concerned with elevation angles less than 45° for which we will expect a greater absorption temperature [7] than the 260°K used by Wulfsburg.

6.3 Solar Noise

The only significant discrete noise source for the TDRS ground antenna will be the sun. The measured solar noise temperature [8] at 15 GHz is 15,100°K.

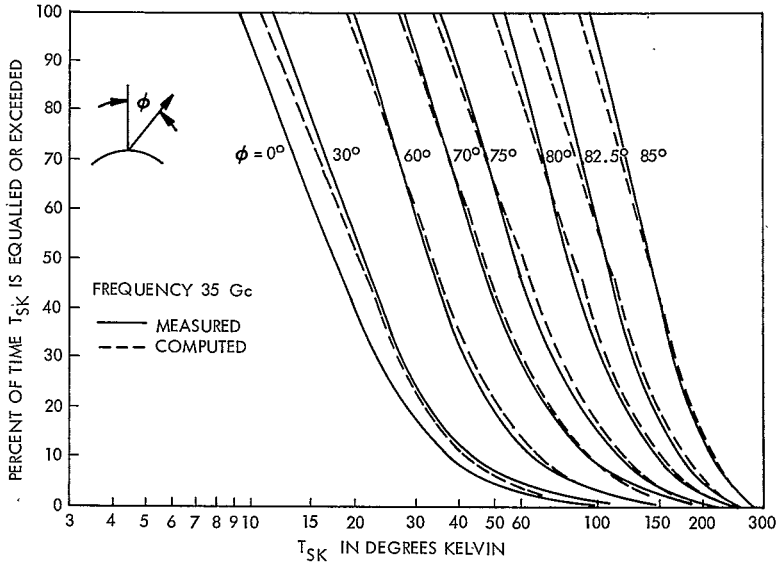

Figure 6-7. Measured and Computed Sky Temperature Distributions (Reference 6)

The sun angle as seen from earth is 0.534°. The 3 db beamwidth of the TDRS ground antenna will be approximately one-tenth of the sun angle. With a system noise temperature of 125°K for the antenna, the reduction in CNR at the ground for a TDRS eclipse of the sun will be 21 db. The appearance of the sun in side-lobes will not reduce the CNR more than 5 db and is well within our 10 db margin. An eclipse cannot be avoided for the 15 to 45° range of elevation angle for the TDRS spacecraft. Figure 6-9 indicates the envelope of the apparent solar orbit as defined by its trajectory during summer solstice and during winter solstice. The line labeled "DRS" defines the locus of positions of the TDRS spacecraft as seen from GSFC for it to remain in synchronous orbit.

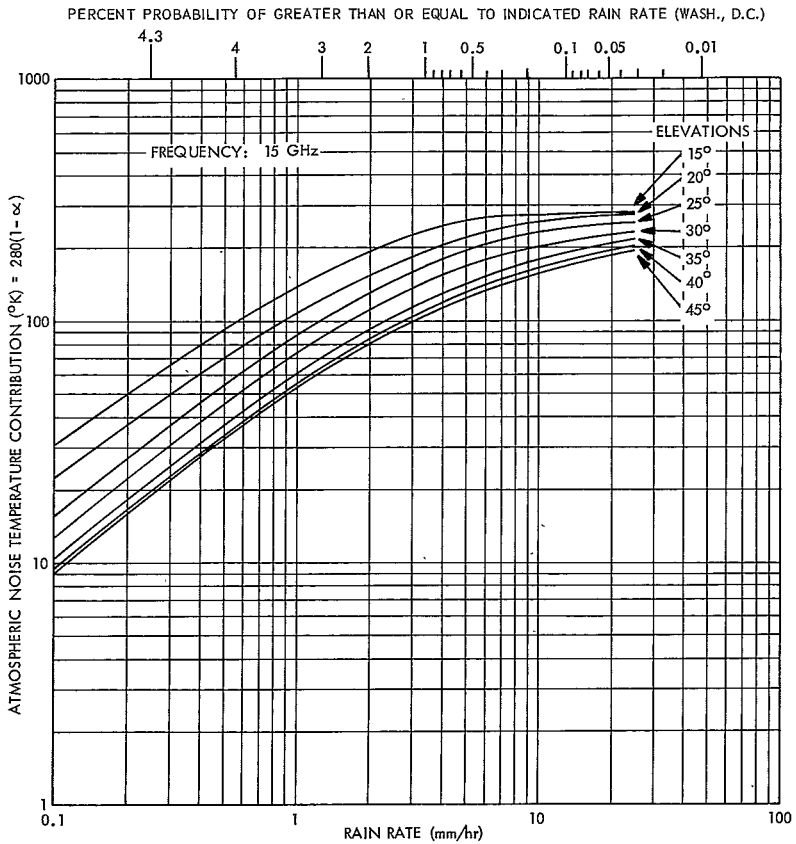

Figure 6-8. Sky Noise Temperature vs Rain Rate

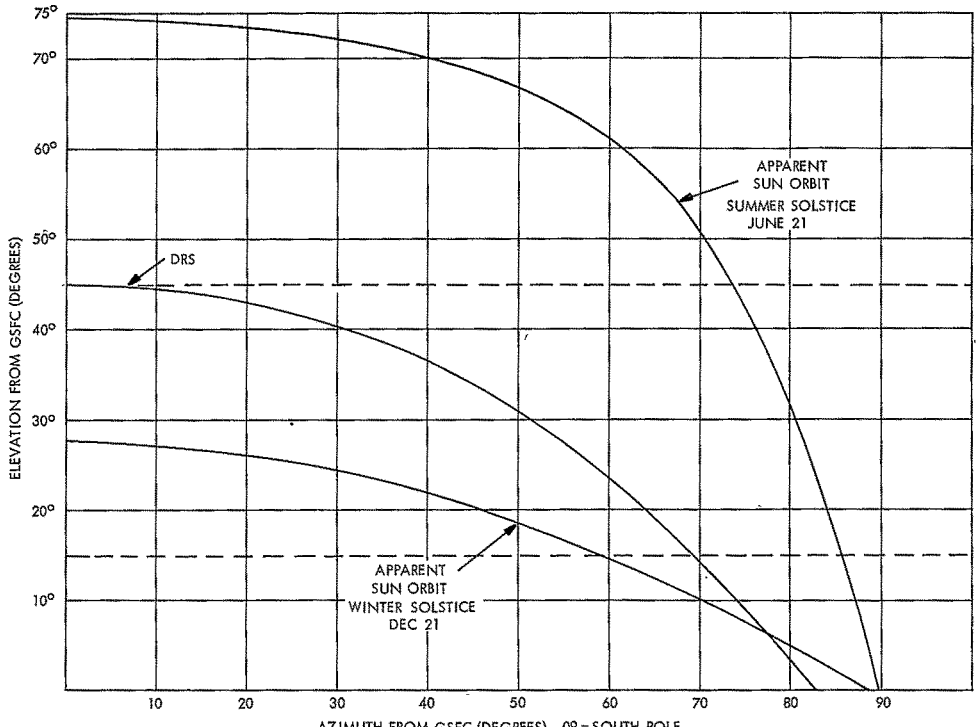

Figure 6-9. Envelope of Apparent Solar Orbit

The sun's apparent orbit will cross the locus of TDRS positions twice a year. The duration of sun jamming will be approximately two and one-half minutes per day on two consecutive days amounting to a total of 10 minutes per year. Since sun jamming is deterministic, it could be avoided by judiciously moving the TDRS spacecraft twice each year to avoid the eclipse periods. Since the duration of severe solar interference is short and since it can be avoided if necessary, the effects imposed by solar noise are not considered to be a significant limitation on the TDRS to ground communication link at K_u-band.

REFERENCES FOR SECTION 6

1. Deep Space Communication and Navigation Study, Bell Telephone Laboratories, Final Report Contract NAS 5-10293, May 1, 1968. Prepared for the Goddard Space Flight Center, Greenbelt, Md.

2. Millimeter Communication Propagation Program, Raytheon Company, Final Report Contract NAS 5-9523, Nov. 1, 1965. Prepared for the Goddard Space Flight Center, Greenbelt, Md.

3. Millimeter Communication Propagation Program Extension, Raytheon Company, Final Report Contract NAS 5-9523, February, 1967. Prepared for the Goddard Space Flight Center, Greenbelt, Md.

4. Altshuler, Edward E., Earth-to-Space Communications at Millimeter Wavelengths, Air Force Cambridge Research Laboratories report AFCRL-65-566 August 1965.

5. The Climatic Handbook for Washington, D.C., Weather Bureau Technical Paper No. 8, U.S. Department of Commerce, Jan. 1, 1949.

6. Wulfsburg, Karl N., Apparent Sky Temperatures at Millimeter — Wave Frequencies, Air Force Cambridge Research Laboratories report AFCRL-64-590, July 1964.

7. Blake, L. V., The Noise Temperature of Antennas and Receiving Systems, paper presented to IEEE PTG-AP, Washington, D.C., April 16, 1963.

8. Wulfsburg, Karl N., Solar Temperature Measurements at 15 and 35 GC, Air Force Cambridge Research Laboratories report AFCRL-65-75, February 1965.

7 RADOME

The use of a radome to protect a 95-foot diameter reflector with 0.03 inch rms (1 sigma) surface tolerance appears at first to be advantageous. This section reviews pertinent considerations and shows that the accumulated water film loss during rainfall makes a radome intolerable. It is for this reason that no Deep Space Network (DSN) antennas are fitted with radomes. On the other hand, no DSN reflectors are located in snowfall areas and so the TDRS reflector at Greenbelt, Maryland would have this unique problem. The reflector panels of a K_u-band reflector (sponsor and location classified) recently completed in Europe are treated with a teflon resin cured by a high fusing temperature. The resultant surface has an unusually high corrosion resistance and snow does not accumulate on the surface. Minimal-pressure fans are used on the reflector edge blowing toward the vertex for added insurance against snow accumulation. Thermal gradients, resulting from self-shadowing, are not a problem with DSN reflectors* because excellent reflective paints with heat scattering beads are used on the surface. It is assumed that a teflon coating could be so colored and treated.

The metal space frame radome was determined to be the most suitable type for the TDRS application. It is least expensive and easiest to erect, has longest life without deterioration, provides the least risk factor in high winds, and has lowest maintenance cost. Figure 7-1 indicates comparative cost of a radome covered reflector and an exposed reflector. It is derived from a Bell Telephone Laboratory formula as modified in Section 10 of this report. Figure 7-2 shows that the weight of a 95-foot reflector so protected could be reduced by 2.4×10^5 lbs. A 130-foot diameter radome (Figure 7-3) would enclose a 95-foot reflector;

*Private conversation with Mr. Arthur C. Ludwig of NASA/JPL

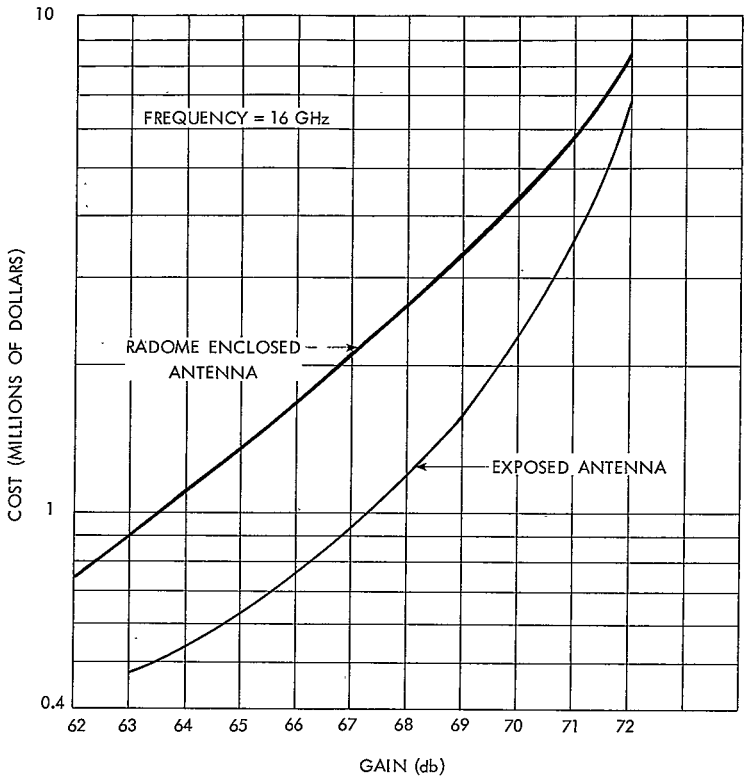

Figure 7-1. Relative Cost, Radome vs No Radome

however, as will be shown later space frame losses require greater gain and hence a larger antenna aperture diameter for equivalent performance.

7.1 Radome RF Losses

Metal space frame radome design techniques have been greatly refined since 1965 when Kay [1] discussed electrical design, and the characteristics of the

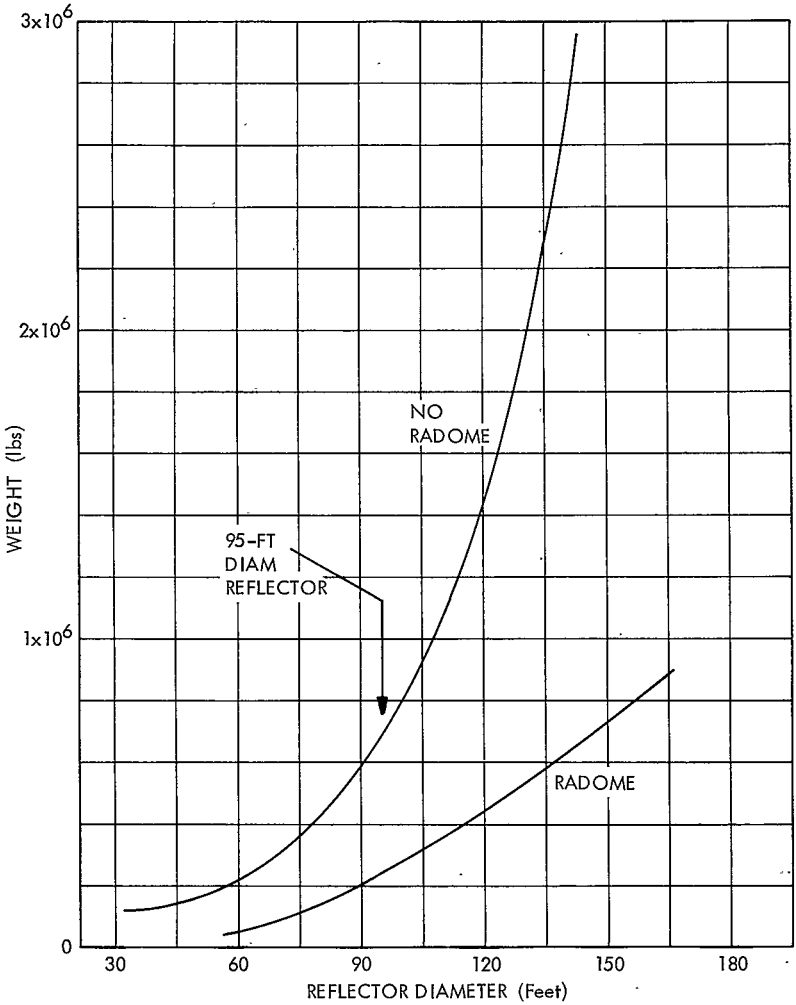

Figure 7-2. Reflector Antenna Total Weight (Reference 10)

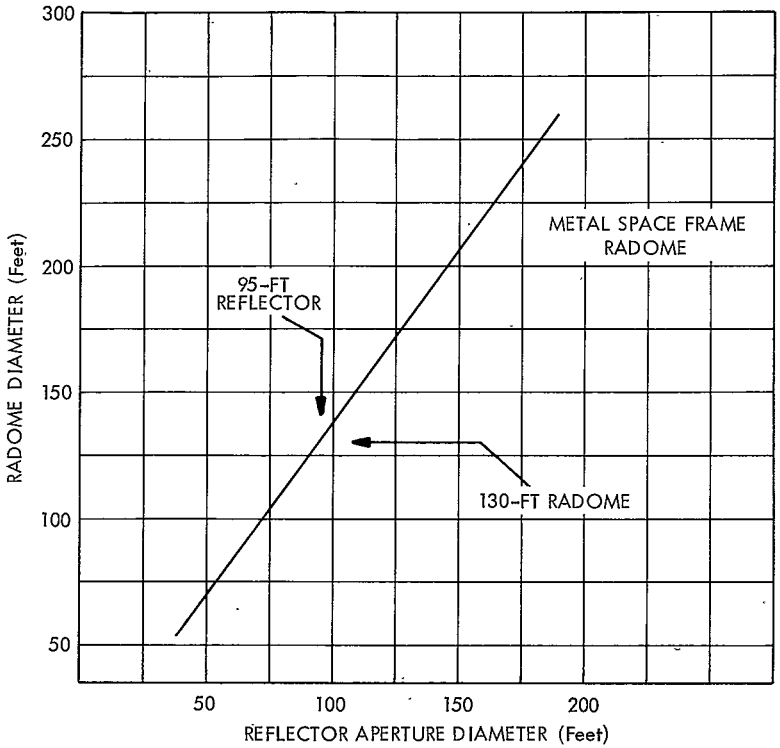

Figure 7-3. Required Size of Radome

Haystack metal space frame radome were published [2]. An Electronic Space Structures Corporation metal space frame radome (ESSCO Model M-110-86) was described [3] in 1968 providing minimal blockage and RF loss. Figure 7-4 illustrates a panel from this minimal blockage space frame radome. The equation on Figure 7-4 for computing effective blockage was developed by Ruze [4], and states that the fraction of the antenna aperture which is blocked is

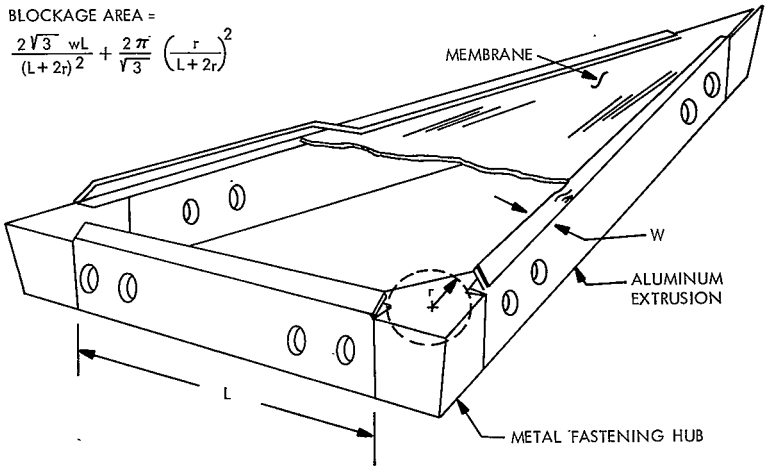

Figure 7-4. Typical Metal Spaceframe Panel ESSCO Model M-110-86

$$\eta_m + \eta_n = \frac{2\sqrt{3}\,wL}{(L + 2r)^2} + \frac{2\pi}{\sqrt{3}}\frac{(r)^2}{L + 2r} \qquad (7\text{-}1)$$

where

η_m = the membrane blockage

η_n = the hub blockage

w = frame width

L = frame side length

r = equivalent radius of hub.

The loss in axial gain due to blockage is computed by Ruze [5] by weighting and normalizing the area computed (Eq. 7-1) by the illumination taper. This computed loss is plotted in Figure 7-5 where it can be seen to be 0.38 db at 15 GHz for the modern design. Computed values are shown in Figure 7-5 to agree with measured values of blockage loss.

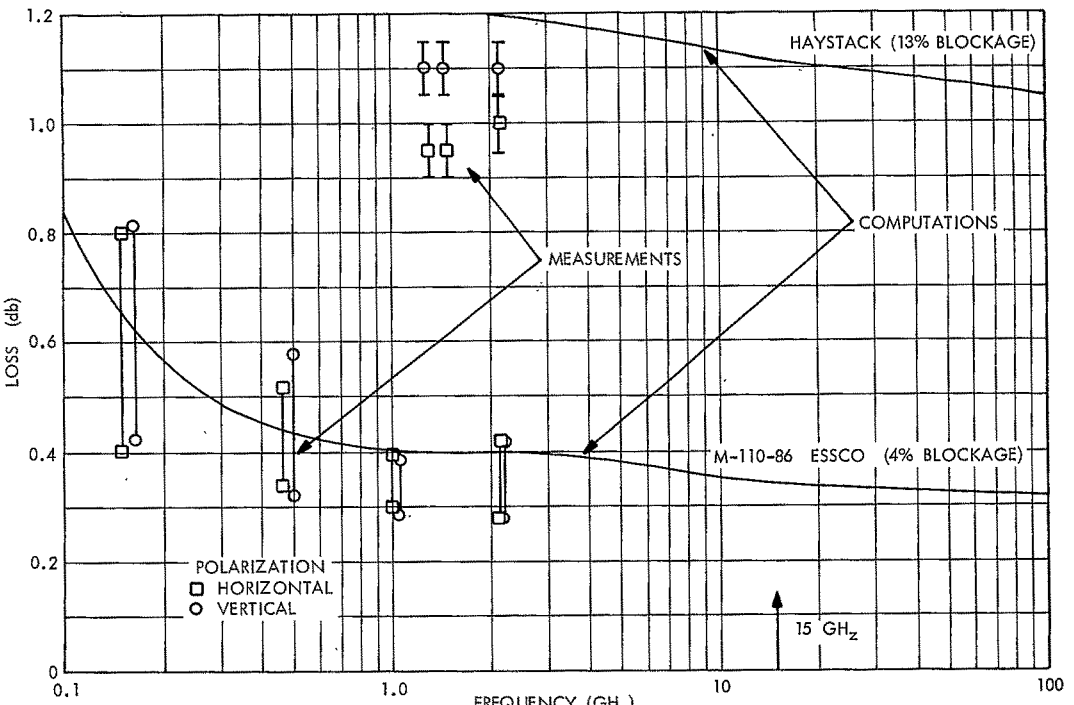

Figure 7-5. Metal Spaceframe Blockage Loss

In addition to blockage loss, two components of membrane loss must be considered: ohmic loss and reflection. The panel ohmic loss is shown by Ruze [6] to be

$$\frac{2\pi t}{\lambda} \sqrt{\epsilon} \tan \delta \tag{7-2}$$

where t = panel thickness (typically 0.050 in.), ϵ = dielectric constant (4.0 for fiberglass at 15 GHz), and tan δ = loss tangent (0.014 for fiberglass at 15 GHz). Substituting values in Eq. 7-2, the ohmic loss is determined to be only

$$\frac{2\pi\ 0.05}{0.78} \quad (4)\left[(0.014)\right] \quad = \quad 0.015 \text{ db} \tag{7-3}$$

The panel reflection loss is shown by Ruze [7] to be

$$\left(\frac{\pi\delta}{\lambda}\right)^2 (\epsilon - 1)^2 \quad = \quad 0.65 \text{ db} \tag{7-4}$$

Total loss for a dry radome is summarized in Table 7-1. The noise temperature contribution for a dry radome is dependent only on absorbed energy (ohmic losses) and is insignificant.

An additional, and far greater, loss is incurred when a radome is wet as during rainfall. Water on a radome can affect both RF transmission and the noise temperature. These effects can be reduced by using epoxy-impregnated fiberglass membranes and various mylar-tedlar coatings such as silicone or teflon. The effect of rain depends not only on the amount of water on the radome but especially on its distribution. The amount of water accumulation depends on rain rate and radome size. Water collection is proportional to the square of the radome diameter, whereas run-off is proportional only to circumference. If the run-off would be in uniform film (which it never is) the energy scattered could

Table 7-1

Total Metal Space Frame Loss (Dry)

Space Frame Blockage	0.38 db
Membrane Losses:	
Ohmic	0.015
Reflection	0.650
Astigmatism	—
Thickness Variation	—
Boresight Shift Loss	—
Total Loss	1.045 db

be said to be dependent on the square of the film thickness in wavelengths. Wat actually tends to run off in rivulets and this can be encouraged by design. Scat tered energy is proportional to the cube of the stream diameter in wavelengths Both the residual film thickness and stream diameter depend inversely on the average run-off velocity. Therefore, treating the surface and designing the sur face to increase run-off velocity and to encourage formation of small diameter rivulets lessens the electromagnetic effect.

Calculations of the effect of water are complex and measured data is sparse. Only two sets of measured data exist. Transmission loss for the Andover radome (a 0.07-inch thick air supported fabric) is 1 to 2 db for rainfall of 0.1 to 2.5 mm/hr. Noise temperature increases from 25 to 70°K for the same conditions. This data does not apply to a metal space frame radome. A 55-foot metal space frame radome was sprinkled with garden hoses at ESSCO [8] and it was found that losses

were an order of magnitude lower than those cited above for the Andover radome. However, these measurements were made using a crude simulation of rain and ESSCO has admitted the need for more representative testing of space frame radomes coated with non-wetting agents. Table 7-2 is derived from a published report [9] of the Weather Bureau. Although it was published two decades ago, it covers observations over a 60-year period and is considered to be representative of present conditions. Figure 6-5 shows rainfall rates versus percentage of occurrence. Table 7-2 and Figure 7-5 show that heavy rainfall occurs only 0.3% of the time and moderate rainfall only 1.5% of the time while 80% of the time it does not rain at all.

Table 7-2

Rainfall Rates For The Washington Area

Type	Rate in/hr	Rate mm/hr	Percentage of Time Occurred
Light	0.01	0.25	3.0%
Moderate	0.1	2.54	1.5
Heavy	1.0	25.40	0.3
Very Heavy	1.7	43.20	—
Heaviest Ever Recorded		86.90	(Sept. 12, 1934)

Rain run-off on a radome surface was described earlier as involving water film flow and water streaks or rivulets. Film flow is slow whereas rivulets reach the velocity of free-falling raindrops (typically 800 inches per second for 1.5 mm diameter drops). Film thickness is estimated [11] to be

$$t = 0.584\,[QR]^{7/12}\ \text{mils}, \qquad (7\text{-}5)$$

where R = radome radius in feet and Q = rain in millimeters per hour. This data is plotted in Figure 7-6 which shows theoretically uniform film thickness for given rates of rainfall for the size radome required. Figure 7-7 shows the transmission loss at 15 GHz for uniform film thickness accumulated by rainfall rates in this geographical region. Using Figures 7-6 and 7-7, it was possible

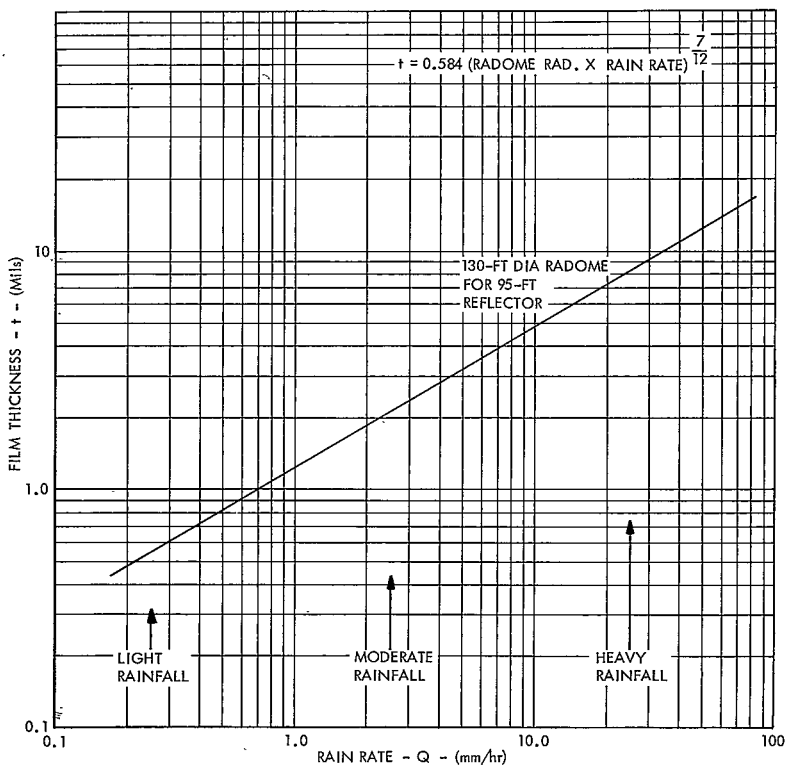

Figure 7-6. Thickness of Rain Film on Radome

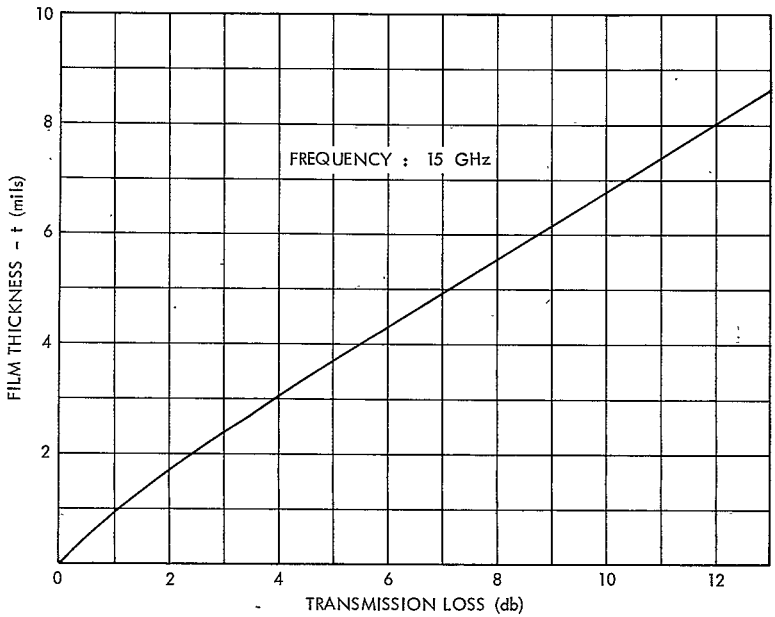

Figure 7-7. Water Film RF Loss (Reference 11).

to plot Figure 7-8 which shows the transmission loss as a result of water film thickness at 15 GHz. This curve represents a worst possible case because the situation can be improved by causing the uniform film of water to run off in rivulets instead. Hence the loss of 11 db for heavy rainfall (25.4 mm/hr) could be reduced by running the water off at high velocity. Quantative loss values are not available for this condition.

7.2 Noise Temperature Due to Radome

Noise temperature is a result of RF absorption by water on a radome. Very sparse information is available on noise temperature due to a water film on a

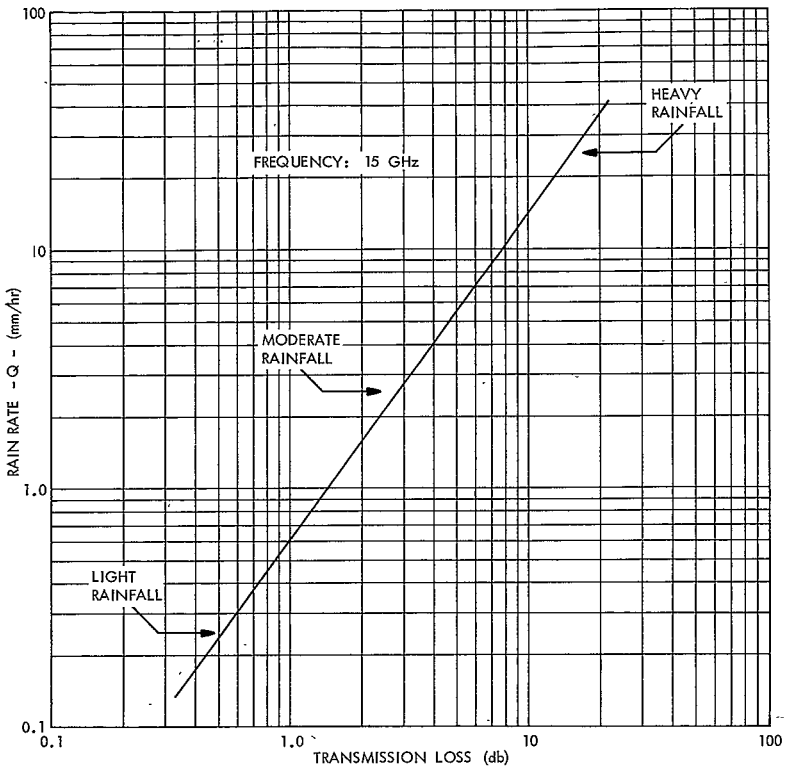

Figure 7-8. Water Film Loss for Metal Spaceframe Radome (Reference 11)

metal space frame radome. Assuming a uniformly thick film of water at a temperature of 290°K, noise temperature can be calculated from the equation $T = 290 (1 - \alpha_s)$ where α_s is the fraction of the power absorbed by the water film. This information is plotted in Figure 7-9 with the use of Figure 7-7 data showing RF absorption for various film thicknesses. It should be noted that the component of the loss in Figure 7-8 due to reflection [12] from the water film does not contribute to the noise temperature.

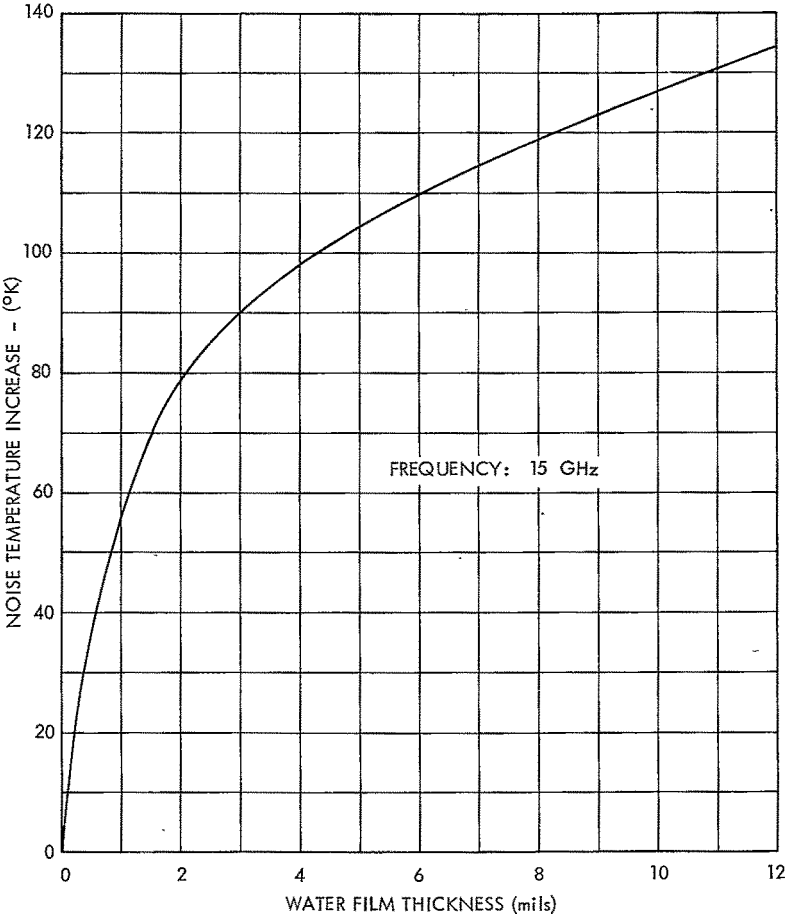

Figure 7-9. Noise Temperature Due to Water Film (Reference 11)

7.3 Feasibility of a Radome

A metal space frame radome is considered to be the best choice of a radome type; however, it is seen that use of a radome incurs a substantial performance penalty. Even if the radome gain loss were zero for a dry radome, a water film would add approximately 10 db gain loss. This loss must be added to the atmospheric attenuation in heavy rain which is shown in Figure 6-4 to be an additional 10 db at 30° elevation angle in heavy rainfall. It is concluded that the increase in attenuation and noise temperature rule out the use of a radome. Even with improvements in radome design to reduce water accumulation, a significant reduction in radome cost is required to make such systems economically feasible.

REFERENCES FOR SECTION 7

1. Alan F. Kay, "Electrical Design of Metal Space Frame Radomes", IEEE Trans AP-13, 2, March 1965, p. 190

2. H. G. Weiss, "The Haystack Microwave Research Facility", IEEE Spectrum 11: 190-192, Feb. 1965

3. Electronic Space Structures Corporation, Proposal 19.86 for 110-Foot Metal Space Frame Radome, (referenced with permission)

4. John Ruze, A Large Radio-Radar Telescope — CAMROC Design Concepts Vol. 1, Jan. 1967, p. 7-3

5. Ibid. Vol. II, p. 1-5

6. Ibid. Vol. I, p. 7-19

7. Ibid. Vol. I, p. 7-12

8. Cohm, A. and Smolski, A., "Effect of Rain on Satellite Communication Earth Terminal Rigid Radome", Microwave Journal, Vol. 9, No. 9, Sept. 1966, p. 111

9. Weather Bureau Technical Paper No. 8, Climatic Handbook for Washington, D.C., U.S. Department of Commerce, Jan. 1949

10. A Study to Evaluate the Effects of a Radome Environment on the Performance and Cost of a Large-Diameter Radio Telescope, Rohr Corporation, Oct. 21, 1966, p. A-4.

11. Ruze, CAMROC, Vol. II, p. 2-5

12. B. C. Blevis, "Losses Due to Rain on Radomes and Antenna Reflecting Surfaces," IEEE Trans. AP-13, January, 1965, p. 175.

8 CONTROL SYSTEM

8.1 Target Dynamics

In this application the target to be tracked is a synchronous satellite and its motion with respect to the antenna is of importance in the consideration of the servo system. The assumption is made that this satellite has a motion similar to that of ATS-3 and ATS-5. The pass of the satellite as seen from the antenna describes a figure eight. The time for completion of this figure eight is 24 hours. It is further assumed that this figure eight is regular and symmetrical. Based on these assumptions, antenna axis rates are established in Figure 8-1. Maximum velocity requirements are very low, 0.0002°/sec., which is an order of magnitude lower than the sidereal rate of 0.00417°/sec. However, the satellite would remain within the desired 1/10 BW pointing accuracy of 0.005° (95' diameter single aperture antenna) for only 27 seconds. Hence, the need for a tracking antenna is established.

8.2 Tracking Loop Considerations

In studying the feasibility of this antenna it is necessary to evaluate the various tracking errors in order to establish the overall system performance. Hence, it is necessary to make several assumptions to permit numerical evaluation. It will be assumed that a conventional Type II servo is used with rate feedback. The block diagram of the tracking loop (low frequency approximation) is shown in Figure 8-2. Since this antenna is exposed to the environment, it is assumed that maximum achievable servo bandwidth will be used in order to minimize wind errors. The rate and position bandwidths can be found by using a relationship from Reference 1:

APPARENT MOTION OF SATELLITE AS SEEN FROM ANTENNA:

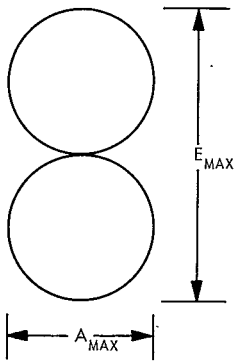

$E_{MAX} = 2.5°$

$A_{MAX} = 0.75°$

TIME OF COMPLETION OF FIGURE EIGHT IS 24 HOURS

FOR ELEVATION:

$$E = 2.5 \cos \frac{2\pi}{24} t = 2.5 \cos 0.262\, t$$

$$\dot{E} = -(2.5)(.262) \sin 0.262\, t$$

$$\dot{E}\ \text{max} = (2.5)(.262) = 0.666°/\text{hr} = 0.000185°/\text{sec}$$

$$\ddot{E} = -(2.5)(.262)^2 \cos 0.262\, t$$

$$\ddot{E}\ \text{max} = (2.5)(.262)^2 = 0.174°/\text{hr}^2 = 0.0000483°/\text{sec}^2$$

FOR AZIMUTH:

$$A = 0.75 \sin \frac{2\pi}{12} t = 0.75 \sin 0.524\, t$$

$$A = (0.75)(0.524) \cos 0.524\, t$$

$$A\ \text{max} = (6.75)(0.524) = 0.393°/\text{hr} = 0.000109°/\text{sec}$$

$$\dot{A} = -(0.75)(0.524)^2 \sin 0.524\, t$$

$$A\ \text{max} = (0.75)(0.524) = 0.206°/\text{hr} = 0.0000572°/\text{sec}^2$$

Figure 8-1. Antenna Axis Rates

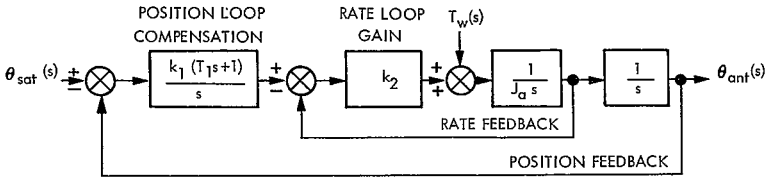

TERMINOLOGY:

θ_{sat} (s) = ANGULAR POSITION OF SATELLITE, RADIANS
θ_{ant} (s) = ANGULAR POSITION OF ANTENNA AXIS, RADIANS
Tw (s) = WIND TORQUE, FT. - LBS.
k_1 = POSITION LOOP GAIN
T_1 = POSITION LOOP TIME CONSTANT, SECONDS
k_2 = RATE LOOP GAIN
J_a = ANTENNA INERTIA, SLUG FT^2
s = LAPLACE OPERATOR

Figure 8-2. Block Diagram of Tracking Loop

$$\omega_c = \frac{\omega_r}{3} = \frac{\omega_n}{6} \tag{8-1}$$

where

ω_c = position loop bandwidth, rad/sec

ω_r = rate loop bandwidth, rad/sec

ω_n = lowest structural resonance, rad/sec

With the aid of this relationship the gains k_1 and k_2 and the time constant T_1 can be evaluated. For the rate loop:

$$\omega_r = \frac{\omega_n}{2} = \frac{k_a}{J_a} \tag{8-2}$$

or

$$k_2 = 1/2\ \omega_n\ J_a$$

For the position loop:

$$\omega' = k_1 = 0.636\ \omega_c = 0.636\ \frac{\omega_n}{6}$$

or

$$k_1 = 0.011\ \omega_n^2 \tag{8-3}$$

where

ω' = frequency at which crossover occurs if $T_1 = 0$, rad/sec

Stability considerations establish the relationship for the time constant T_1:

$$\frac{1}{T_1} = 0.398\ \omega_c = 0.0664\ \omega_n$$

$$T_1 = 15.1\ \frac{1}{\omega_n} \tag{8-4}$$

Figure 8-3 shows the Bode plot of the system. Over 20 db attenuation exists at the frequency at which antenna resonance occurs; this amount should be sufficient for stability purposes.

8.3 Errors Due To Wind Torque

One of the major factors that limit the tracking accuracy of this antenna is the error caused by wind gusts on the antenna. A method for computing this error is given in Reference 2. Mean wind torque can be computed using Eq. 5-1, but there exists a fluctuation about that mean of

$$T_{wf} = 2 k_w V_0 V_1(t)$$

where

T_{wf} = wind torque fluctuation, ft.-lbs.

$V_1(t)$ = standard deviation of wind velocity, mph

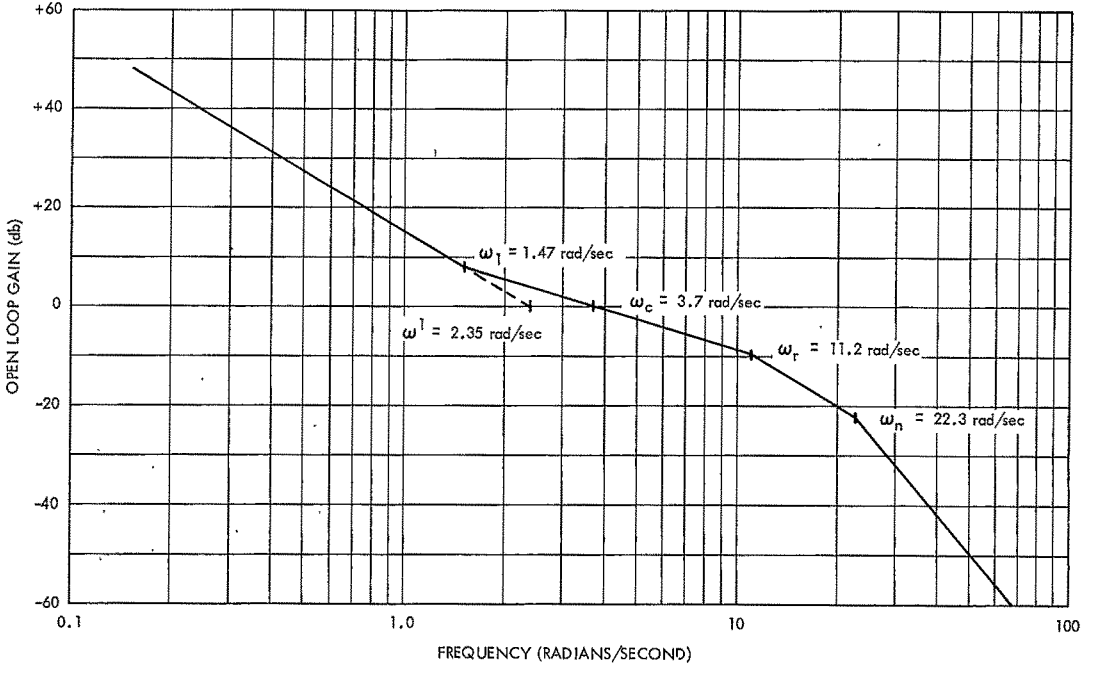

Figure 8-3. Bode Plot for Position Loop

The assumption is made in Reference 2 that the standard deviation is 25% of the mean wind velocity, hence T_{wf} can be redefined as

$$T_{wf} = 1/2\, k_w\, V_0^2$$

The power density spectrum of the wind torque can be written as

$$\phi_{ww}(s) = \frac{T_{wf}}{\pi} \frac{W_0}{s^2 + \omega_0^2} \tag{8-6}$$

where

$\phi_{ww}(s)$ = power density spectrum, (ft.-lbs.)^2/rad/sec

ω_0 = corner frequency of spectrum, rad/sec

$\approx$ 0.11 rad/sec as given by Reference 3.

The error due to wind torque is given by the relationship:

$$\epsilon_w^2 = \frac{1}{2\pi j} \int_{-j\infty}^{j\infty} \left| G_w(s) \right|^2 \phi_{ww}(s)\, ds \tag{8-7}$$

where

ϵ_w = error due to wind torque, radians

$G_w(s)$ = torque system transfer function.

The torque system transfer function can be obtained by setting $\theta_{SAT}(s) = 0$ in Figure 8-2 and rearranging the block diagram as shown in Figure 8-4. Using this diagram it can be found that

$$G_w(s) = \frac{\theta_{ant}(s)}{T_w(s)} = \frac{s}{J_a\, s^3 + k_2\, s^2 + k_1\, k_2\, T_1\, s + k_1\, k_2} \tag{8-8}$$

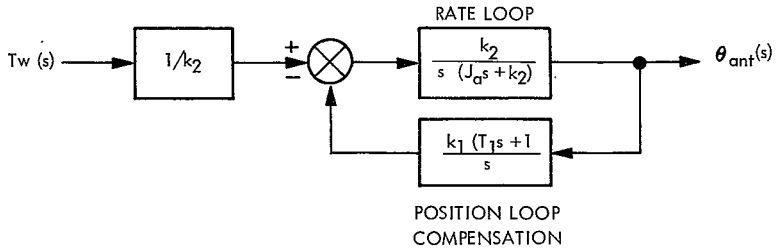

Figure 8-4. Block Diagram of Tracking Loop, Rearranged for Torque Input

Making use of Eqs. 8-2, 8-3 and 8-4 in Expression 8-8 yields

$$G_w(s) = \frac{\frac{1}{J_a}\, s}{s^3 + 0.5\,\omega_n\, s^2 + 0.083\,\omega_n^2\, s + 0.0055\,\omega_n^3} \qquad (8\text{-}9)$$

Combining 8-5, 8-6 and 8-9 in Expression 8-7 results in

$$\epsilon_w^2 = \frac{1}{4\pi} \frac{k_w^2\, \omega_0\, V_0^4}{J_a^2} \left(\frac{1}{2\pi j}\right) \int_{-j\infty}^{+j\infty} \frac{s}{s^3 + 0.5\,\omega_n\, s^2 + 0.083\,\omega_n^2 s + 0.0055\,\omega_n^3} \Bigg|^2 \frac{ds}{s^2 + \omega_0^2}$$

$$= \frac{1}{4\pi} \frac{k_w^2\, \omega_0\, V_0^4}{J_a^2} \left(\frac{1}{2\pi j}\right) \int_{-j\infty}^{+j\infty} \frac{c(s)\, c(-s)}{d(s)\, d(-s)}\, ds = 4.55\, \frac{k_w^2\, \omega_0\, V_0^4}{J_a^2}\, I_4$$

The solution of integral I_4 appears in Reference 2 (page 372) and without going through the mathematics the result can be written as:

$$\epsilon_w^2 = 2.58\, \frac{k_w^2\, V_0^2}{J_a^2}\, \frac{4.55\,\omega_n + 1}{\omega_n^3\,(\omega_n^3 + 1.59\,\omega_n^2 + 1.1\,\omega_n + 0.24)}$$

Taking the square root of above expression yields

$$\epsilon_w = 1.61 \frac{k_w V_0^2}{J_a} \sqrt{\frac{4.55\omega_n + 1}{\omega_n^3 (\omega_n^3 + 1.59\omega_n^2 + 1.1\omega_n + 0.24)}} \qquad (8\text{-}10)$$

To get a numerical solution to above expression for a 95-foot antenna, reference is made to Figures 5-3, 5-4 and 5-1 for some of the constants required:

$k_w = 670$ ft.-lbs./(mph)^2

$J_a = 2 \times 10^6$ slug ft^2

$\omega_n = 3.55$ cps $= 22.3$ rad/sec

Wind maxima can be found from Figure 8-5 for the Washington, D.C. area. This curve has been compiled using Reference 8-4. Since the wind does not exceed 29 mph 99% of the time

$V_0 = 30$ mph.

Substituting above constants into 8-10 yields

$$\epsilon_w = 0.025° \qquad (8\text{-}11)$$

For other wind speeds and antenna sizes the error can be found in a similar fashion and is plotted in Figure 8-6.

8.4 Errors Due To Friction

The second important error contributor to the overall tracking accuracy is the error due to friction. This error is predominant at extremely low speeds and assumes the form of a limit cycle. The magnitude of this error can be estimated by using a relationship from Reference 1

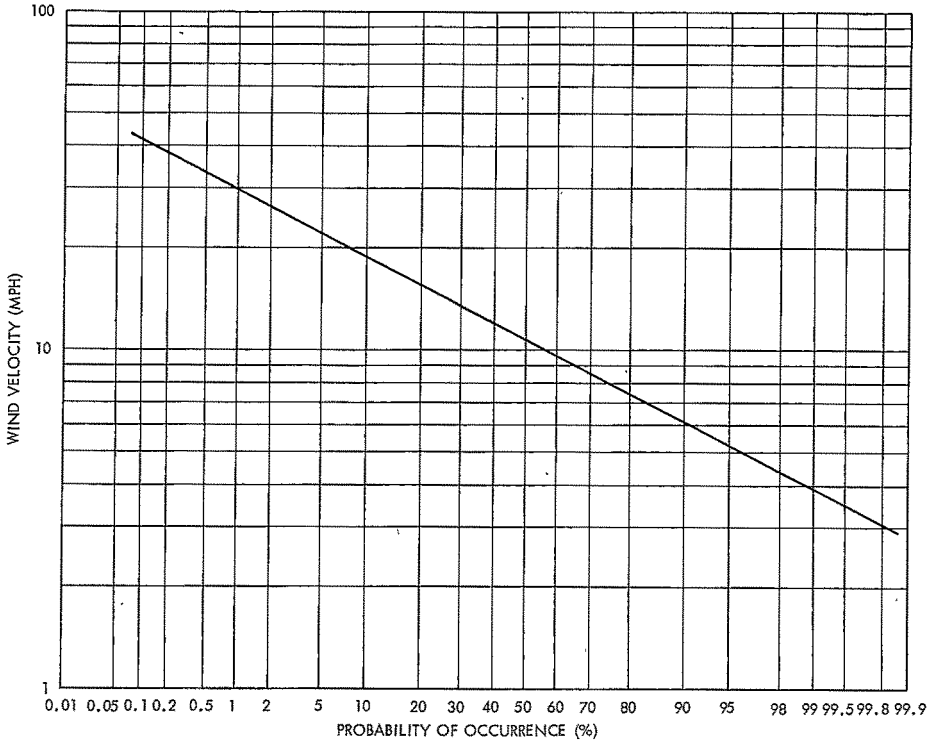

Figure 8-5. Maximum Wind Speeds for the Washington, D.C. Area

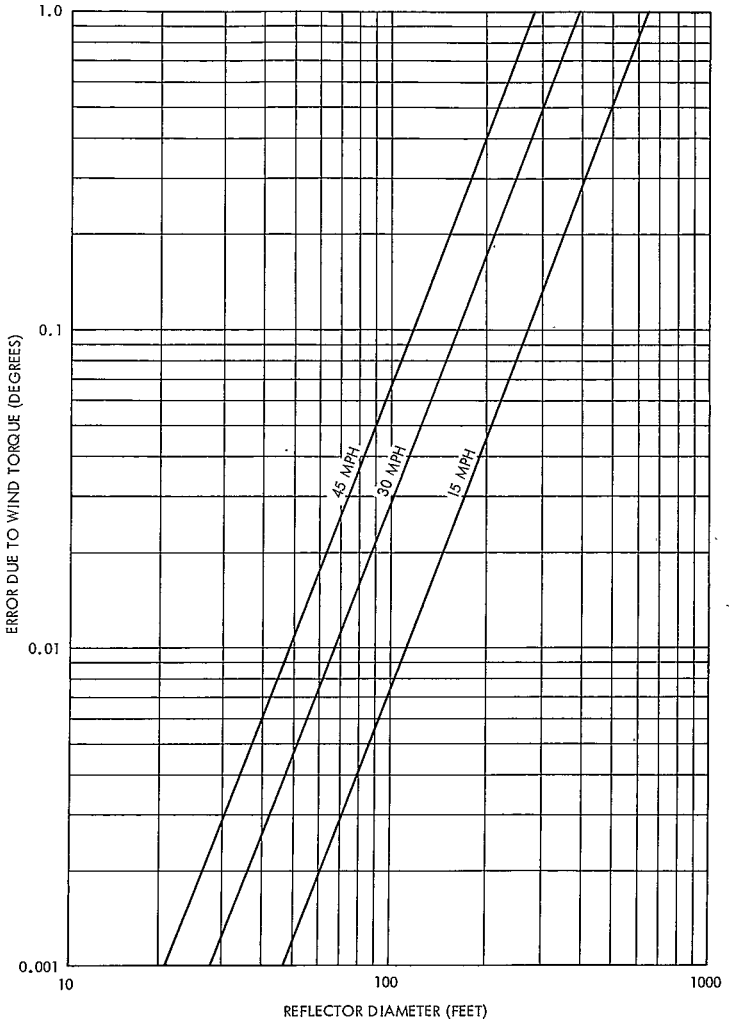

Figure 8-6. Errors Due to Wind Torque vs Reflector Size

$$\epsilon_f = \frac{12\ T_f}{J_a \omega_n^2} \tag{8-12}$$

where

ϵ_f = error due to friction, radians

T_f = friction torque (Coulomb), ft.-lbs.

Friction torque can be found from Figure 5-2. Substitution of friction torque and values for inertia and natural frequency for a 95-foot antenna yields

$$\epsilon_f = \frac{(12)\ (8.4 \times 10^4)}{(2 \times 10^6)\ (5 \times 10^2)} = 1.04 \times 10^{-3}\ \text{rad} = 0.060°$$

The error due to friction exceeds the required tracking error considerably. By judicious design, especially using digital techniques, this error can be reduced. However, the most effective way of reducing this error is by the use of hydrostatic bearing, which will substantially decrease the friction torque. A decrease in friction by a factor of twenty can be expected, hence the error will be reduced to 0.003°. This error is essentially independent of antenna size.

8.5 Other Contributing Errors

There are other errors, that contribute to the overall tracking error and these are computed below:

(1) Error due to Thermal Noise at Receiver: This error can be estimated by using a relationship from Reference 5

$$\epsilon_{th} = \frac{B}{K_m\ (S/N)\ (f_r/\beta_n)}$$

where

ϵ_{th} = error due to thermal noise, degrees

B = beamwidth of antenna = 0.051°

S/N = signal-to-noise ratio of error channel

= 30 db = 10^3

k_m = error slope for monopulse receiver = 1.57 deg/deg

f_r = receiver bandwidth = 50 cps

β_n = servo noise bandwidth $\approx 2\omega_c$ = 1.18 cps

Substitution into above equation yields

$$\epsilon_{th} = \frac{0.051}{1.57\ (10^3)\ (50/1.18)} = 1.5 \times 10^{-4} \text{ degrees}$$

This error is small because of the high signal-to-noise ratio expected in the error channel. Figure 8-7 shows how this error varies for variou signal-to-noise ratios and for various antenna sizes.

(2) Error due to Dynamic Lag of Servo: For a Type II servo this error is given by the relationship

$$\epsilon_d = \frac{\ddot{\theta}_{max}}{k_1}$$

where

ϵ_d = error due to dynamic lag, degrees

$\ddot{\theta}_{max}$ = maximum acceleration

= $\ddot{A}_{max}$ = $(5.72 \times 10^{-5})^0$/sec^2 (from Figure 8-1)

k_1 = acceleration gain = 0.011 ω_n^2 (from Eq. 8-3)

= 5.5/sec^2

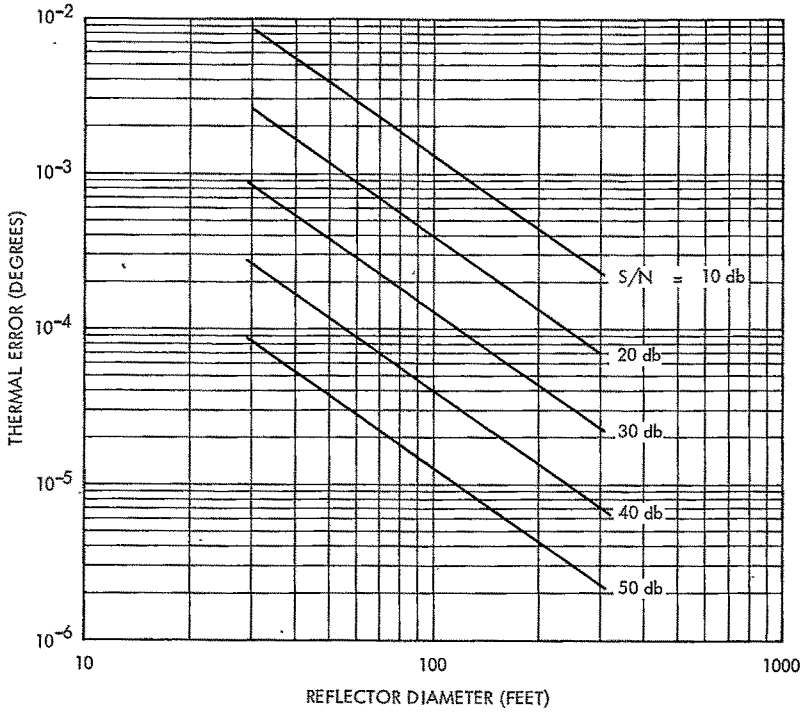

Figure 8-7. Thermal Error vs Reflector Size

Substitution yields:

$$\epsilon_d = \frac{5.72 \times 10^{-5}}{5.5} = 1.04 \times 10^{-5} \text{ degrees}$$

Similar to the thermal error, this error is very small and can be neglected. This error is small because the target acceleration as seen

from the antenna is very small. This error decreases rapidly as antenna size is decreased.

(3) Error Due to Atmospheric Scintillation: The power spectrum of scintillation is given in Reference 5 as

$$\phi_{ss}(s) = k_s \frac{\omega_s^2}{\omega_s^2 + \omega^2} \tag{8-13}$$

where

$\phi_{ss}(s)$ = power density spectrum of scintillation, degrees^2/rad/sec

k_s = constant

ω_s = corner frequency estimated by Reference 5 to be about 15.7 rad/sec

The mean amplitude of scintillation, S_{rms}, is assumed to be 0.001°. Hence, the constant k_s can be evaluated:

$$(S_{rms})^2 = \int_0^\infty \phi_{ss}(s)\, d\omega = k_s \omega_s \int_0^\infty \frac{\omega_s}{\omega_s^2 + \omega^2} d\omega$$

$$= \frac{\pi k_s \omega_s}{2}$$

Solving above for k_s and substitution of values yields:

$$k_s = \frac{2}{\pi \omega_s}(S_{rms})^2 = \frac{2}{15.7\pi} 10^{-6} = 4.05 \times 10^{-8} \tag{8-14}$$

The scintillation error then can be computed from

$$\epsilon_s^2 = \frac{1}{2\pi j} \int_{-j\infty}^{j\infty} |G_s(s)|^2 \phi_{ss}(s)\, ds \qquad (8\text{-}15)$$

where

ϵ_s = scintillation error, degrees

$G_s(s)$ = system transfer function

The exact system transfer function $G_s(s)$ can be found using Figure 8-2. However, a first order approximation to this function will be used:

$$G_s(s) = \frac{\theta_{ant}(s)}{\theta_{sat}(s)} = \frac{1}{\frac{1}{\omega_c} s + 1} \qquad (8\text{-}16)$$

The integral given by 8-15 is of the same form as 8-7 hence, the same method of solution can be used. Substitution of 8-13, 8-14 and 8-16 into 8-15 and solution of the integral yields:

$$\epsilon_s^2 = \frac{k_s}{2\left(\frac{1}{\omega_c} + \frac{1}{\omega_s}\right)} = 6.14 \times 10^{-8}$$

and taking the square root

$$\epsilon_s = 2.48 \times 10^{-4}$$

ıin this error is small and can be neglected when comparing the wind and friction errors. Figure 8-8 shows how this error varies with antenna size.

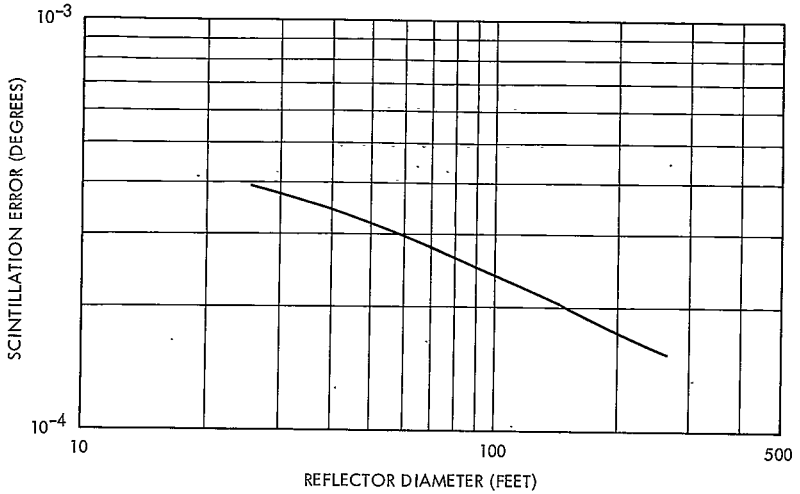

Figure 8-8. Scintillation Error vs Reflector Size

8.6 Overall Tracking Accuracy

Error components contributing to the overall tracking accuracy are listed in Table 8-1. As is evident, wind and friction errors are predominant. Fortunately, these two errors can be assumed to be exclusive, i.e., the greater of the two is present at any given time. When considering an overall tracking accuracy of 0.005° it becomes clear that hydrostatic bearings have to be used to reduce the friction error.

The total error is the root-mean-squared sum of the component errors and is given in Table 8-2. The total tracking error of the system is the vector sum of the individual axis errors and is also tabulated in Table 8-2 on a one sigma and three sigma basis. This table shows that the total tracking error at 30 mph wind velocity is 0.0355° which is in excess of the desired tracking accuracy of

Table 8-1

Component Errors

Mechanical error (see Section 5-5)	4.70×10^{-4} degrees
Wind error at 10 mph	2.78×10^{-3}
20 mph	1.11×10^{-2}
30 mph	2.50×10^{-2}
40 mph	4.45×10^{-2}
Friction error, standard bearings	6.00×10^{-2}
hydrostatic bearings	3.00×10^{-3}
Thermal error	1.58×10^{-4}
Dynamic Lag	1.04×10^{-5}
Scintillation	2.48×10^{-4}
Noise (assumed)	2.00×10^{-4}

Table 8-2

Total Errors

(hydrostatic bearings assumed)

Wind Velocity, mph	0	10	20	30	40
Total Error per Axis, 1σ	0.00306	0.00306	0.0112	0.0251	0.0446
Total Error System, 1σ	0.00433	0.00433	0.0158	0.0355	0.0632
Total Error System, 3σ	0.0130	0.0130	0.0474	0.107	0.189

0.005° by a factor of 7. The tracking error is also shown in graphical form in Figure 8-9. By combining the tabulated tracking error and the wind probability for the Washington, D.C. area (Figure 8-5) a probability model can be established and is shown in Figure 8-9. For the single antenna (0.1 db loss) the tracking accuracy will be 0.005° or less 64% of the time. For the array the required tracking accuracy of 0.009° will be held for 83% of the time. A more detailed presentation of tracking reliability as a function of antenna configuration is given in Section 9-4 of this report.

It should be recalled that computations leading to the total tracking errors are based on many assumptions and empirical data and therefore, a tolerance for accuracy has to be allowed. In addition, computations have been based on conventional control system design; introduction of a computer controlled antenna using either adaptive or optimal control techniques may lead to a more precise system.

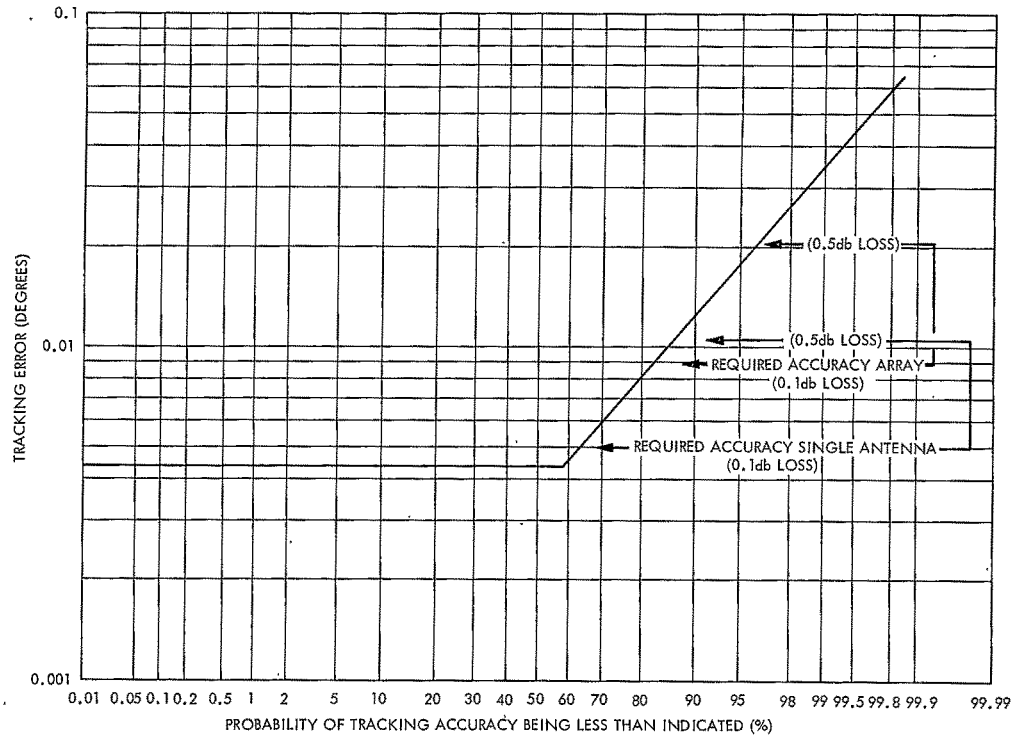

Figure 8-9. Probability Distribution of Total Tracking Error

REFERENCES FOR SECTION 8

1. G. Bierenson. "Relation Between Structural Compliance and Allowable Friction in Servomechanism", IEEE Transactions on Automatic Control, January 1965

2. G. C. Newton, L. A. Gould, J. F. Kaiser. Analytical Design of Linear Feedback Controls, John Wiley, 1964

3. J. W. Titus. Wind-Induced Torques Measured on a Large Antenna, Report 5549, Naval Research Laboratory, 1960

4. U.S. Weather Bureau, The Climatic Handbook for Washington, D.C. Technical Paper No. 8, 1949

5. D. K. Barton, Radar System Analysis, Prentice-Hall, Inc., 1965

9 SYSTEM CONSIDERATIONS

9.1 System Noise Temperature

The noise temperature of the TDRS ground antenna was determined from the equation

$$T_s = \alpha T_a + 290 (1 - \alpha) + 290 (NF - 1) \qquad (9\text{-}1)$$

where α includes all antenna losses prior to the preamplifier, assumed to be 0.5 db, and NF is the noise figure of the receiving system referred to the input of the preamplifier. Current developments in wideband parametric amplifiers indicate that a noise figure of 0.5 db at K_u-band with 2 GHz bandwidth will be achievable soon with further varactor diode improvements (sponsor and location classified). Assuming that this goal will be achievable with reliability by the mid 1970's, a total receiving system noise figure of 1.0 db is reasonable.

The antenna temperature (T_a) used in Eq. (9-1) during precipitation was taken to be the atmospheric noise temperature calculated previously and plotted in Figure 6-8. The system noise temperature is plotted in Figure 9-1 versus rain rate at three elevation angles for a 1.0 db noise figure receiving system. A similar graph in Figure 9-2 indicates system noise temperature versus rain rate for an identical antenna enclosed in a radome. The expression below was used to determine system noise temperature with a radome.

$$T_s = T_a \alpha_t + T_r \alpha_f + 290 (1 - \alpha_f) + 290 (NF - 1)$$

where

$$\alpha_t = \alpha_r \cdot \alpha_f$$

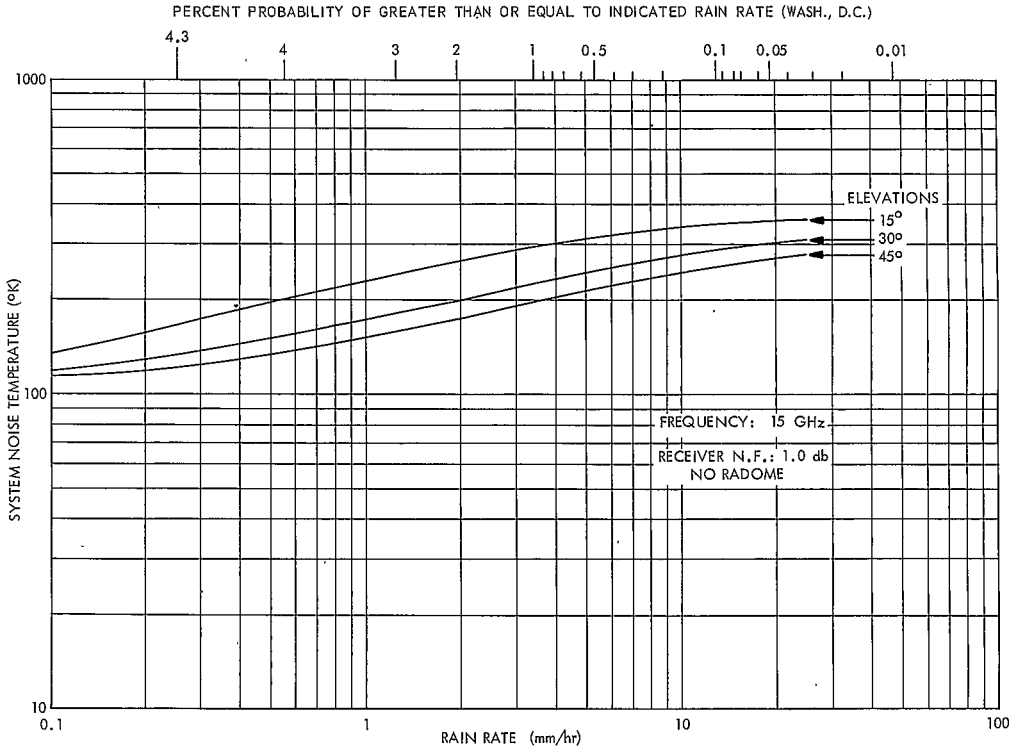

Figure 9-1. System Noise Temperature vs Rain Rate, No Radome

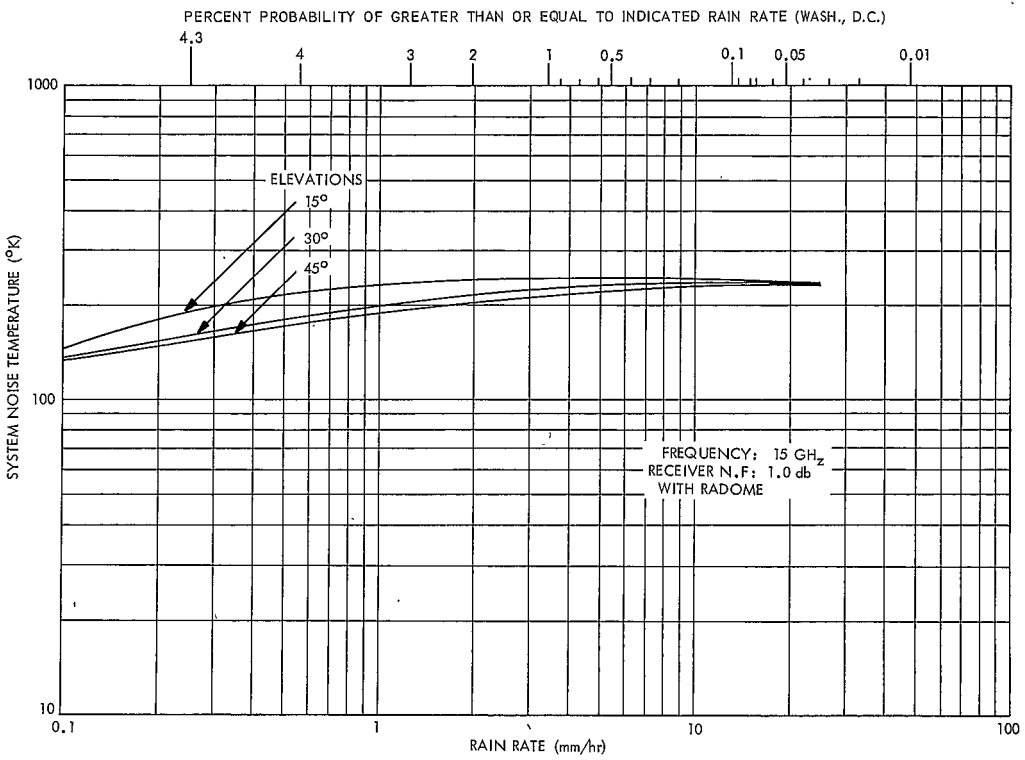

Figure 9-2. System Noise Temperature vs Rain Rate, with Radome

α_r = transmission coefficient of the radome and water accumulation on the radome

α_f = transmission coefficient of feed (0.5 db loss)

T_a = atmospheric noise temperature

T_r = noise temperature of radome

NF = receiving system noise figure referred to input of preamp

The values of radome noise temperature (T_r) and transmission coefficient (α_r) were derived in Section 7 of this report. Several representative values of ℓ_r and T_r are given in Table 9-1 for a space frame radome without a water repellant surface. The lack of significant experimental data on water repellant surfaces prevents an evaluation of their characteristics.

Table 9-1

Radome Characteristics, F = 15 GHz

Loss (dry)	Rain Rate	Water Film Thickness	Water Atten.	T_r	Loss (net) ℓ_r
1.05 db	0.25 mm/hr	0.55 mills	0.7 db	37°K	1.75 db
1.05 db	2.54	2.15	2.7	81	3.75
1.05 db	25.40	8.40	12.6	120	13.65

The effect of receiver noise figure can be seen in Figures 9-3 through 9-5. In these curves, system noise temperature versus rain rate is plotted for four values of receiver NF: 0.5, 1.0, 2.0, and 3.0 db.

9.2 Carrier to Noise Ratio

The system noise temperature versus environmental conditions has been plotted in the previous section. A similar set of curves for attenuation were

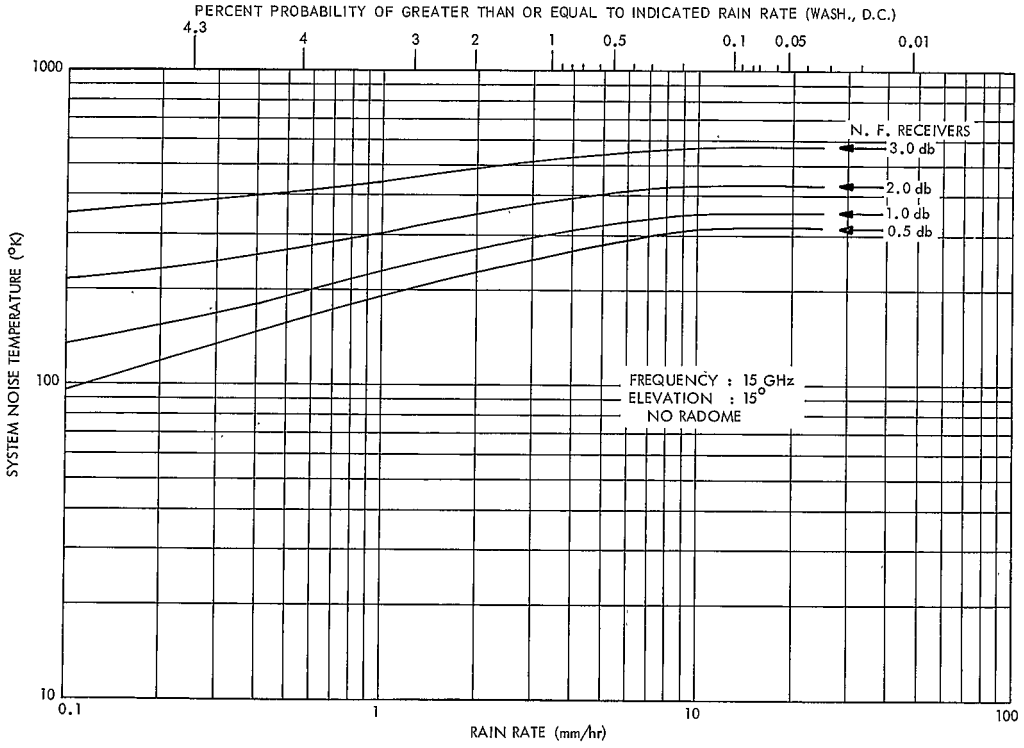

Figure 9-3. System Noise Temperature vs Rain Rate, 15° Elevation

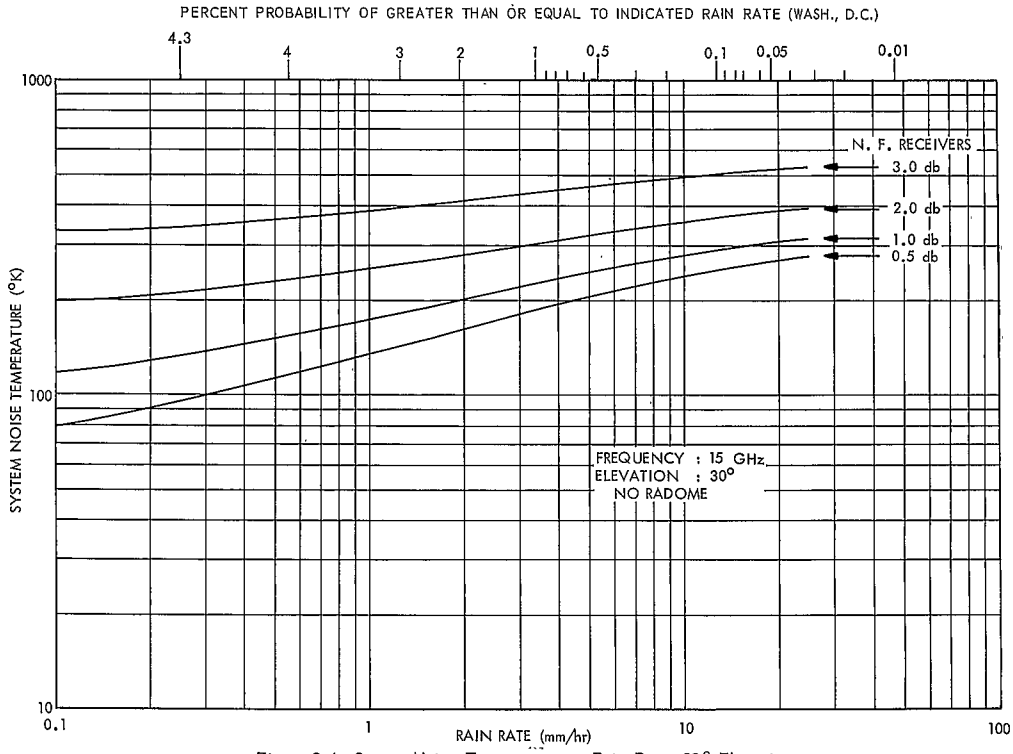

Figure 9-4. System Noise Temperature vs Rain Rate, 30° Elevation

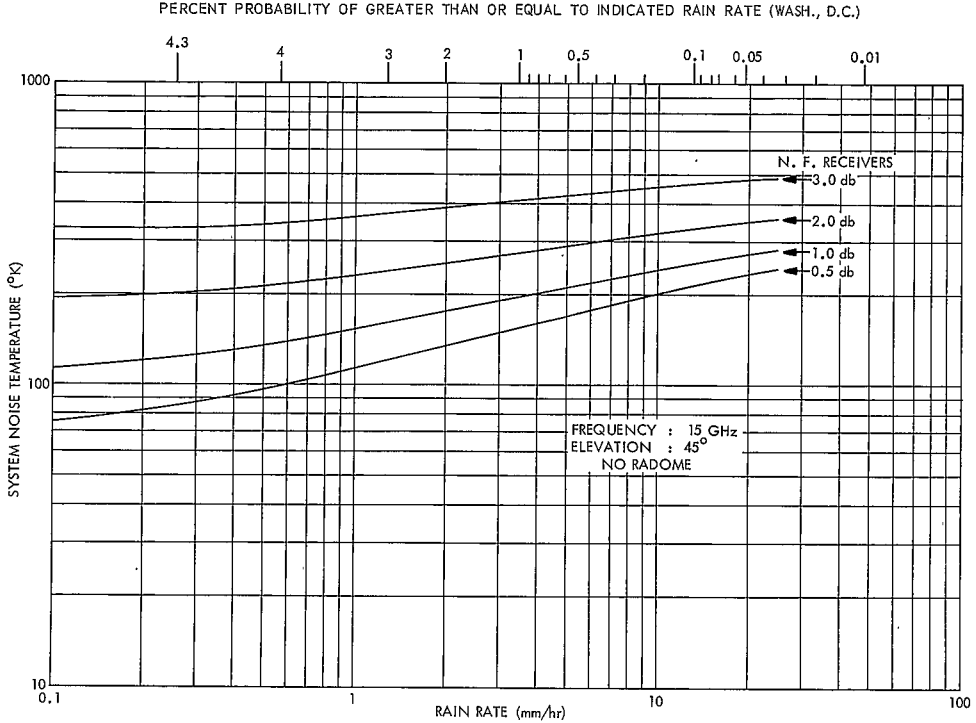

Figure 9-5. System Noise Temperature vs Rain Rate, 45° Elevation

plotted in Figure 6-4. From these curves, the resultant reduction in CNR can be calculated relative to clear sky conditions. In the CNR reduction curves that follow, the reference CNR was based upon a system noise temperature for clear sky and no radome. The reference values are given below for the receiver noise figures considered.

Receiver NF	Clear Sky System Noise Temperature
0.5 db	85.8°K
1.0 db	124.8°K
3.0 db	339.8°K

The CNR reduction vs rain rate for a system with a 1.0 db receiver noise figure is plotted in Figure 9-6. An identical antenna enclosed in a radome (Section 7 of this report) would experience a CNR reduction as shown in Figure 9-7. [It should be noted that the radome enclosed antenna must provide 1 db greater gain and be correspondingly larger to achieve the equivalent gain of an exposed antenna (Section 7-1).] The effect of the radome is to produce an additional 4 db reduction in CNR under moderate rain (2.5 mm/hr) and 12 db under heavy rain (25 mm/hr). Looking at this from another point of view, an antenna oriented at 30° elevation with no radome would not exceed 10 db reduction in CNR more than 0.2% of the time as compared to 1.0% for an antenna with radome. The CNR reduction for systems without radome and receiver noise figures of 0.5 db and 3.0 db are plotted in Figures 9-8 and 9-9.

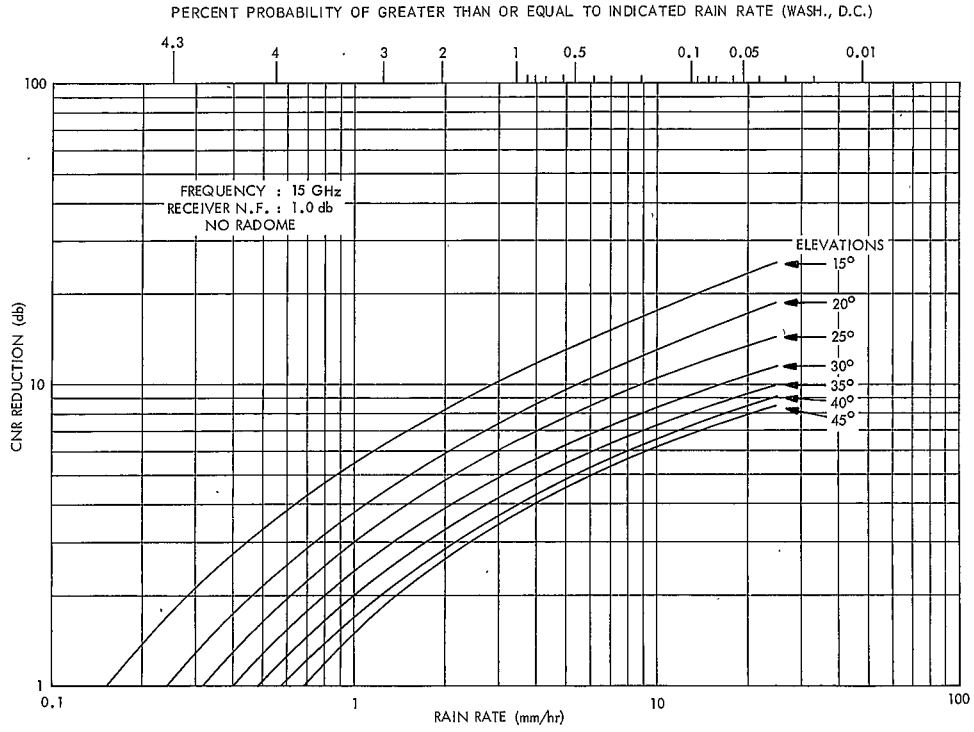

Figure 9-6. CNR Reduction va Rain Rate, 1.0 db NF Receiver

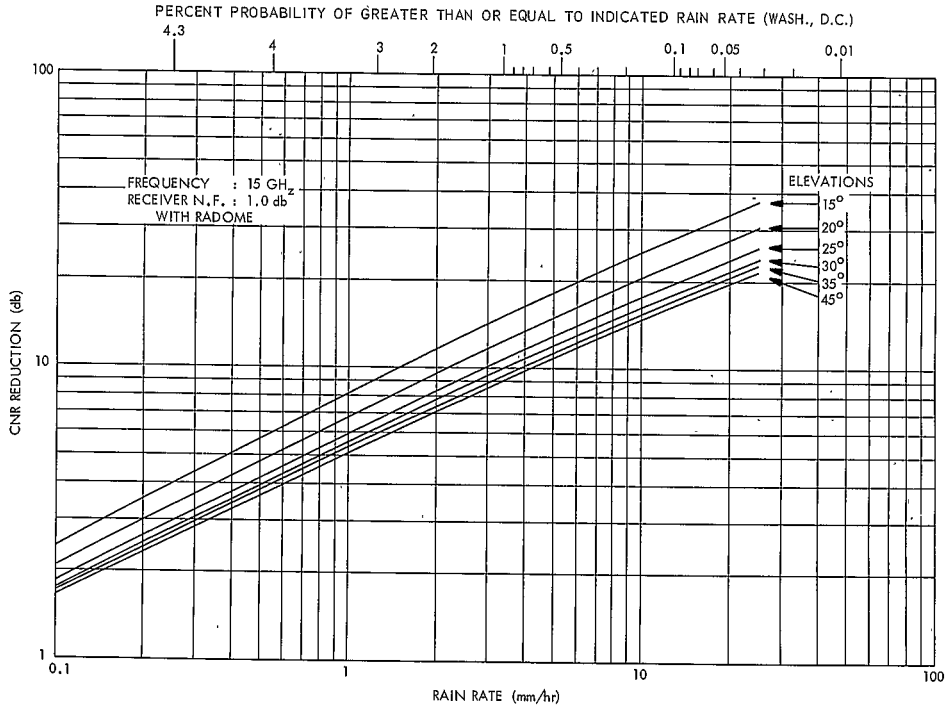

Figure 9-7. CNR Reduction vs Rain Rate, 1.0 db NF, with Radome

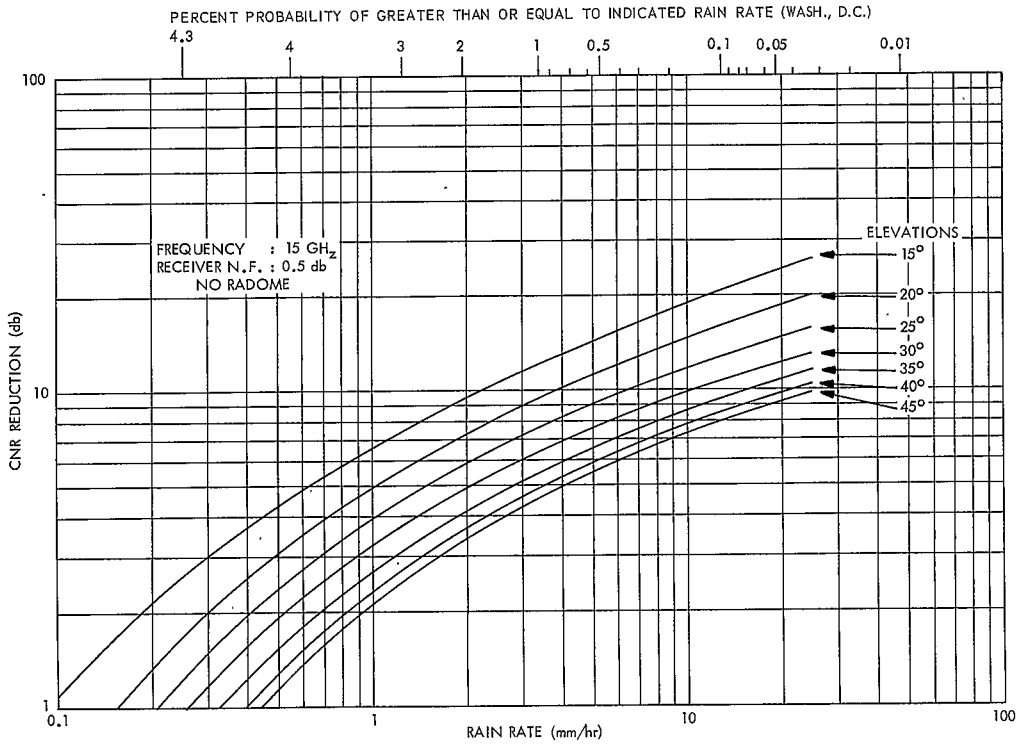

Figure 9-8. CNR Reduction vs Rain Rate, 0.5 db NF Receiver

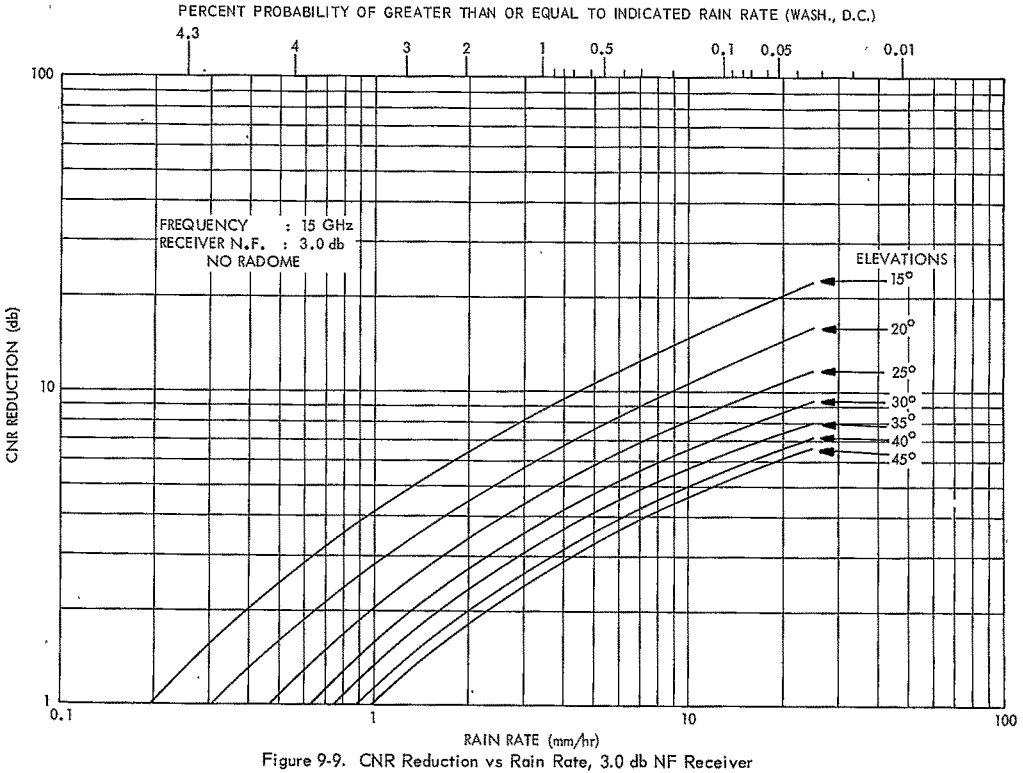

Figure 9-9. CNR Reduction vs Rain Rate, 3.0 db NF Receiver

9.3 Communication Performance

The link calculation for the TDRS to ground K_u-band communications channel is given in Table 9-2. The EIRP for the DRS Spacecraft was defined by the gain parameters of Table 2-1 and an assumed 2 db loss in transmission line from the transmitter to the antenna. An atmospheric loss of 0.2 db was assumed corresponding to the humid, clear sky conditions of Figure 6-3. The system noise temperature of 124.8°K was based upon a 1.0 db NF receiving system, an assumption that appears reasonable for the mid 1970's. A ground antenna gain of 70 db

Table 9-2

Link Calculations, F = 16 GHz

Transmitted Power (20 watt)	+43 dbm
Spacecraft Gain (4' Dish, 55% efficiency)	+43.5 db
Spacecraft Losses	-2.0 db
EIRP	+84.5 dbm
Space Loss	-208.8 db
Atmospheric Attenuation (Clear, 30° elevation)	-0.2 db
Feed Losses	-0.5 db
Signal Power Into Preamplifier	-125.0 dbm
Noise Power (T_s = 124.8°K, 2 GHz BW)	-85.7 dbm
Required Carrier to Noise Ratio (CNR)	30 db
Minimum Ground Antenna Gain	69.3 db
Margin	0.7 db
Required Ground Antenna Gain	70 db

is necessary to achieve the required 30 db CNR. No radome is assumed in the link calculations for reasons that were discussed in Section 7.

The effect of receiving system noise figure on ground antenna gain requirements is substantial. The table below indicates the gain required to achieve a 30 db CNR under humid clear sky conditions. Although further reduction in receiver noise figure below the 1.0 db assumed realistic in the link calculations

NF	T_s	Gain Required
0.5 db	85.8°K	68.4 db
1.0 db	124.8°K	70 db
3.0 db	339.8°K	74.3 db

will reduce the required antenna gain, meteorological effects will increase the CNR reduction in unfavorable weather.

Meteorological conditions greatly affect link performance as discussed in Section 9.2 of this report. The requirements for the communications link permit a 10 db reduction in CNR under unfavorable weather without significantly affecting full-operation. Based upon the curves in Figures 9-6 through 9-9, Table 9-2 was constructed indicating the percentage probability of exceeding a 10 db CNR reduction versus spacecraft elevation angle. Further reductions in CNR are not catastrophic and can be tolerated if the probability of occurrence is acceptably low. Table 9-3 lists the percentage probabilities of exceeding 20 db reduction in CNR.

The effect of a radome can clearly be seen in Tables 9-3 and 9-4 as compared to an identical antenna with no radome. The communication link is degraded but not to an extent that precludes their use. It should be noted that recent developments in water repellant membrane coatings (Section 7) could reduce the

Table 9-3

Probability of Exceeding 10 db CNR Reduction

Elevation of Spacecraft	NO RADOME			WITH RADOME
	3.0 db N.F.	1.0 db N.F.	0.5 db N.F.	1.0 db N.F.
15°	0.7%	1.3%	1.8%	2.6%
20°	0.2%	0.5	0.9	1.8
25°	0.07	0.2	0.4	1.3
30°	*	0.07	0.17	1.0
35°	*	0.03	0.08	0.8
40°	*	*	0.04	0.75
45°	*	*	0.03	0.7

*< 0.03%

Table 9-4

Probability of Exceeding 20 db CNR Reduction

Elevation of Spacecraft	NO RADOME			WITH RADOME
	3.0 db N.F.	1.0 db N.F.	0.5 db N.F.	1.0 db N.F.
15°	0.06%	0.10%	0.15%	0.41%
20°	*	*	0.03	0.18
25°	*	*	*	0.10
30°	*	*	*	0.07
35°	*	*	*	0.06
40°	*	*	*	0.05
45°	*	*	*	0.04

*< 0.03%

probabilities in Tables 9-3 and 9-4. However, until measured performance data for these techniques is available the radome characteristics in the above tables must be assumed.

Now that both CNR reduction and reliability have been discussed, estimates of reliability in the communications link can be made. The TDRS is assumed 60° longitude from GSFC. Assuming a 1.0 db receiver noise figure and no radome, the link reliability of providing at least 20 db CNR (10 db CNR reduction from the 30 db maximum) will be 98.7%. For providing at least 10 db CNR, the reliability is 99.9%.

These reliability figures can be significantly increased by a 5° increase in elevation to 20°. The reliability for this satellite configuration is given in Table 9-5. The TDRS spacecraft must be within 53° longitude of GSFC to provide the reliability given in Table 9-5. The reliability of the communications link for

Table 9-5

Propagation Link Reliability

Minimum CNR	Link Reliability (NO RADOME)	Link Reliability (WITH RADOME)
10 db	99.97%	99.82%
20 db	99.5 %	98.2 %
30 db	95 %	95 %

a 53° longitude relative to GSFC is considered a minimum for the TDRS to ground communications channel. Overall system reliability including equipment and tracking as well as communication link reliability must also be considered, but these considerations are beyond the scope of this report.

The most unreliable part of the ground antenna is the receiver front end. In a single aperture system, a failure here results in complete failure of the system. Periodic maintenance on the front end and refrigeration equipment will also require down time for the entire system. The multi-aperture array, however, exhibits a graceful failure. The failure of a single front end, although more likely to occur since there are now four, will result in a 1.3 db loss in gain for the array. The simultaneous failure of three of the four elements will reduce the gain by only 4.7 db. The multi-aperture array is a much more attractive configuration when a continuous uninterrupted communication channel is required.

9.4 Tracking Performance

The TDRS ground antenna is of necessity a high performance system. The antenna must provide a 70 db gain communication channel and must simultaneously track the TDRS spacecraft. The gain requirement is achievable with current state of the art technology (Section 4.1). The feed system necessary to track the TDRS spacecraft will be a complex multimode configuration (Section 4.2) if a single aperture ground antenna is chosen. Even with an acceptable RF tracking system, the tracking function is seriously impaired by the servo pointing accuracy of the system (Section 8). An AZ/EL pedestal with a hydrostatic bearing on the azimuth

axis is not sufficient to give the system an acceptable tracking reliability. Table 9-6 summarizes the tracking reliability of a 70 db gain single aperture antenna based upon wind loads characteristic of the Washington, D.C. area. This data is derived from Section 8 of this report.

Table 9-6

Tracking Performance of a 95' Diameter Antenna

Tracking Accuracy	Resulting Gain Loss	% Probability of Occurrence, Unfavorable Wind Conditions
0.005°	0.1 db	37%
0.010°	0.5 db	12%
0.014°	1.0 db	8%
0.020°	2.0 db	4%
0.025°	3.0 db	2.5%

An array of four antennas on a single pedestal is as cost effective as a single aperture antenna for achieving 70 db gain (Section 10). The array is attractive from both a tracking and a reliability point of view. Each array element will be 42 feet in diameter and mounted in a square cluster as in Figure 4-9. The cross sectional area of the array is roughly identical to that for the single aperture antenna and therefore the wind loading will be the same for these two alternative configurations. However, since the array is adaptively phased to remove phase differences on the received information prior to combining, the pointing loss of the array is determined by the antenna patterns of the array elements. For 42-foot diameter elements, the tracking reliability is given in Table 9-7.

Table 9-7

Tracking Performance of a Four Element Array of 42' Diameter Antennas on a Single Pedestal

Tracking Accuracy	Gain Loss	% Probability of Occurrence, Unfavorable Wind Conditions
0.009°	0.1 db	17%
0.021°	0.5 db	3.5%
0.028°	1.0 db	1.8%
0.041°	2.0 db	0.5%
0.050°	3.0 db	0.35%

The array also simplifies the RF tracking requirements. Contrary to the requirements of a single aperture antenna, the array elements require only a sum mode output. The tracking error channels are formed in the combining receiver which measures and removes the phase of the array element channel prior to combining. A one milliwatt pilot transmitted by the TDRS spacecraft and a 20 KHz tracking noise bandwidth in the receiver would provide more than 30 db CNR in the error channel. The square arrangement of the array elements would provide error channels in each of two orthogonal directions for the servo system.

Although Table 9-7 indicates that the TDRS spacecraft will fall outside the 3 db BW of the array under wind conditions that occur 0.35% of the time in the Washington, D.C. area, the probability of the spacecraft actually being outside the 3 db BW is a much smaller value. It is the wind gusting (Section 8-3) that determines the pointing error, not the average wind velocity.

The selection of the multi-aperture array on a single pedestal presents one other attractive feature for this configuration. The central region of the array has not been used thus far. For an array of 42-foot diameter elements, a 17-foot diameter section exists in this central region. An acquisition antenna could be positioned within that region as in Figure 9-10. This acquisition antenna (3 db BW = 0.25°) would have a Cassegrain tracking feed arrangement that would facilitate initial acquisition of the TDRS spacecraft and provide tracking information to bring the spacecraft within the tracking region of the full array. Under unfavorable wind conditions, the acquisition antenna would reduce the probability of occurrence of conditions that would cause loss of signal or track to less than 0.03% as opposed to the 0.35% figure for the multi-aperture array alone. Again it should be remembered that the probability of the satellite actually being outside the range of the acquisition antenna is much less than 0.03%.

The use of a radome would eliminate the wind errors and greatly increase tracking performance. However, the exposed 4 element array has already been shown to provide an acceptable tracking capability. The tracking reliability given in Table 9-7 is based upon the worst case wind direction for the antenna. The actual tracking reliability can realistically be expected to be much higher than indicated. However, the communication link reliability of Tables 9-3 and 9-4 are based upon precipitation conditions that can be confidently expected in the Washington area. Therefore, based upon total system performance, the radome should not be used for the TDRS ground antenna.

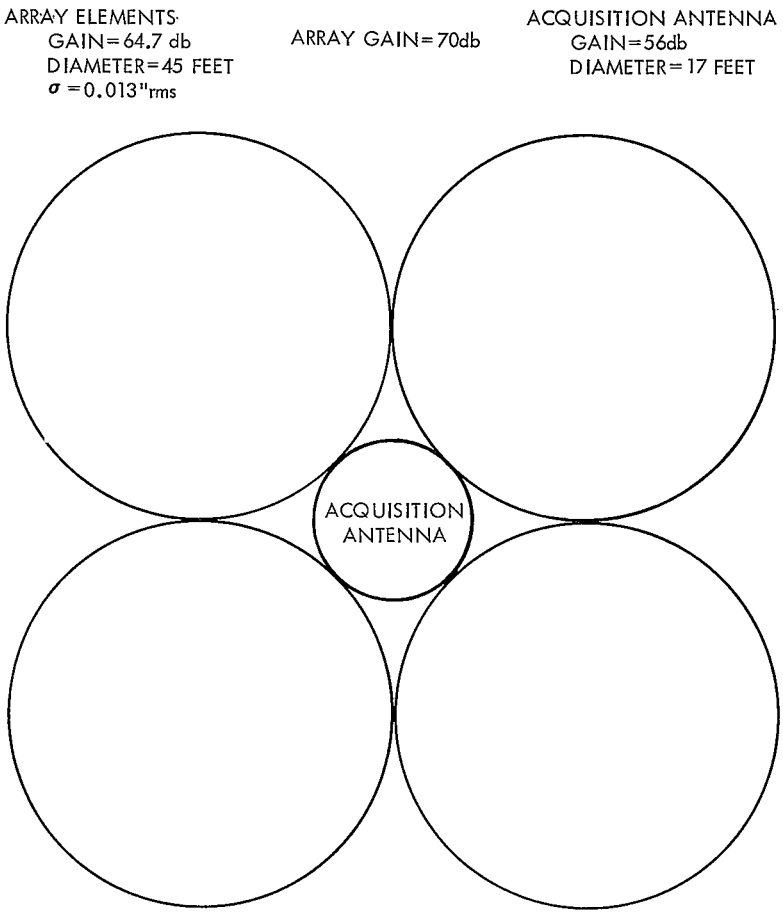

Figure 9-10. Four Element Array on a Single Pedestal With Acquisition Antenna

10 ECONOMIC CONSIDERATIONS

The TDRS ground station is a complex facility that requires a detailed cost analysis. This Section limits itself to covering only the antenna costs and those electronics that affect a tradeoff between antenna configurations. An economic analysis of the two feasible antenna configurations is presented in this Section: a single reflector antenna and a four element array on a common pedestal.

10.1 Single Reflector Antenna

A cost model for large reflector antennas was constructed by Bell Telephone Laboratories [1] recently, under contract to GSFC. The model for exposed reflector antennas is given in Eq. 10-1. Structure, pedestal, drive and control costs are included in this model.

$$\$ = a_1 D^{-1/3} e^{D/45} \qquad (10\text{-}1)$$

$\$$ = cost in dollars

D = antenna diameter in feet

$a_1 = 6.7 \times 10^5$

Eq. 10-1 was obtained by fitting a curve to three well known existing antenna systems (Figure 10-1). All three antennas were built by the Rohr Corporation and good surface tolerance information is available for each structure. BTL recommends the use of Eq. 10-1 for a range of antenna diameters from 10 to 250 feet.

In determining its cost model, BTL assumed that rms surface accuracy and antenna diameter were related by the expression

$$\sigma = 10^{-5.37} D^{3/2} \qquad (10\text{-}2)$$

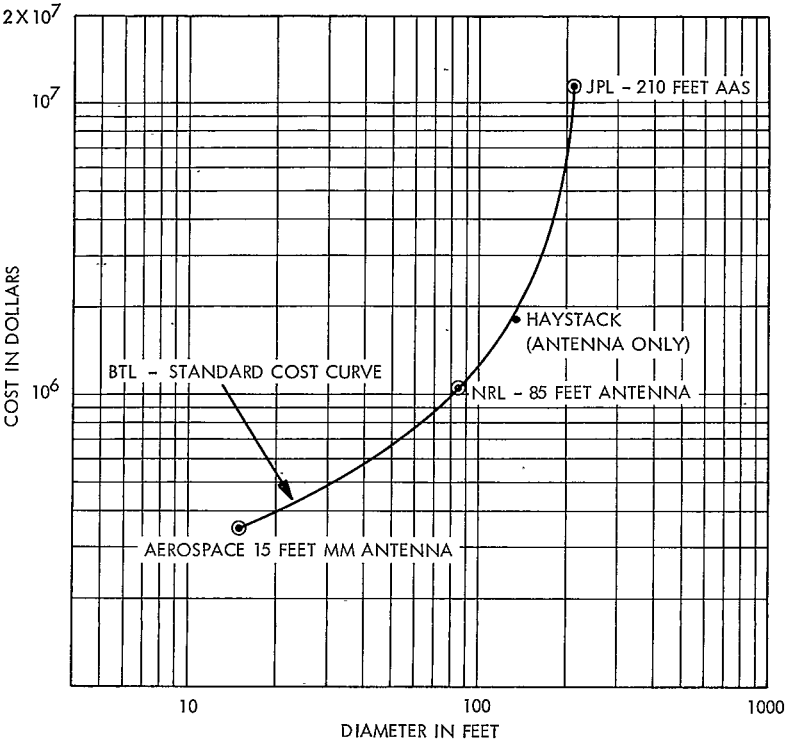

Figure 10-1. Cost vs Diameter for Basic Antenna Structures

for exposed antennas. Figure 10-2 illustrates the BTL criterion as well as the older JPL criterion [4]. The curve indicating the upper limit in the present state of the art is taken from Figure 4-4 of this report. The maximum gain for the $\sigma = 10^{-4.6} D$ curve is 73 db. Based upon this current state of the art, the surface tolerance assumed in Eq. 10-2 is inaccurate. The BTL cost model (Eq. 10-1) was adjusted in light of the new surface tolerance relation by adding

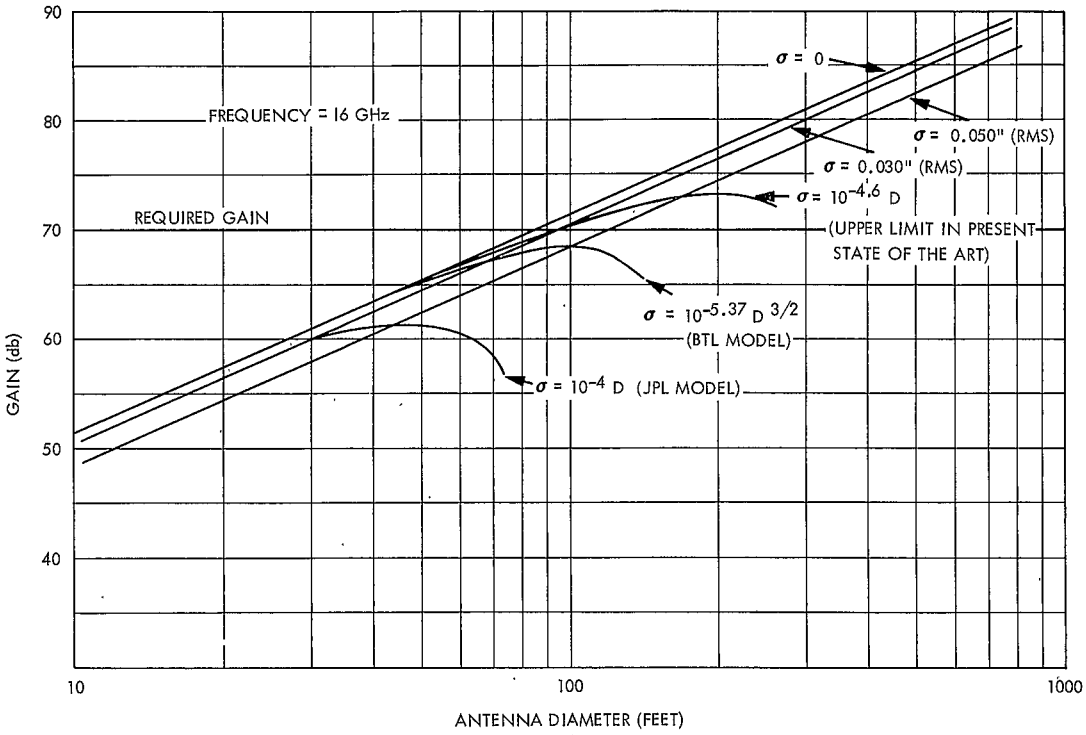

Figure 10-2. Gain-Limit Antennas for Various Sigma Criteria

a quality factor to the expression. The quality factor relates an incremental change in rms surface accuracy ($\Delta\sigma$) to an incremental change in cost ($\Delta\$$). This approach was first introduced by Stack [2] and is expressed as

$$\sigma = \frac{\sigma_0}{x} \qquad (10\text{-}3)$$

where

σ = actual rms surface accuracy

σ_0 = rms surface accuracy from Eq. 10-2

x = quality factor

Adjusting Eq. 10-1 in light of Eq. 10-3 we get a new cost expression [1]:

$$\$ = a_1 D^{-1/3} e^{(a_2 D + x - 1)}$$

where

$a_1 = 6.7 \times 10^5$

$a_2 = 2.22 \times 10^{-2}$

The array on separate pedestals was discussed in Section 4.3 and shown to b unacceptable since it can not provide the required bandwidth. This configuration will, therefore, not be considered further in this Section.

The BTL study also developed a cost-diameter relation for antennas enclosed by radome. After correcting for surface tolerance as with the exposed antenna case, the cost relation is given by

$$\$ = e^{(x-1)} \left[a_3 D^{1.3} - a_4 D^{1.85}\right] + a_4 D^{1.85}$$

where

$\$$ = cost of antenna and radome, including pedestal, drive and control equipment

$a_3 = 6.7 \times 10^3$

$a_4 = 1.28 \times 10^2$

Note that the quality factor (x) is associated with the antenna portion only, since it has no effect on radome costs. The cost of exposed and radome enclosed antennas as a function of gain are given in Figure 7-1.

10.2 Array of Reflector Antennas

The gain requirement can also be achieved with an array of smaller aperture antennas. The array elements can be mounted on separate pedestals or on a common pedestal [3]. In either case the array elements are adaptively combined and provide a total array gain of

$$G_T = G_E + 10 \log N$$

where

G_T = total array gain

G_E = array element gain

N = number of elements

In estimating the cost of an array on a common pedestal, the reflector, feed, and backup structure are assumed to comprise 35% of the cost of a conventional antenna system with the pedestal, drive and control equipment comprising the remaining 65%. This cost division closely matches the costs of the 40' antenna recently installed at the Goddard Network Test and Training Facility (NTTF). Under this assumption, the cost of the array on a common pedestal is given by

$$\$_A = N(0.95^{\log_2 N})(0.35\ \$_E + C_F) + 0.65\ \$_S$$

where

$\$_S$ = cost of a gain equivalent single reflector antenna from Eq. 10-4

$\$_E$ = array element costs from Eq. 10-4

C_F = front end costs = \$80K

The term $(0.95^{\log_2 N})$ is the learning factor of manufacturing N identical antennas. This learning factor is commonly used in cost estimations of this type [1,4]. The 1.0 db receiver noise figure assumed for the system will require a front end and refrigeration costing \$80K per antenna.

10.3 Cost Effectiveness

The most attractive ground antenna configuration is the one that provides the best performance per dollar cost. The performance criterion will be the total antenna gain. System noise temperature is assumed identical for each configuration. A comparison of the cost effectiveness of an exposed antenna and a radome enclosed antenna is given in Figure 10-3. At the required 70 db gain, the radome enclosed antenna is much less cost effective and therefore undesirable. The radome enclosed antenna system is also unattractive under precipitation as discussed in Section 9.2 of this report.

The cost effectiveness of the two feasible antenna configurations is presented in Figure 10-4. At the required 70 db gain, the single antenna and the array of four dishes on a common pedestal are about equally cost effective. The cost effectiveness criterion used in the analysis was gain. Tracking capability, acquisition and reliability did not contribute to the results. These considerations, however, are important and must be considered along with cost effectiveness in determining the optimum antenna configuration. The system performance of the alternative configurations are discussed in Section 9 of this report.

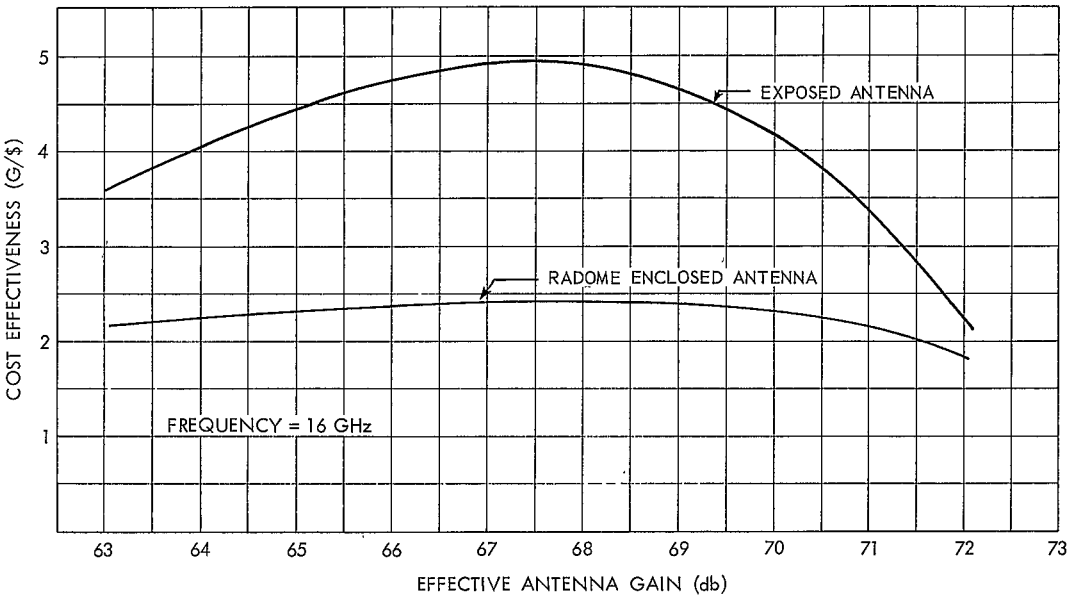

Figure 10-3. Cost Effectiveness of Exposed and Radome Enclosed Antennas

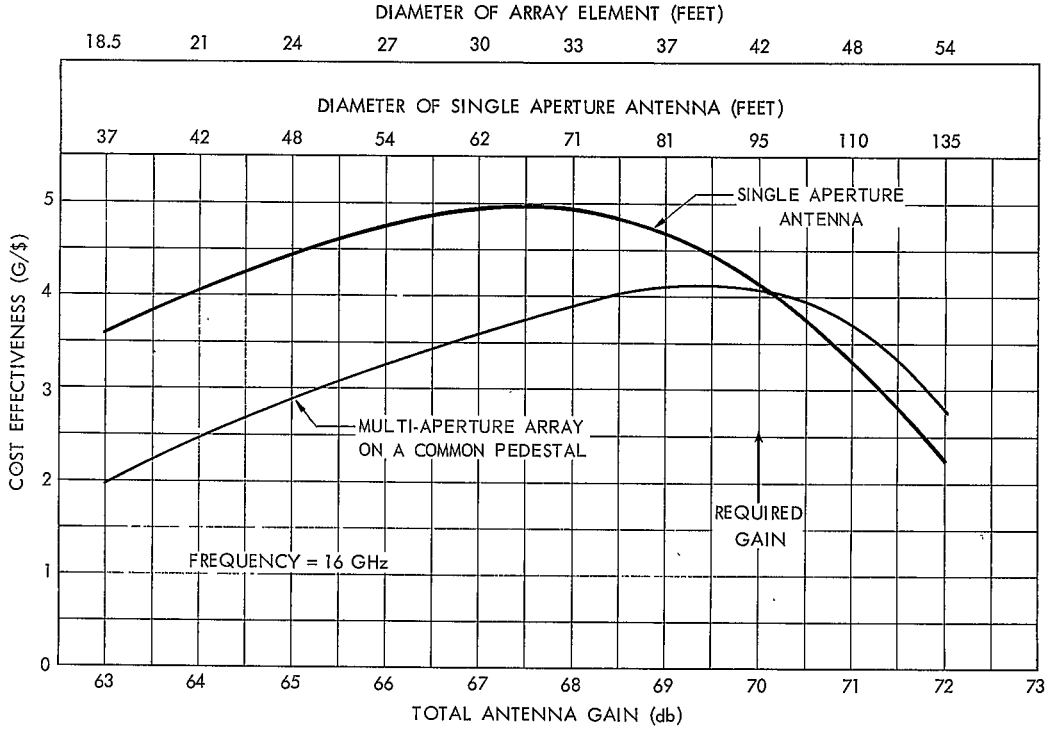

Figure 10-4. Cost Effectiveness of Alternative Configurations